Copyright

by

Bradley Donald Koester

2000

Panel Zone Behavior of Moment Connections Between Rectangular Concrete-Filled Steel Tubes and Wide Flange Beams

by

Bradley Donald Koester, B.S.C.E., M.S.

Dissertation

Presented to the Faculty of the Graduate School of
The University of Texas at Austin
in Partial Fulfillment
of the Requirements
for the Degree of

Doctor of Philosophy

The University of Texas at Austin

May 2000

Panel Zone Behavior of Moment Connections Between Rectangular Concrete-Filled Steel Tubes and Wide Flange Beams

Approved by
Dissertation Committee:

_____
Joseph A. Yura

_____
James O. Jirsa

_____
Richard W. Furlong

_____
Michael D. Engelhardt

_____
Morris Stern

To my Mother

In Loving Memory of Donald Alfred Koester
1931 – 1998

Acknowledgments

I would like to start by thanking Dr. Joseph Yura. Your generous nature and patience with me through the completion of this project was invaluable. I have learned to look at various phenomena, engineering related or not, from very interesting points of view. In addition, I've enjoyed your wonderful sense of humor. Sometimes I laugh to myself while recalling entertaining discussions or anecdotes. Also I would like to thank Dr. James Jirsa. Your assistance on this project and your insights have helped me a great deal. I appreciate your guidance and participation in discussions. Thanks also to the rest of the Dissertation Committee: Professors Richard Furlong, Michael Engelhardt and Morris Stern. I would like to acknowledge the enthusiastic cooperation of Professor Hiroshi Noguchi and Dr. Kazuhiro Uchida of Chiba University in Japan. Their assistance and validation of our tests using their analysis was very valuable during their nine-month visit to Texas during 1997. Also, I would like to thank Professor James Ricles and Ph.D. Candidate Shih-wei Peng of Lehigh University for their collaboration. Without the financial support of the National Science Foundation, this research project would not have been possible.

Next I'd like to express a deep thanks to the Ferguson lab staff, many members of whom have move on to other things. Thanks go to: Laurie Golding, Sharon Cunningham, Wayne Fontenot, Blake Stassney, Ray Madonna, Mike Bell, Regina Forward, Ruth Goodson, Patrece Reese, Kelly Gorham, Dijaira Smith, and of course, Edgar! A special thanks goes out to the spirit of April Jenkins. Your heart was ever flowing, and you'll be missed by all of us who had a chance to share in your life.

Friends at Ferguson Lab made the experience priceless. Thanks to Reagan and Jerry Herman, Sergio and Suzanna Brena, Paul Ziehl, Chuck and Maria Veronica Barnes, Fernando Ulloa, Jeff Schmitz, Charles Bowen, Robert Frosch, Robbie Barnes, Scott and Sheryl Civjan, Jeannine Amos, Yajai and others for your great sense of humor and for the fun. Then there are the newcomers this year who have been a refreshing breath of air into this lab, with all of the social activities and such: Tink, Anna, Jenny, Hagenberger, Michele, and all the rest. It's dangerous to name people for fear of missing anyone.

Jeff and Pam West. You two are great. I appreciate the time we've spent together, and especially have enjoyed watching Jack and Bennett grow up. I look forward to more good times, and am pleased that you have decided to stay in Austin. Your friendship and support has been invaluable to me. Jeff Wouters, it's been great getting to know you, and I appreciate your candor and sincerity. Dave and Jill Glassco, you two are wonderful. It's been great getting to know you. I look forward to many more fun times, working with you, and watching your band Blue Millennium evolve. To The Recliners, Russell Young, Neal, Mike, Brent and Dennis, it's been great working to help promote your band, and I wish you continued success.

Glenn Gomez. How can I thank you enough for your flexibility and support that has made this dissertation possible in the wake of a booming business venture. Allowing me the time and space to wrap this work up, as well as providing administrative support during this period so that I could disappear for a while, is the true mark of faith and trust. Much thanks Glenn, Doug, Courtney, and Dave, the CDstreet.com team!

Mom. Your love and support during this academic phase in my life has been the cornerstone of this accomplishment. Through tough times managing Dad's illness, we've managed to make things work for all of us. Dad would be smiling right now. I appreciate all you've done for me, for your faith and love. Pam, Steve, Aaron and Steph: thanks for the fun times and support, and I look forward to our next visits.

Thank you Dad, wherever you are, for your humor, kindness, and unending well of generosity and spirit. You'll be with us always.

Sincerely,

Austin, TX
May 2000

Brad Koester

Panel Zone Behavior of Moment Connections Between Rectangular Concrete-Filled Steel Tubes and Wide Flange Beams

Publication No. _____

Bradley Donald Koester, Ph.D.
The University of Texas at Austin, 2000

Supervisors: Joseph A. Yura and James O. Jirsa

During the 1990s, guidelines for the detailing of composite joints for seismic safety have been proposed and adopted. Such guidelines were based on the testing of composite joint subassemblies under cyclic loads. The role of the confined concrete core in composite joints has been documented and quantified for systems using steel shapes encased in concrete, as well as for other mixtures of reinforced concrete and structural steel. The need to understand the role of the concrete core in moment connections utilizing concrete-filled tube (CFT) columns still exists.

In this research program, the split-tee through-bolted moment connection between wide-flange steel beams and concrete-filled tubes was studied. The aim of the study was to understand the role of the confined concrete core in transferring forces through the joint. Fifteen half-scale panel-zone specimens were designed and tested to model the shear behavior of the split-tee connection. Following an analysis of the results of the panel-zone tests, six full-scale moment connections were designed and tested. Variables studied were: concrete compressive strength, the *b/t* ratio (slenderness) of the steel tube walls, and the split-tee contact area against the steel tube.

Following an analysis of the test data, design criteria for the concrete contribution to the joint strength are presented, and recommendations are made for the inclusion of CFT systems in the design recommendations for composite joints. Suggestions are made for further research.

Table of Contents

Table of Figures xiv

List of Tables xviii

1. Introduction 1

1.1 Composite / Hybrid Structural Systems 1

1.2 Composite Connections 3

1.2.1 Connections in Steel Reinforced Concrete (SRC) Systems 4

1.2.2 Connections to Concrete-Filled Tube (CFT) Systems 10

1.3 Development of Through-Bolted Moment Connections to CFTs 12

1.3.1 Research in Japan 12

1.3.2 Research in the US – Joint US / Japan Program 14

1.4 Research Program 17

1.5 Panel Zone Behavior 18

1.5.1 The Concrete Compressive Strength Variable: f'_c 20

1.5.2 The Slenderness Ratio Variable: b/t 20

1.5.3 The Tee-Width Parameter: $\%b$ 22

1.6 Outline of Research Program 22

2. Half-Scale Panel-Zone Tests 24

2.1 Description of Tests 24

2.2 Test Setup 25

2.2.1 Measurements and Data Acquisition 28

2.3 Specimen Descriptions and Details 32

2.3.1 Series A Specimens 33

2.3.2 Series B Specimens 34

2.3.3 Series C Specimens 34

2.4 Testing Procedure 39

3. Experimental Results from Panel-Zone Tests 40

3.1 Panel Zone Tests 40

3.2 Series A: Specimen 8.4A, 8.6A and 8.8A 40

3.3 Series B: Specimens 8.4B, 8.6B, and 8.8B 49

3.4 Specimen 8.MB 54

3.5 Series C Specimens 55

3.5.1 Reference Specimens 8.PC and 8.P2C 55

3.5.2 Specimen 8.RC 58

3.5.3 Specimen 8.DC 61

3.5.4 Specimen 8.SC 64

3.5.5 Specimen 8.SAC 65

3.5.6 Specimen 8.BC 67

3.6 Series C Results Tabulated 68

3.7 Validity of Panel-Zone Tests 69

4. Analysis of Panel-Zone Tests for the Development a Behavioral Model 72

4.1 Contributions to Joint Shear Strength 72

4.2 Evaluation of the 8-inch Tube Series 73

4.2.1 Series C “Cut-out” Specimen Analysis 74

4.2.2 Summary of Cut-out Series 80

4.3 Development of Behavioral Model 81

4.3.1 Shear Strength by the Kanatani Model 83

4.3.2 ACI-ASCE Committee 352 Term for V_c 85

4.3.3 Relationship Between V_c and f'_c for CFTs 86
4.3.4 Trial Models 89
4.3.5 Effect of *b/t* Ratio 93
4.3.6 Variation of the Tee Width Against the Tube 94
4.4 Summary of Panel-Zone Analysis 96
5. Tests on Full-Scale Connections **99**
5.1 Description of Tests 99
5.2 Specimen Descriptions and Details 100
5.2.1 12” x 12” CFT Connections 101
5.2.2 16” x 16” CFT Connections 101
5.2.3 Beam Sizes 102
5.2.4 Structural Tees Used 103
5.2.5 Through Bolts 104
5.3 Specimen Fabrication 105
5.3.1 Drilling of Tube Sections and Insertion of Placeholders 105
5.3.2 Concrete 108
5.3.3 Specimen Assembly 109
5.3.4 Post-tensioning 110
5.3.5 Welding 110
5.4 Test Setup 110
5.4.1 Loading System 111
5.4.2 Measurements and Data Acquisition 112

5.5 Testing Procedure 114

6. Application of Model to Full-Scale Connection Tests 116

6.1 Description of Tests 116

6.2 12 inch CFT – Results 116

6.3 CFT.1 116

6.3.1 Net-section Fracture 117

6.3.2 Increase in net-section for remaining 12 inch CFTs 119

6.4 CFT.2 120

6.4.1 Beam Behavior 120

6.4.2 Bolt / Tee Behavior 123

6.4.3 System Performance and Panel Zone 124

6.5 CFT.3 and CFT.4 126

6.5.1 Comparisons between CFT.2, CFT.3 and CFT.4 129

6.5.2 Common Behavior in the 12 inch CFTs 132

6.6 Application of Panel Shear Equations to 12 inch Square CFT Specimens 133

6.7 A Simplified Model 134

6.7.1 Significance of *b/t* and Confinement 135

6.7.2 Observed Effects Related to b / t and tube thickness 136

6.8 16 inch CFT – Results 137

6.9 CFT.5 138

6.9.1 System Performance and Panel Zone 138

6.10 CFT.6 143

6.10.1 System Performance and Panel Zone 143

6.11 Behavior of 16 inch CFT Moment Connection Specimens 148

6.12 Contributions of Steel and Concrete, Compared 150

6.13 Synopsis 152

7. Summary and Conclusions **154**

7.1 Summary 154

7.2 Recommendation for Shear Calculation 157

7.3 Limitations 158

7.4 Suggestions for Future Research 158

Appendix A: Finite Element Analysis **159**

A.1 Introduction 160

A.2 Experimental Program 163

A.2.1 Panel-Zone Test Specimens and Variables 163

A.2.2 Testing Procedure 164

A.2.3 Experimental Results 165

A.3 Finite Element Analysis 168

A.3.1 Finite Element Analysis of Panel Zone Test 169

A.3.2 Finite Element Analyses of Beam - Column Joint Test 173

A.4 Conclusions 178

Appendix B: Design Shear Check **181**

Appendix C: As-Built Connection Dimensions **184**

Bibliography **191**

Vita **195**

Table of Figures

Figure 1.1 - IDS Center Floor Plan (Viest, 1997) 2
Figure 1.2 - Encased Composite Column in Rigid Frames (Viest, 1997) 4
Figure 1.3 - Examples of Japanese SRC Construction (Ogura et al, 1990) 5
Figure 1.4 - Steel Beam to Encased Column Connection (Viest, 1997) 6
Figure 1.5 - Classification of Joint Types 8
Figure 1.6 - Definition of Effective Width for Reinforced Concrete Joint 9
Figure 1.7 - Effective Width for Two Types of Composite Joints Utilizing Steel Encased in Concrete (a) Extended FBP, and (b) Wide FBP 9
Figure 1.8 – Examples of Composite Connections Used in Japanese Construction 11
Figure 1.9 - Example CFT Connection Types (Viest 1997) 12
Figure 1.10 - End-Plate Through-Bolted Connection (Kanatani et al, 1985) 13
Figure 1.11 - Split-Tee Through-Bolted Connection (Kanatani, et al 1985) 14
Figure 1.12 - Split-Tee Through-Bolted Connection (Ricles et al, 1997) 16
Figure 1.13 - Split-tee Through-bolted Connection 17
Figure 1.14 - Tension and Compression from Beam Moments Resolved by Joint Forces 18
Figure 1.15 - Vexp / Vtheory Related to b / t (Tomii 1988) – Solid: Cyclic, White: Monotonic 21
Figure 2.1 - Panel Zone Test Setup – Plan View 25
Figure 2.2 - Schematic of Test Setup, Cyclic Load P Applied at Ends 26
Figure 2.3 – Reaction Blocks Simulate Tee Forces 26
Figure 2.4 - Test Setup Idealization 27
Figure 2.5 - Variation of Bearing Surfaces to Simulate Tee Width 28
Figure 2.6 - Panel Zone Instrumentation 29
Figure 2.7 - Panel Zone Instrumentation (During Test) 29
Figure 2.8 - Specimen 8.M-B Tested Under Flexure 34
Figure 2.9 - Specimen 8.BC Details 36
Figure 2.10 - Reinforcement for 8.B-C 36
Figure 2.11 - Inserting Cage into 8.B-C 36
Figure 2.12 - Specimen 8.RC, Rectangle of Steel Removed 37
Figure 2.13 - Rectangular Cutout 37
Figure 2.14 - Specimen 8.SC, Slot Removed 37
Figure 2.15 - Narrow Slot Cutout 37
Figure 2.16 - Specimen 8.DC, Steel Tension Tie 38
Figure 2.17 - Diagonal Strap Left in Place 38
Figure 3.1 - Definition of End Displacement and Panel Shear 41

Figure 3.2 – 8.4A Load / Displacement Curve 42
Figure 3.3 - 8.6A Load / Displacement Curve 42
Figure 3.4 - 8.8A Load / Displacement Curve 43
Figure 3.5 - Panel Zone Distortion 44
Figure 3.6 – 8.4A Panel Zone Distortion 44
Figure 3.7 – 8.6A Panel Zone Distortion 45
Figure 3.8 – 8.8A Panel Zone Distortion 45
Figure 3.9 - Comparison Between Linear Pot and 1-Sided Strain Gauge – 8.4A 46
Figure 3.10 – Interior Damage to 8.4A 47
Figure 3.11 – General Crack Direction in 8.4A (Area of Contact Denoted by 4" x 4" Squares on Side) 48
Figure 3.12 – Contact Face Exposed 48
Figure 3.13 – 8.4B Load / Displacement Curve 49
Figure 3.14 – 8.6B Load / Displacement Curve 50
Figure 3.15 – 8.8B Load / Displacement Curve 50
Figure 3.16 - 8.4B Panel Zone Distortion 52
Figure 3.17 – 8.6B Panel Zone Distortion 52
Figure 3.18 – 8.8B Panel Zone Distortion 53
Figure 3.19 - Specimen 8.MB Load-Displacement 54
Figure 3.20 - Specimen 8P.C Load -Displacement 56
Figure 3.21 - Specimen 8P2.C Load-Displacement 57
Figure 3.22 - Specimen 8P.C Panel Distortion 57
Figure 3.23 - Specimen 8P2.C Panel Distortion 58
Figure 3.24 - Specimen 8.RC 59
Figure 3.25 - Specimen 8R.C (rectangular cut-out) 59
Figure 3.26 - 8.RC Average Diagonal Concrete Strain - Tension 60
Figure 3.27 - 8.RC Average Concrete Panel Strain – Compression 61
Figure 3.28 - Specimen 8.DC (instrumentation removed) 62
Figure 3.29 - Specimen 8D.C (diagonal steel strap) 63
Figure 3.30 - Specimen 8.DC Strain in Steel Tension Strap (average both sides) 63
Figure 3.31 - Specimen 8.DC Compression Diagonal Concrete Strain 64
Figure 3.32 - Specimen 8S.C (narrow slot cut-out) 65
Figure 3.33 - Specimen 8.SAC (Sand in Panel) 66
Figure 3.34 - Specimen 8.BC (Rebar-Enhanced) 67
Figure 3.35 - Shear vs. Panel Distortion for 8.BC 68
Figure 3.36 – Specimen 8.4A Results Compared to FEM Model (Uchida, et al 1998) 70
Figure 3.37 – Specimen 8.8A Diagonal Panel Zone Displacement FEM Comparison (Left: Compression, Right: Tension) Uchida et al (1998) 70
Figure 3.38 - FEM Stress Contour Comparison (Uchida et al, 1998) 71
Figure 4.1 – Specimen 8.RC (X-X: Axis of Bending) 75

Figure 4.2 – Relationship Between Shearing Force P and Fixed End Moments M 75
Figure 4.3 - 8.DC Steel Contribution in Shear 78
Figure 4.4 - Specimen 8.SC 80
Figure 4.5 - Kanatani Model for Predicting Shear Strength of Square CFT Section 83
Figure 4.6 - Illustration of Kanatani Concrete Term 84
Figure 4.7 – Log-Log Plot of Vc Versus f'c for Specimens with Constant b/t=32. 89
Figure 4.8 - Equations Compared to Normalized Test Data 92
Figure 5.1 - Split-Tee Through-Bolted Connection 99
Figure 5.2 - Cruciform Shaped Specimen in Test Setup 100
Figure 5.3 - Hole Pattern for Specimens CFT.1 through CFT.4 106
Figure 5.4 - Filling the tubes with concrete (left), and vibrating (right). 109
Figure 5.5 - Test Setup for Full-Scale Specimens 111
Figure 5.6 - Loading System: Ram Applied to Column Top 112
Figure 5.7 - Panel Zone Instruments 113
Figure 5.8 - Displacement History 115
Figure 6.1 – Specimen CFT.1 Load-Displacement Curve 117
Figure 6.2 – Net Section Fracture on Top Tee Bolt Line 118
Figure 6.3 – Fractured Column with Beams Removed 119
Figure 6.4 – Specimen 2 Beam Yield Pattern at 2.0% Drift 121
Figure 6.5 – Specimen CFT-2, Beam Web at 4.5% Drift 121
Figure 6.6 – Initiation of Tee Prying around 2.0% Drift 122
Figure 6.7 – Specimen CFT-2 at conclusion of test: 5.0% Drift 122
Figure 6.8 - Influence of Test Setup Geometry on Top-Tee Prying 123
Figure 6.9 – Specimen CFT.2 Load-Displacement Curve 124
Figure 6.10 – CFT.2 Shear vs. Panel Distortion 125
Figure 6.11 – Excavation of CFT.2 Concrete – Removal of Loose Material 126
Figure 6.12 – Specimen CFT.3 Load-Displacement Curve 127
Figure 6.13 – CFT.3 Shear vs. Panel Distortion 128
Figure 6.14 – Specimen CFT.4 Load-Displacement Curve 128
Figure 6.15 – CFT.4 Shear vs. Panel Distortion 129
Figure 6.16 - Shear vs. Drift Envelope for 12 inch Series 130
Figure 6.17 - Panel Distortion Envelope, 12 inch Series 131
Figure 6.18 – Equations Compared Against Normalized Test Results 134
Figure 6.19 – Specimen CFT.5 138
Figure 6.20 – Specimen CFT.5 Joint Shear vs. Drift Curve 139
Figure 6.21 – CFT.5 Extent of Beam Flange Yield at 2.0% Drift 139
Figure 6.22 – CFT.5 at 3.0% Drift: Tee Prying, Panel Zone Undamaged 140
Figure 6.23 – CFT.5 Shear vs. Steel Panel Distortion 141
Figure 6.24 – Extent of Beam Yield at 3.5% Drift 141
Figure 6.25 – K-Line Fracture of Tee 142

Figure 6.26 – Specimen CFT.6 Joint Shear vs. Drift Curve 144
Figure 6.27 – CFT.6 Shear vs. Steel Panel Distortion 144
Figure 6.28 - Joint Shear vs. Story Drift Envelope for CFT.5 and CFT.6.....145
Figure 6.29 - Joint Shear vs. Steel Panel Distortion Envelope 145
Figure 6.30 – CFT.6 with Panel-Zone Exposed and Intact.....147
Figure 6.31 – CFT.6 Extent of Interior Concrete Panel-Zone Distress – Hairline Diagonal Cracking 147
Figure 6.32 - CFT.5 Normalized Shear vs. Distortion.....149
Figure 6.33 - CFT.6 Normalized Shear vs. Distortion.....149
Figure 6.34 - Joint Shear vs. Story Drift for CFT.5 and CFT.6 150
Figure 6.35 - Steel Panel Shear Contribution for CFT.5.....151
Figure 6.36 - Steel Panel Shear Contribution for CFT.6.....152

List of Tables

Table 1-1 – Coefficient γ for R / C Joints (from ACI-ASCE Committee 352) 7
Table 2-1 - Panel-Zone Specimens 32
Table 2-2 - Steel Properties of Square HSS Sections 33
Table 3-1 - Series A Results 43
Table 3-2 - Series B Results 53
Table 3-3 - Series C Measured Capacities 68
Table 4-1 – Estimated Vc for Selected Specimens 82
Table 4-2 - Comparison of Concrete Predicted Strength 88
Table 4-3 - Four Equations Normalized to Test Data (NORM=V_{calc}/V_{test}) 92
Table 4-4 - Series A and Series B Results 96
Table 5-1 – Measured Properties of Concrete-Filled Tube Sections 101
Table 5-2 - Wide-Flange Beam Properties 103
Table 5-3 – Measured Dimensions of Split Tees 104
Table 5-4 - Through-Bolts Used and Tensile Strength of the Group Based on AISC LRFD Tables 105
Table 6-1 – Tabulated Results for 12” Tube Series 132
Table 6-2 - Tabulated Results for 16" Tube Series 146

1. Introduction

1.1 Composite/Hybrid Structural Systems

The innovative use of composite or "hybrid" structures is gaining popularity worldwide because of its economy and impact on seismic safety and performance. When performance is measured in terms of strength, stiffness and ductility, composite systems can perform better than the sum of their parts through the symbiotic participation of concrete and steel. Conventional reinforced concrete construction is one of the earliest forms of composite construction. The addition of reinforcing steel to plain concrete made it possible to design for tensile forces in concrete members despite the fact that plain concrete is not reliable under tension.

Typical composite building systems utilize steel structural shapes embedded inside concrete (steel reinforced concrete systems - SRC), or wrapped around concrete (concrete-filled tube systems - CFT). Composite construction in general is not limited to vertical columns or beams. Other forms of composite construction include: coupling walls, shear walls, floor systems, pressure vessels and nuclear reactors, piles, offshore structural members, bridge cable-stays, bridge decks, pavements, and many other applications.

Entire building systems may be regarded as composite. For example, the 57-story IDS Center in Minneapolis, MN (Figure 1.1) employs the use of exterior composite columns, and a concrete core around the elevator shaft system. The building was constructed in 1972, and was one of the earliest examples of

exterior composite columns. Structural steel floor girders span column-free from the interior concrete core to the perimeter frame. Two-story outrigger trusses are located at three widely separated levels along the height of the building. The core is a concrete box with encased steel sections.

One of the key advantages to mixed systems is the efficiency at which buildings can be constructed. Construction of the steel and concrete can take place simultaneously by simply separating the crews by a few stories. In the case of the IDS center, the steel erection crew had a ten-story lead on the concrete crew. Temporary bracing can be used to stabilize the steel members prior to the placement of concrete.

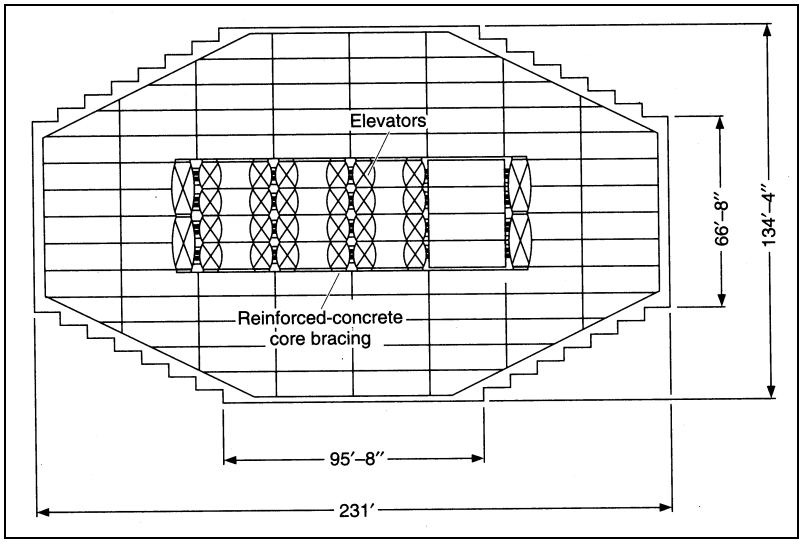

Figure 1.1 - IDS Center Floor Plan (Viest, 1997)

1.2 Composite Connections

The development of composite construction created the need to develop new ways of connecting materials. Moment connections between beams and columns in typical reinforced concrete structures consist of steel reinforcing bars that pass through the joint according to code-required embedment lengths and anchorage details. Steel reinforcement is designed to confine the concrete joint core, and to provide a stable load path for joint shear forces through the column. Detailing of structural steel moment connections involves bolting or welding of materials. Beams are either welded directly to columns, or are attached to columns by bolting to tee stubs, angles, and/or shear tabs. Column webs are typically stiffened with steel plates to transfer beams flange forces through the joint. Composite joints, on the other hand, present a new variety of connection challenges.

Current design provisions in the US dictate that moment connections in seismic zones must remain ductile, and must possess strong-column/weak-beam properties. Under reverse cyclic loading, beams must dissipate energy through plastic beam rotation without failure of either: (a) the connection to the columns, or (b) the columns to which they frame. Forcing plastic hinges into the beams, rather than into the columns, allows structures to remain stable after experiencing severe damage. Collapse prevention in the event of structural failure is a life-saving measure.

1.2.1 Connections in Steel Reinforced Concrete (SRC) Systems

Steel Reinforced Concrete (SRC) systems utilize concrete embedded wide flange steel columns. Figure 1.2 shows an example of a rigid frame composite section. Wide flange beams are attached to the bare steel column during erection. The column is then surrounded by reinforcing bars, stirrups and formwork. After concrete is placed, forms are stripped and moved to the next story. As with the IDS Center example, steel can be erected stories ahead of the concrete crew. The encased steel section confines the concrete within its flanges, and concrete provides added stability to the steel column.

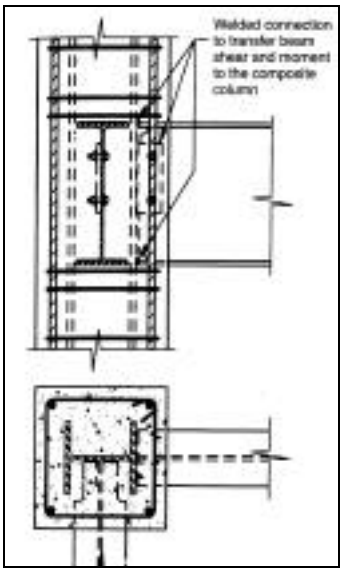

Figure 1.2 - Encased Composite Column in Rigid Frames (Viest, 1997)

SRC construction is widely used in Japanese construction. Figure 1.3 shows some details utilizing a variety of combinations of: vertical joint continuity reinforcement, steel shear panels, stirrup reinforcement, continuous beams, and

assorted stiffeners. These systems are widely used in Japan, but are not cost effective in the US due to labor costs. Most of the connections shown in Figure 1.3 are shop fabricated, and then assembled at the job site.

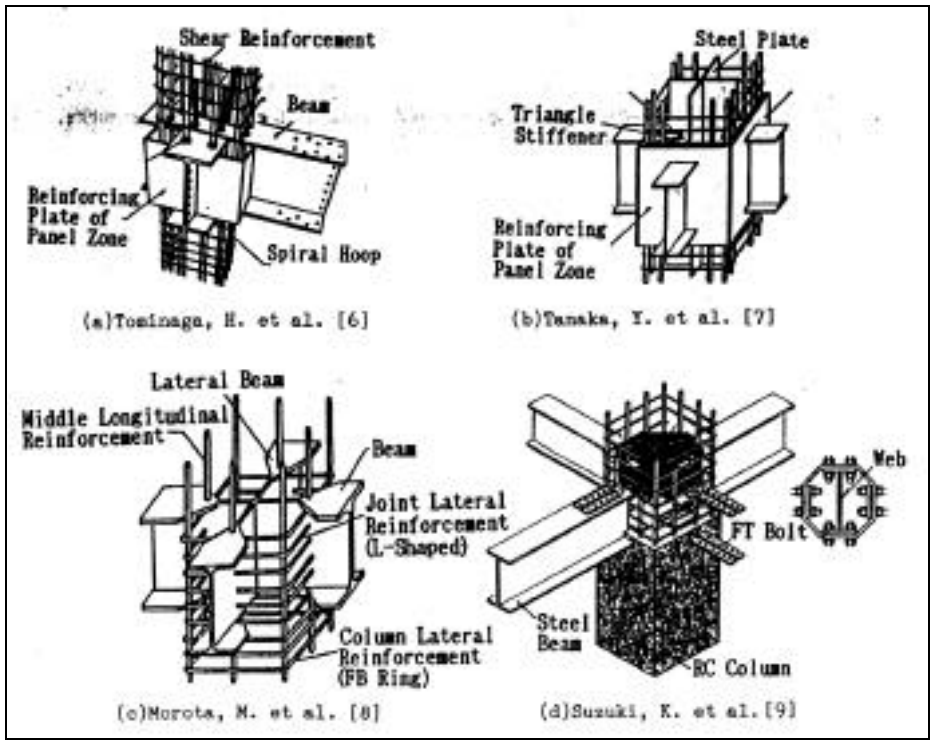

Figure 1.3 - Examples of Japanese SRC Construction (Ogura et al, 1990)

Research by Sheikh (1987) and Deierlein (1988) on SRC joints contributed to the development of "Guidelines for Design of Joints between Steel Beams and Reinforced Concrete Columns" (ASCE Task Committee on Design Criteria for Composite Structures in Steel and Concrete, 1994). Connections utilizing face bearing plates (FBP), web stiffener plates (WSP), embedded steel columns, welded shear studs, steel doubler plates, and vertical joint reinforcement were tested. Joint shear strength was shown to be the sum of the shear capacities of

the individual connection elements: steel webs, concrete compression struts, and compression fields. The concrete contribution was enhanced in some cases by confinement. Joint behavior was characterized by reasonable stiffness at service loads, and adequate ductility at failure loads. An example SRC composite joint is shown in Figure 1.4.

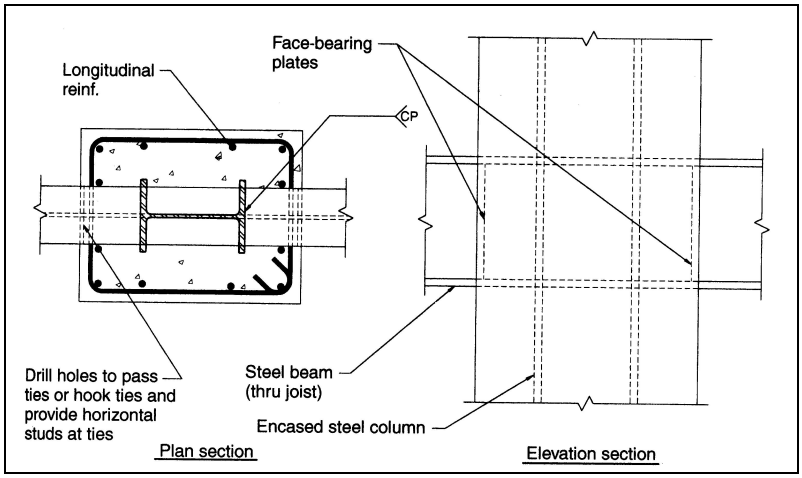

Figure 1.4 - Steel Beam to Encased Column Connection (Viest, 1997)

Prior to the development of the ASCE Task Group composite recommendations, ACI/ASCE Committee 352 had developed recommendations for the design of beam-column joints in monolithic reinforced concrete structures. In the recommendations, moment connections are classified as Type 1 or Type 2. Type 1 joints are those designed according to the ACI 318 Building Code provisions for joints subject to typical loading conditions. Type 2 joints are expected to undergo inelastic deformations, such as those produced by seismic forces. In addition to Type 1 and Type 2 classifications, joints are classified as interior, exterior, or corner type, for a total of six possible joint types (See Figure

1.5). Equation 1.1 is the recommended formula for joint shear strength of the concrete contribution. The appropriate coefficient γ from Table 1-1 is selected based on connection type. Coefficients for interior joints are higher than for exterior joints because the presence of beams on all four sides of the joint improves the confinement of the joint.

$$\varphi V_n \geq V_u$$

$$V_n = \gamma \sqrt{f_c'} b_j h \qquad (1.1)$$

where: $b_j = \dfrac{(b_b + b_c)}{2}$

f_c' is in units of psi, V_n in lbs.

Table 1-1 – Coefficient γ for R/C Joints (from ACI-ASCE Committee 352)

Joint Type	Joint Classification		
	(a) Interior	(b) Exterior	(c) Corner
1	24	20	15
2	20	15	12

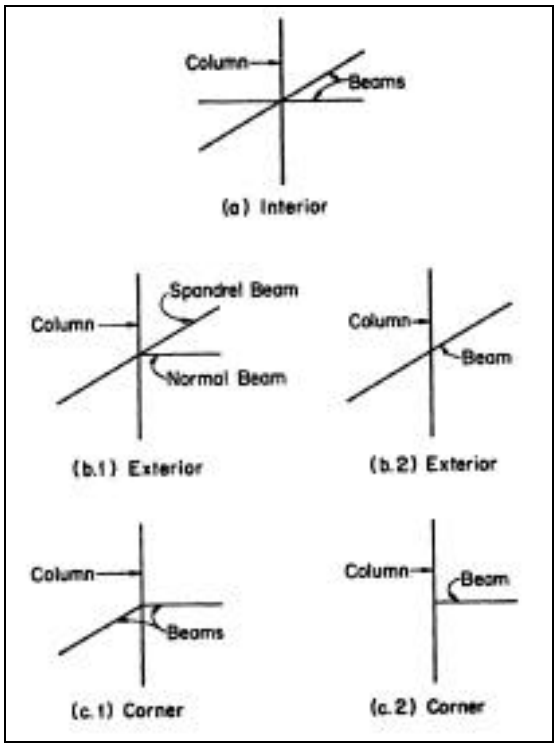

Figure 1.5 - Classification of Joint Types

In Equation 1.1, the term $b_j h$ refers to the shear area of the concrete inside the joint. The term b_j is defined as the effective width of the joint, as shown in Figure 1.6, and represents the average of dimensions b_c and b_b. In the development of recommendations for composite joints (ASCE, 1994), Equation 1.1 for reinforced concrete joints was also shown to be appropriate for the concrete contribution in composite connections when a coefficient of γ=20 is applied. The definition of effective width for two types of face bearing plate (FBP) connections is shown in Figure 1.7. The terms b_j and b in Figure 1.7 correspond to the terms b_c and b_b, respectively.

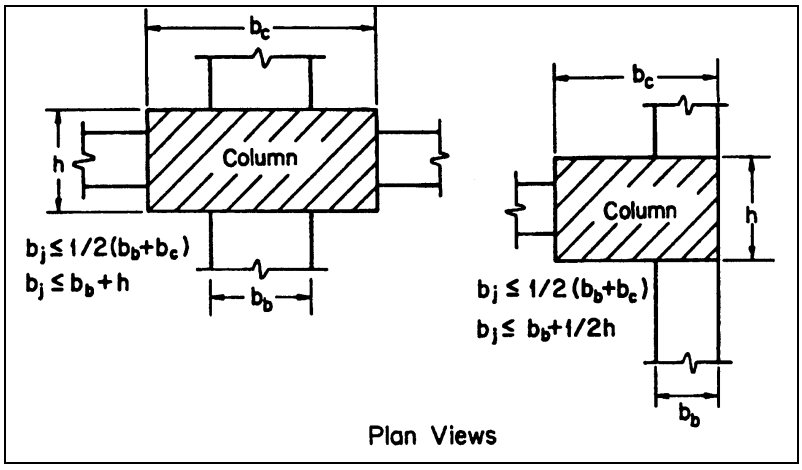

Figure 1.6 - Definition of Effective Width for Reinforced Concrete Joint

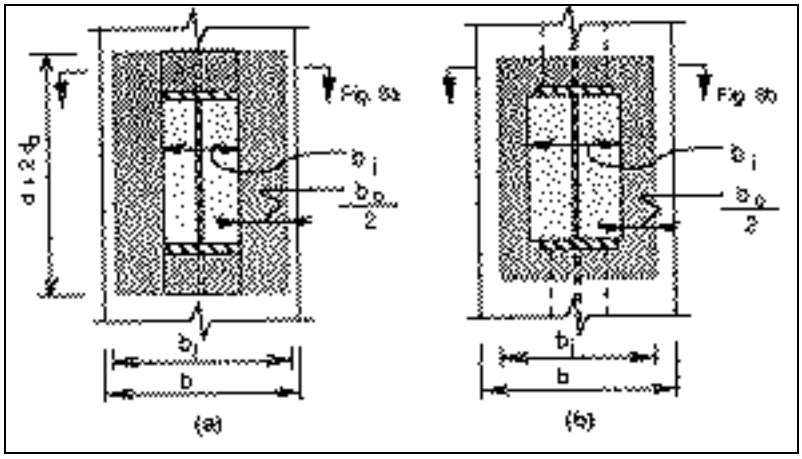

Figure 1.7 - Effective Width for Two Types of Composite Joints Utilizing Steel Encased in Concrete (a) Extended FBP, and (b) Wide FBP

Guidelines for the design of composite SRC joints, based on the ASCE Task Committee recommendations are available (ASCE 1994), but most recently with in-depth discussion in text book form (Viest, 1997). Background of the development of the recommendations and several design examples are presented in Viest.

1.2.2 Connections to Concrete-Filled Tube (CFT) Systems

Composite columns have direct cost advantages over conventional reinforced concrete and structural steel, but economy can be further realized by reducing the need for column formwork. If steel tubes are used for columns rather than W-shapes, then formwork is no longer needed, so the direct benefit includes formwork cost savings. Concrete cover is no longer present, so spalling of the concrete is not a possible failure mechanism. When hollow steel tubes are used in place of wide flange column sections, and act to contain the concrete, additional benefits result. The side shear panels of a steel tube can be analogous to the web of a wide flange column section. Because steel confines the concrete, internal reinforcement may not be necessary. Concrete also acts to prevent buckling of the steel shape.

The need to develop reasonable and cost-effective means of connecting the steel beams to the concrete-filled tubes presents another challenge. In Japan, CFT systems are used with complex connection details involving extensive welding and cutting procedures to produce strong ductile connections. Figure 1.8 shows a few examples of tubular connections with intricate welded stiffener details. In the Japanese AIJ code for CFTs, the concrete strength is not allowed to be included in joint shear calculations, but is allowed to be included in column axial strength calculations. Such connections in the US would be impractical because of the nature of competing trades and labor costs. In addition, seismic risk affects the entire country of Japan, so considerably more resources have been

available to study and develop structures for optimum seismic performance, and the level of complexity in the construction is accepted.

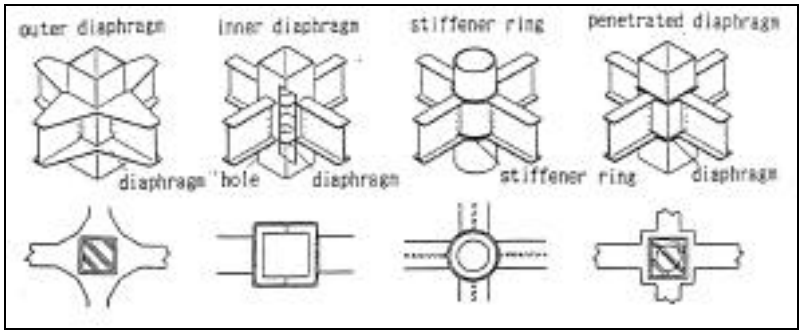

Figure 1.8 – Examples of Composite Connections Used in Japanese Construction

Design recommendations for US construction presented by Viest (1997) refer to example connections that utilize anchor bolts, embedded elements, and steel through-beam connection possibilities (Figure 1.9). The relatively thin plate of the steel tube often prohibits connecting steel beams directly to the tube. This is especially true in seismic areas. According to Viest, welding directly to the steel tube should be avoided to prevent: (a) separation of the steel tube from the concrete core due to flange tensile forces, (b) large residual stresses in the steel due to restraint of the other connecting elements, and (c) possible compromise of the confinement due to the additional stresses on the steel tube. Design examples for connections of the type shown in Figure 1.9 can be found in the text. Other types of connections, such as the through-bolted connections of Figure 1.10 and Figure 1.11 are not included, but are in need of clear design recommendations

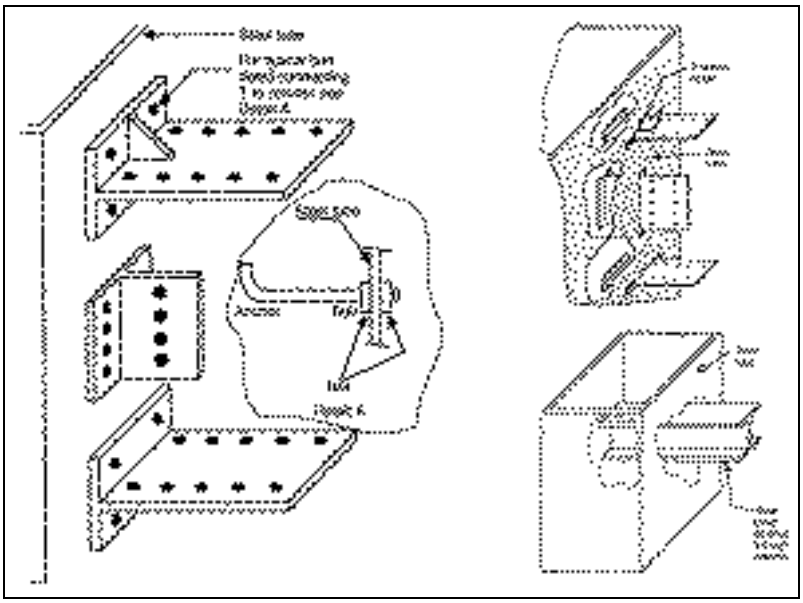

Figure 1.9 - Example CFT Connection Types (Viest 1997)

1.3 Development of Through-Bolted Moment Connections to CFTs

1.3.1 Research in Japan

Through-bolted moment connections, as shown in Figure 1.10 and Figure 1.11, were tested by Kanatani, et al (1987). Research was motivated by the need to evaluate connections that experience less local damage to the steel tube walls due to beam flange forces. In addition, connecting beams to CFTs using through-bolted connections was investigated to eliminate difficulties associated with on-site welding of beams to columns. He studied prefabricated moment connections in which wide flange steel beams were shop-welded to end plates (Figure 1.10), and then bolted to the partially filled CFT columns on-site. He also studied the split-tee through-bolted connection as shown in (Figure 1.11). Both connections were designed to transfer joint shear forces without the aid of

internal stiffeners or exterior diaphragms. Test data showed that the split-tee through-bolted connection, when compared to internally and externally stiffened welded connections with identical beam and column sizes, was able to perform as good or better than welded specimens in terms of strength. Test data from cyclic load tests showed that when the b/t of the steel tube was 42, the failure was caused by local buckling of the column flange.

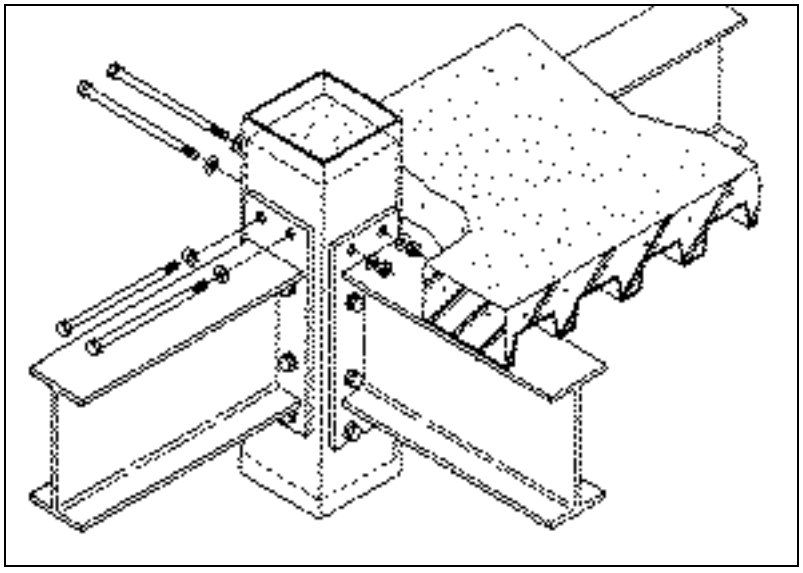

Figure 1.10 - End-Plate Through-Bolted Connection (Kanatani et al, 1985)

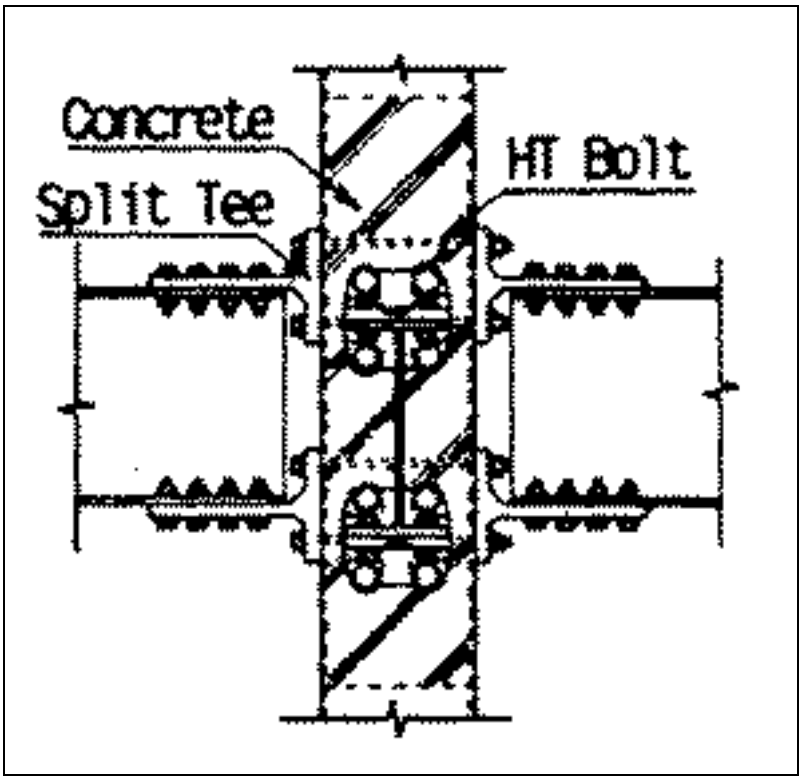

Figure 1.11 - Split-Tee Through-Bolted Connection (Kanatani, et al 1985)

1.3.2 Research in the US – Joint US/Japan Program

The work of Kanatani et al (1987) provided data to support the value of the split-tee connection, which is more constructible and feasible in the US than connections requiring difficult fabrication details, such as those in Figure 1.8. Ricles et al (1998) at Lehigh University studied various CFT moment connections as part of an independently sponsored research program. The timing of his research program was such that he was able to continue his work on CFT moment connections directly into the Joint US/Japan Cooperative Research Program on Hybrid and Composite Construction. The planned duration of the

joint program was five years; however, the US side was directly involved during the last three years of the program. Research on the US side was sponsored by the National Science Foundation, and included joint meetings between researchers in the US and Japan. The effort was aimed at increasing awareness of each others' activities, and at helping to broaden the knowledge base of the state of the art in composite construction, especially with regard to seismic performance.

Under the US/Japan Cooperative Research program on Composite and Hybrid Structures, Lehigh University and The University of Texas at Austin were charged with the task of studying moment connections utilizing rectangular concrete-filled tube columns and wide flange steel beams. The two universities submitted independent proposals, and were awarded research projects. Prior to the start of the University of Texas research program, which is the focus of this dissertation, Ricles tested connections between steel beams and CFT columns. Both schools agreed on a common connection type to study, and met to discuss division of tasks to avoid unnecessary overlap between the two programs.

The split-tee through bolted connection of Figure 1.12 is Specimen number C6 from the Lehigh testing program, and is typical of connections common to both research programs. Lehigh test results showed that the split-tee through-bolted connection was robust enough to allow full plastic hinges to develop in the beams. Connections were tested to 5% inter-story drift. For this connection, both welding and bolting were used as a means of connecting beams

to the tee stems. Welding tees to beam flanges, compared to bolting, was shown to result in more stable hysteresis because welding eliminated the potential for bolt-hole elongation in the beam flanges and pinched hysteresis as had been observed for the tees which were bolted to the beams.

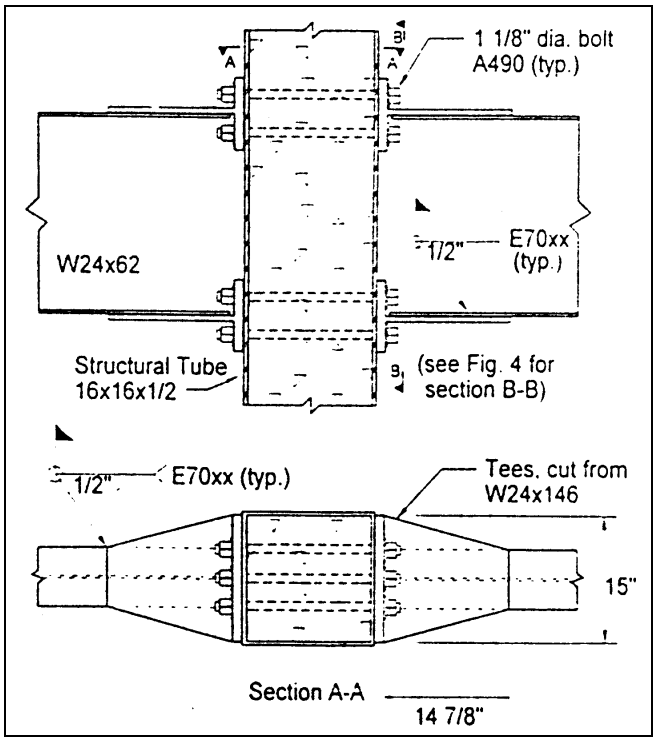

Figure 1.12 - Split-Tee Through-Bolted Connection (Ricles et al, 1997)

It was decided that the research at Lehigh University would focus on the design and development of the steel component of the connection—to be responsible for the design and testing of the tees, through bolts, and connection details in order to make a robust connection. Research at The University of Texas would be to focus on the strength of the internal concrete compression strut within the panel zone, namely the interior joint shear force transfer mechanism

through the interior of the joint, by failing the joint. It is for this reason that the focus of the Texas program was on the behavior of the encased concrete, and how the concrete contributes to the overall joint shear strength, but not on the design of bolts or the tees.

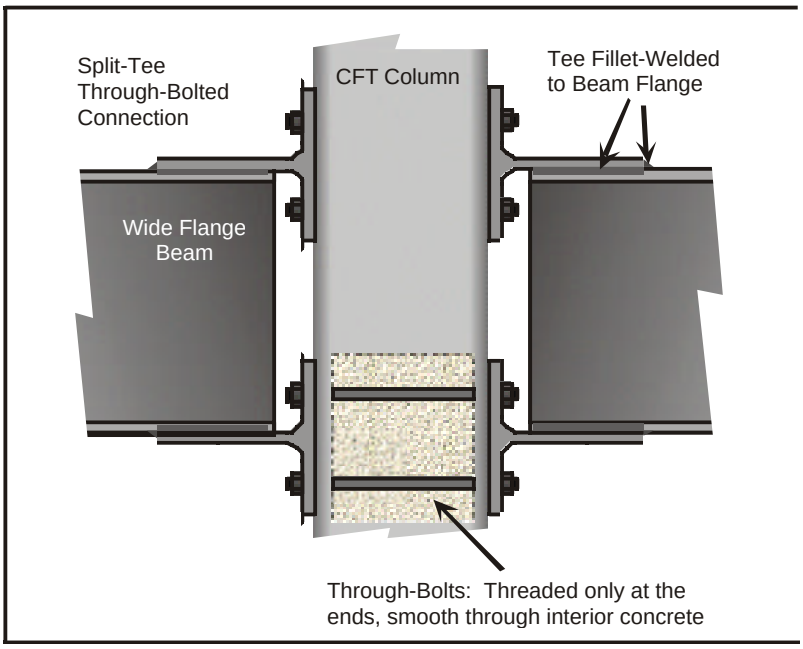

Figure 1.13 - Split-tee Through-bolted Connection

1.4 Research Program

A connection typical of the type studied in this research program is shown in (Figure 1.13). Contributions to the joint strength of the CFT system are studied by isolating variables, and results of the tests are used to develop design recommendations. Reverse cyclic loading is used in the absence of axial load. Figure 1.14 shows how the internal joint forces are assumed to transfer the beam flange forces due to reverse cyclic beam moments. The split-tee connection

applies forces to the joint only in compression. When tees are in tension, the tensile force is taken by the through-bolt to the other side, and provides an additional compressive force to the compression tee. Force transfer through the concrete is assumed to act as a compression strut.

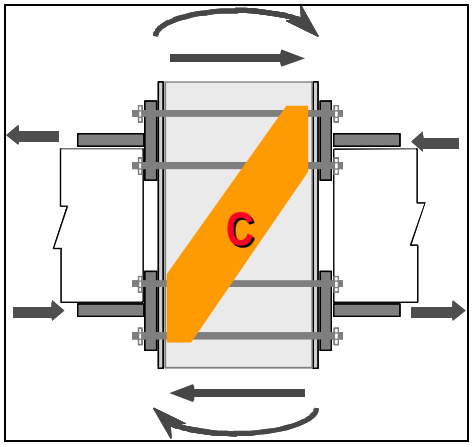

Figure 1.14 - Tension and Compression from Beam Moments Resolved by Joint Forces

1.5 Panel Zone Behavior

The Texas research program focused on the strength and behavior of the interior of the panel zone. Under reverse cyclic loading, moment connections that are idealized as fully restrained (FR), actually deform in shear in the region of the joint, namely the panel zone. Considerable research has been conducted to understand the behavior of steel panel zones of steel columns in FR moment resisting structural steel frames. By definition, only connections between beams and columns that rigidly hold the angles between the beams and columns in the connection can be considered fully restrained. Connections that were historically

thought of as fully restrained were in fact only partially restrained because of the deformation of the panel zone. The behavior of steel panel zones has been widely studied, and it was shown by Fielding (1994) that analyzing the impact of the deformation of panel zones when analyzing frame behavior is necessary, and that analytical models taking into account reduced stiffness of the panel in the post-yield range provide reasonable results. Krawinkler and Mohasseb (1987) studied the effects of panel zone deformations on the story drifts of steel framed structures. They concluded that the panel shear stiffness was a combination of both the web shear stiffness and to a lesser extent the flexural stiffness of the column flanges. Also it was shown that the shear-displacement behavior included a distinct elastic region, followed by a yield plateau with a slight stiffness, and finally strain-hardening. Using a tri-linear model to incorporate panel zone behavior into frame analysis, Schneider (1998) concluded that models that neglect the effects of panel-zone distortion can underestimate overall story drift by as much as 10%, and overestimate base shear strength by 30% for the steel frames used in that study.

In composite connections, the concrete also participates in the development of shear forces within the panel zone. It was shown by Deierlein (1988) that the concrete contribution of the shear panel strength for SRC systems could be predicted. Within the CFT split-tee through-bolted connection, the concrete contribution needs to be understood and quantified. The shear strength of the concrete core within this type of connection is the aim of this study, and three variables are chosen for study.

1.5.1 The Concrete Compressive Strength Variable: f'_c

Of interest in the study of the panel zone behavior is the influence of concrete strength. As shown earlier in the discussion of Section 1.2.1, a relationship between concrete compressive strength and the shear capacity of joints in reinforced concrete and composite joints has been used for design. Attention in this research will focus on the validity of current models when applied to the split-tee through-bolted connection.

1.5.2 The Slenderness Ratio Variable: *b/t*

Tomii (1988) showed that slenderness of the steel tube had a direct effect on the shear strength of concrete-filled tubes. Figure 1.15 shows that for lower *b/t* ratios, higher ratios of experimental maximum shear to theoretical maximum shear were obtained. The results were more significant for monotonically loaded specimens (white markers) with high axial load, and less for the cyclically loaded specimens (solid markers). Data presented in Figure 1.15 for cyclic loading at no axial load, which is similar to the conditions of the research program of this dissertation, is not as compelling. An examination of the b / t variable is included in this test program.

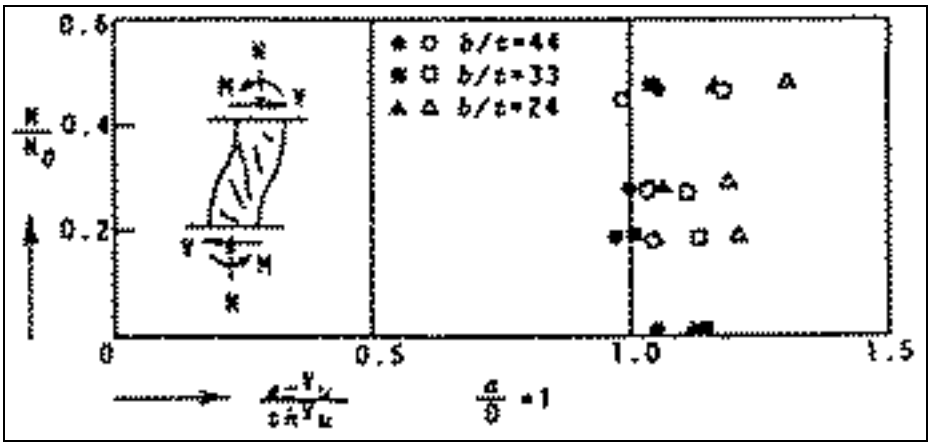

Figure 1.15 - Vexp/Vtheory Related to b/t (Tomii 1988) – Solid: Cyclic, White: Monotonic

There is consensus among the ACI 318 Building Code, the AIJ Code in Japan, and the AISC LRFD Specification with regard to slenderness limits on the steel used in rectangular concrete-filled tubes. Although the equations are written somewhat different between the codes, the end result is the following limit:

$$\frac{b}{t} \le \sqrt{\frac{3E_s}{f_y}} \quad \text{for each face of width } b \qquad (1.2)$$

The AISC LRFD also requires that the steel area must be at least 4% of the total cross sectional area of the section in order to be designed in accordance with the AISC specification. Slenderness limits were imposed to: (a) ensure sufficient longitudinal yield stress develops in the steel tube prior to buckling, (b) ensure rotational capacity is large enough to form plastic hinges in the columns, and (c)

ensure that energy dissipation is sufficient to allow a badly damaged structure to survive strong earthquakes.

1.5.3 The Tee-Width Parameter: *%b*

Also in the study will be an examination of the effect of the tee-width parameter, which refers to the width of the split-tee connection flange relative to the width of the CFT column. This variable is studied to determine if the concrete core varies its contribution to the overall joint strength if the connection does not cover the entire width of the section. Tee width would likely have a serious effect on the joint shear transfer mechanism of bare un-filled tubes due to buckling, so it is desired to relate the effects of tee-width, if any, to the concrete-filled case.

1.6 Outline of Research Program

The following is a general outline of the research program presented:

1. The design and testing of fifteen 1/2 scale CFT specimens idealizing the panel zone of the split-tee through-bolted connection by simulating tee forces against the joint.
2. Analysis of collected data to isolate various contributions to joint shear strength.
3. Comparison of findings to existing models for composite joints, and development of new equations, or coefficients.
4. Application and comparison of proposed model to the test results of four full-scale moment connection specimens designed to fail in the panel zone.
5. Refinement of model based on results.

6. Examination of two full-scale moment connections not designed for panel zone failure to evaluate the force transfer mechanism through the joint.
7. Recommendations, Conclusions and Suggestions for Future Research

2. Half-Scale Panel-Zone Tests

2.1 Description of Tests

The behavior of the split-tee through-bolted connection was studied initially by testing specimens idealizing the connection zone. The concrete compression strut within the split-tee through-bolted connection was assumed to act as a significant load path for shear force transfer through the joint. Because the split-tee connection has no internal or external diaphragms to aid in the force transfer, the concrete was expected to be the primary means for transferring large beam flange forces through the joint.

Variables studied in this research included: variation in the contact width of the tee against the tube, change in concrete strength, and slenderness of the steel tube wall (b/t ratio). The objective of the tests was to determine quantitatively the contribution of the confined concrete core to the force transfer through the joint. The panel-zone was instrumented and monitored to assess the distribution of forces in the joint.

By conducting specialized panel-zone tests, the behavior of concrete-filled steel tubes subjected to stress conditions similar to that of actual CFT through-bolted connections was examined in a way that did not require the fabrication of the entire beam-column assembly as was done later in the research program. As a result, a greater range of variables could be studied. The results of the panel-zone tests would be used to choose a reasonable set of variables and parameters for the full-scale connection specimens.

2.2 Test Setup

The test setup was designed to simulate forces imposed on the panel-zone region of a CFT-to-wide-flange-beam moment connection subject to cyclic loading. The test set-up is shown in Figure 2.1. Hydraulic rams applied reverse cyclic loads to the ends of the specimen. Reaction blocks simulated compressive tee forces to the joint region.

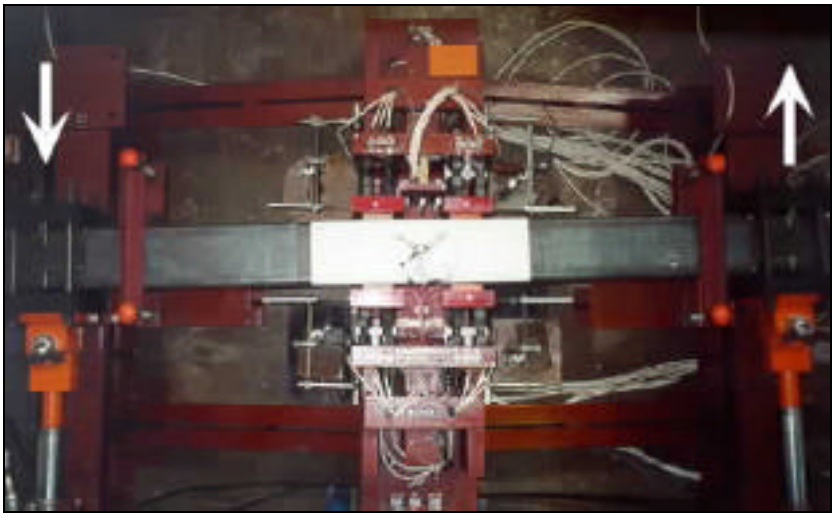

Figure 2.1 - Panel Zone Test Setup – Plan View

The schematic of the setup is shown in Figure 2.2. For each direction of loading, only two of the four reaction blocks were in contact with the tube. Because of symmetry in the idealization, the panel zone shear is theoretically 8P – P = 7P.

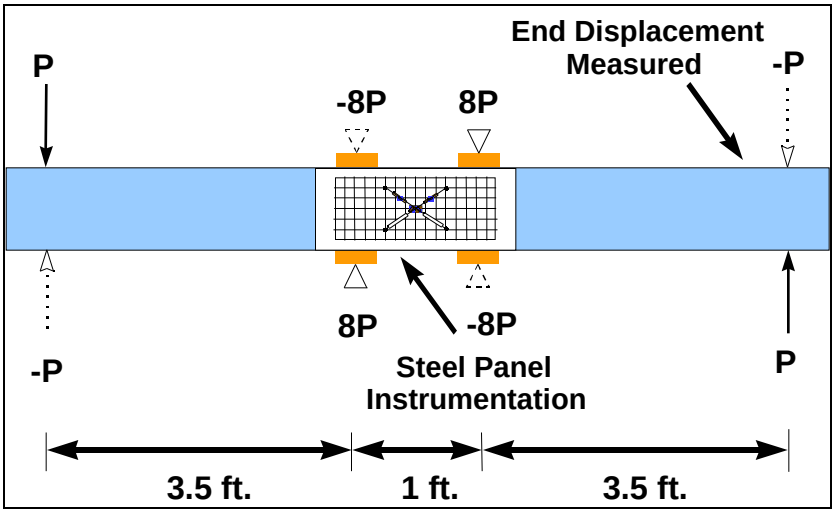

Figure 2.2 - Schematic of Test Setup, Cyclic Load P Applied at Ends

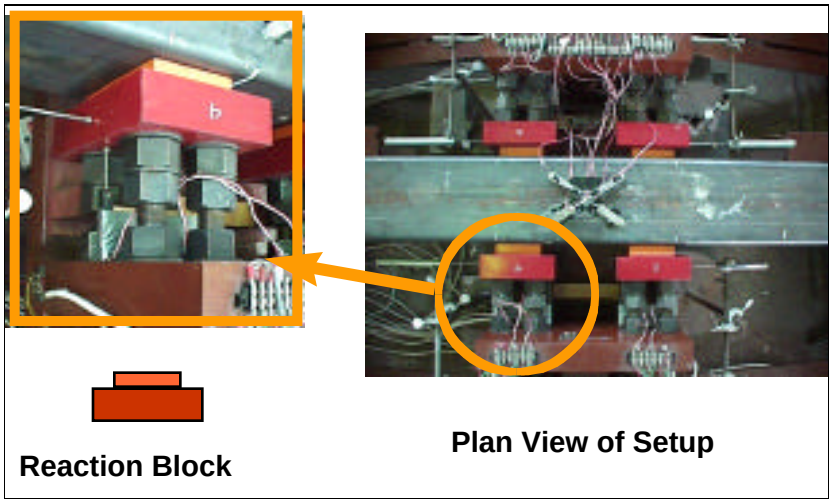

Figure 2.3 – Reaction Blocks Simulate Tee Forces

A close-up of the reaction blocks is shown in Figure 2.3. Each reaction block was fastened to the test setup using four high strength bolts. The bolts were adjusted to provide a tight fit against the specimen prior to testing.

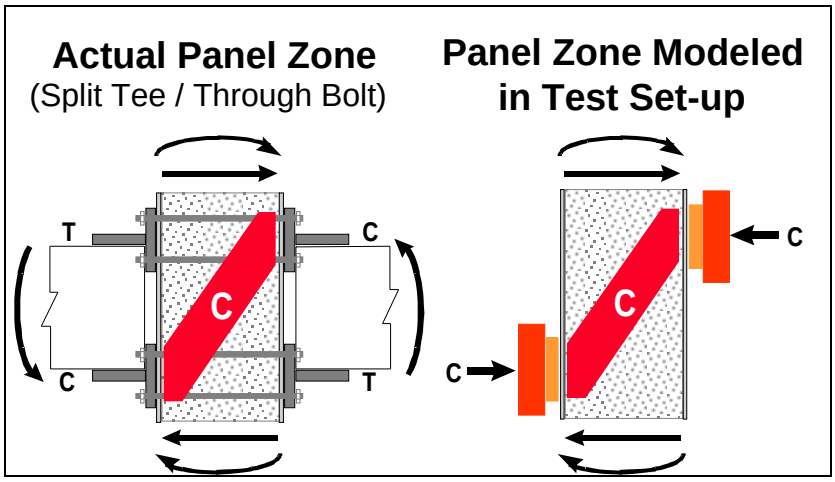

Figure 2.4 - Test Setup Idealization

Figure 2.4 shows an idealization of the connection zone. The panel-zone of the CFT specimen was subjected to concentrated loads acting on rectangular areas representative of the contact area between the CFT and the split-tee. The interesting feature of the split-tee/through-bolted moment connection is that only compressive forces are transmitted to the CFT panel zone from the beams through split tees. When beam flanges are in tension, forces are transmitted via through-bolts to the other side of the column, and act as an additional compressive force to that face of the column. The four reaction blocks of the test setup were designed accordingly. Only two of the four reaction blocks applied forces to the CFT at any one time.

To simulate varying tee widths, bearing surfaces were attached to the reacting blocks as shown in Figure 2.5. Bearing surfaces were adhered to the reaction blocks using epoxy and cap screws. The percentages of tube width that were loaded were 50, 75 and 100%.

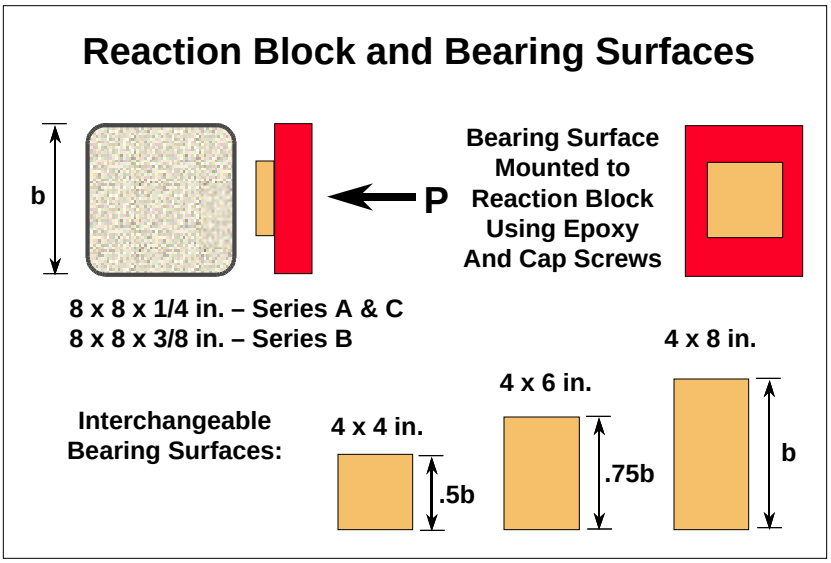

Figure 2.5 - Variation of Bearing Surfaces to Simulate Tee Width

2.2.1 Measurements and Data Acquisition

Because the aim of the panel zone study was to gain an understanding of the behavior of the connection region, measurements in and near the panel zone were of primary interest. Panel zone distortion at the steel surface was measured. Visual inspection was aided by mapping the surface with grid lines scribed through white surface paint. The square grid line spacing on the surface of the specimens was 1 inch. Figure 2.6 shows the location of the panel-zone instruments. Strain gauges, displacement transducers, and strain rosettes were used to measure shear distortions in the steel panel zone. Redundant measurements were taken to: (a) validate the test results, (b) compare the effectiveness of the measurements, and (c) gain insight for future test

instrumentation. Figure 2.7 shows an actual panel zone specimen with instruments in place during testing.

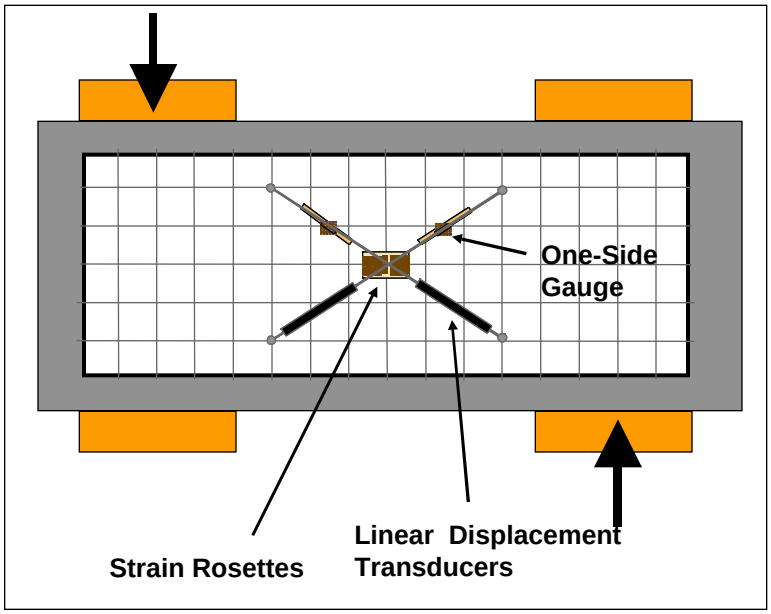

Figure 2.6 - Panel Zone Instrumentation

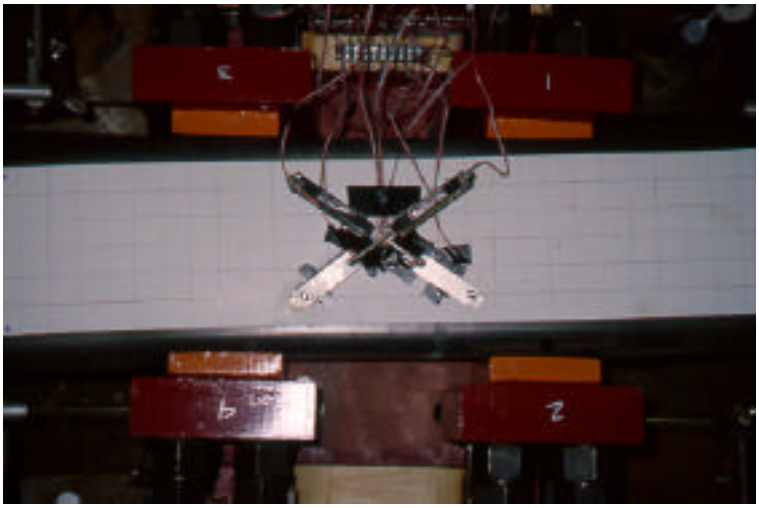

Figure 2.7 - Panel Zone Instrumentation (During Test)

The panel-zone test setup was designed for horizontal testing, such that the panel zone surfaces were oriented parallel to the floor. This allowed the panel zone to be observed by looking down while standing above the specimen. The underside of the panel zone was also visible, but to a limited extent. Both sides of the panel zone had identical instrumentation. Data collected from both sides of the panel zone were averaged.

2.2.1.1 Strain Rosettes

Single strain rosettes were placed on the surface of the steel tube directly at the center of the panel zone where the diagonal lines between the load points crossed. Rosettes were used to determine the state of stress at the center of the steel panel.

2.2.1.2 Diagonal Displacement Transducers

Diagonal displacement transducers were aligned cross-wise near the surface of the steel tube as shown in Figure 2.6. To lessen the effect of bending of the tube near the edges of the diagonal displacements, the effective rectangle used for the diagonal measurements was 4 x 6 inches. The 4 inch dimension corresponded to half of the 8 inch tube width, and allowed the instruments to be located sufficiently away from the edge of the tube. The 6 inch dimension corresponded to half the height of the panel zone (the distance between the compression and tension beam flanges, and the distance between the centers of the reaction blocks). The resulting rectangle had the same aspect ratio as the complete 8 x 12 inch panel zone.

2.2.1.3 Single-Sided Strain Gauges

Diagonal strain measurements were taken on the surface of the steel through the use of single-sided strain gauges. The gauges allow measurements in which the effects of out-of-plane bending of the steel can be removed. Single-sided gauges contain a pair of parallel strain gauges, separated by a fixed distance (3 mm, for example), and molded into a single piece of plastic that is adhered to the surface of the steel. The strain in the center of the steel tube wall can be calculated by extrapolating linearly the strain profile through the thickness of the gauge to the center of the steel to which the gauge is bonded.

2.2.1.4 Load Cells and Pressure Transducers

Load was monitored both through the use of pin-type load cells on the ends of both rams, as well as through pressure transducers connected to the pressure lines to those rams. Because the pressure lines were cross-linked to the double-rodded rams so that equal pressures would exist in opposite directions of the rams, only one pressure transducer was used, and was switched back and forth such that it only monitored the line carrying the acting pressure.

2.2.1.5 Thin Wire Linear Motion Transducers (String Pots)

Thin wire (string) pots were used to monitor displacements of the ends of the specimen. The end displacement was used for plotting load-displacement relationships.

2.3 Specimen Descriptions and Details

Cross section dimensions for the panel zone specimens were scaled from earlier Lehigh tests on full-scale connections (Ricles *et al* (1997)). The list of specimens is shown in Table 2-1. The steel tube outer dimensions were held constant at 8 x 8 inches, which represented cross sectional outer dimensions that were half-scale. Two tube wall thicknesses were used: 0.25 inch in Series A and C, and 0.375 inch in Series B to compare the effects of *b/t*. The specimens were grouped into series A, B and C according to steel used. Material properties for the steel tubes are shown in Table 2-2. Two nominal concrete strengths, 6 ksi and 4 ksi, were used.

Table 2-1 - Panel-Zone Specimens

All Tubes: 8 x 8 in. ASTM A-500 Cold Formed Welded HSS				
Specimen	***t* (in.)**	***%b***	***f'c* (ksi)**	
Pilot	0.25	50	5.5	
8.4A	0.25	50	6.2	
8.6A	0.25	75	6.2	
8.8A	0.25	100	6.2	
8.4B	0.50	50	6	
8.6B	0.50	75	6.1	
8.8B	0.50	100	5.9	
8.MB	0.50	n/a	6.5	
8.PC	0.25	75	3.9	Reference #1
8.RC	0.25	75	3.9	Rectangle Cut-Out
8.SC	0.25	75	4	Slot Removed
8.DC	0.25	75	4	Diagonal Strap
8.BC	0.25	75	5.9	Rebar Enhanced
8.P2C	0.25	75	4.2	Reference #2
8.SAC	0.25	75	n/a	Sand in Panel Zone

Table 2-2 - Steel Properties of Square HSS Sections

Series	Thickness (inches)	Static σ_y (ksi)	Static σ_u (ksi)	Dynamic σ_y (ksi)	Dynamic σ_u (ksi)	% Elongation
A	0.25	54.1	60.0	55.2	61.9	19.0
B	0.375	52.6	54.2	54.9	57.5	26.6
C	0.25	61.5	66.0	63.5	69.0	17.2

2.3.1 Series A Specimens

The specimens of Series A used tubes that were 0.25 inches in thickness, which corresponds to a b/t ratio of 32. In Series A the steel tube properties and dimensions, and concrete strength were constant. The variable in Series A was the size of the bearing area, or the width of the reaction block simulating the applied beam flange forces. This variable will be referred to as the *"tee width"* (or *%b*). As the tee width is reduced the flange force bears on the tube face further away from the steel side panel of the tube. With a smaller tee width, more of the applied force is expected to transfer through the connection by the internal concrete compression strut. Nominal concrete strength was held constant at 6.2 ksi for the three specimens of Series A (see Table 2-1) with varying tee widths. The first specimen of Series A was a pilot specimen used to troubleshoot the setup and instrumentation.

2.3.2 Series B Specimens

Within Series B, all steel dimensions, steel properties, and concrete strengths were held constant as well. The variable used was the same as in Series A, namely the variation of the tee width dimension from 50% to 100% of the tube depth, *b*. The only change between Series A and Series B was the tube thickness, which was 3/8 inch for Series B, and corresponds to a b/t ratio of 21.3.

It was anticipated that changing the tee width would have less effect on force transfer with a smaller b/t ratio. The first three specimens of Series B were used to test this hypothesis. Specimen 8.M-B, the only specimen not tested under panel-zone shear with the test setup, was used only to test the moment capacity of the typical Series B CFT section, and was tested under center-point loading using a 600 kip universal testing machine as shown in Figure 2.8.

Figure 2.8 - Specimen 8.M-B Tested Under Flexure

2.3.3 Series C Specimens

In Series C, the bearing area was held constant at 0.75b (6 in.), but other variables were considered as follows: (1) Variation in concrete strength, 4 ksi for

specimen 8.PC and 6 ksi for 8.P2C; (2) Increase in the moment capacity of the section without enhancing the shear capacity (8.BC and 8.PC); and (3) modifications to isolate various shear strength mechanisms (8.RC, 8.DC, and 8.SC).

2.3.3.1 Specimen 8.BC

The purpose of specimen 8.BC was to increase the flexural capacity without increasing the shear capacity. Comparing the results of 8.BC with reference specimen 8.PC would show whether or not the moment capacity of the CFT section governs the failure load. Flexural enhancement of specimen 8.B-C was accomplished through the installation of 12 - #4 reinforcing bars (Figure 2.9). To eliminate congestion of steel hooks at the ends of the specimen, and to allow concrete access, four of the twelve bars were terminated 2 feet from the end of the specimen. Placement of the reinforcing bar cage is shown in Figure 2.10 and Figure 2.11. No stirrups were located through or near the panel zone, and were included only to hold the longitudinal bars in place.

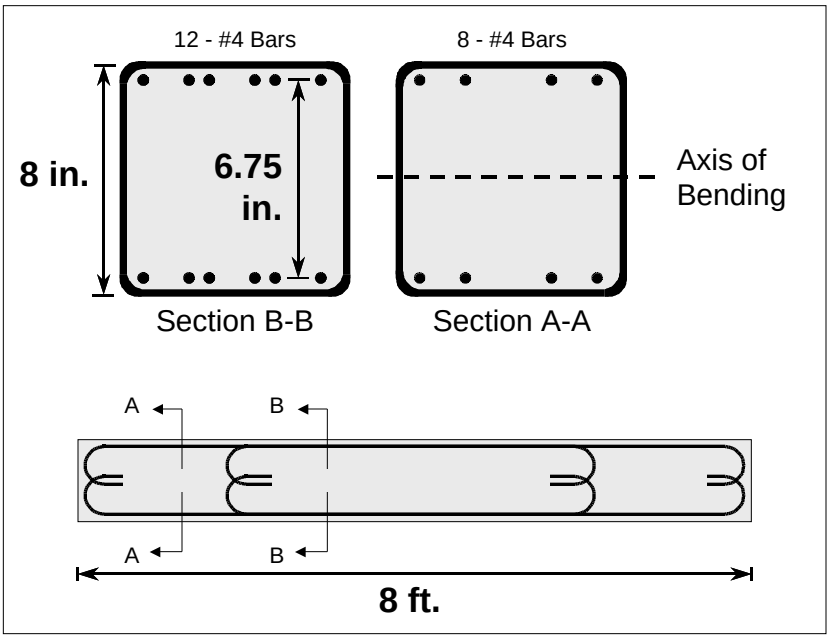

Figure 2.9 - Specimen 8.BC Details

Figure 2.10 - Reinforcement for 8.B-C

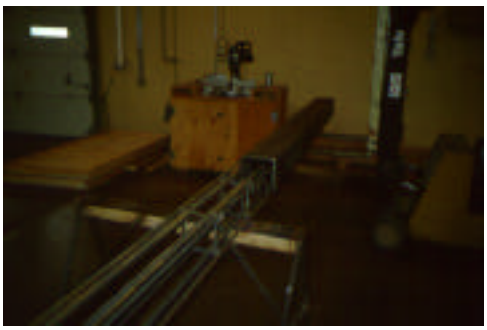

Figure 2.11 - Inserting Cage into 8.B-C

2.3.3.2 Specimen 8.RC – Rectangular Panel Removed

To eliminate the contribution of the steel side panel to the shear strength of the joint, a 12 x 5.5 inch steel panel was removed from the steel tube (See Figure 2.12 and Figure 2.13). The panel was removed from both sides of the steel tube. The missing steel was then replaced with like-thickness foam-core board

inserts prior to concrete placement. The boards were removed to expose the concrete prior to testing.

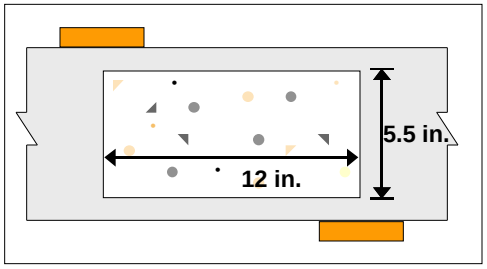

Figure 2.12 - Specimen 8.RC, Rectangle of Steel Removed

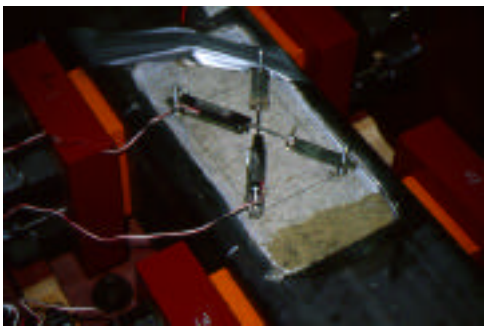

Figure 2.13 - Rectangular Cutout

2.3.3.3 Specimen 8.SC – Slot Removed

In Specimen 8.S-C, a 1.25 x 12 inch slot was cut along the longitudinal axis of the tube (See Figure 2.14 and Figure 2.15). This was done to interrupt the steel panel shear diagonal, but to preserve some concrete confinement.

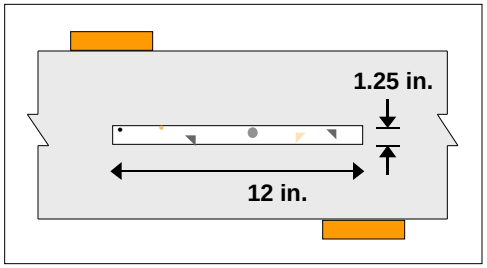

Figure 2.14 - Specimen 8.SC, Slot Removed

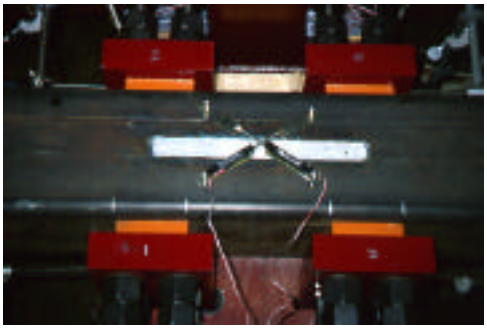

Figure 2.15 - Narrow Slot Cutout

2.3.3.4 Specimen 8.DC – Diagonal Strap Left in Place

In Specimen 8.D-C, a 2 inch diagonal strap of steel was left in the panel zone (See Figure 2.16 and Figure 2.17) after two triangular regions of steel were removed. The diagonal strap provided a well-defined force transfer path for the steel (as a tension brace), but the panel zone steel shear strength and concrete confinement were reduced.

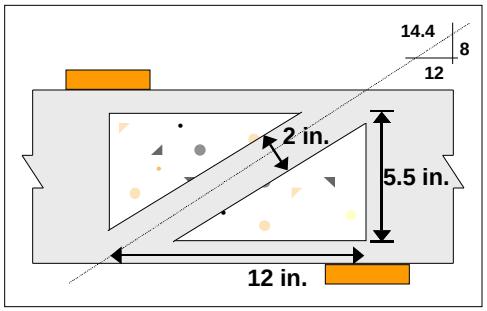

Figure 2.16 - Specimen 8.DC, Steel Tension Tie

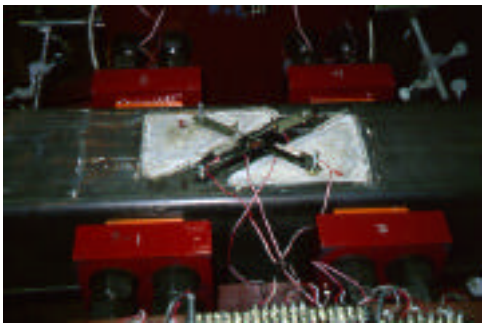

Figure 2.17 - Diagonal Strap Left in Place

2.3.3.5 Specimen 8.SAC – Sand in the Panel

Specimen 8.SAC was used to test a limiting case of a joint that could not mobilize a compression strut. The center 1/3 of the specimen was filled with moist sand. The remainder of the specimen was capped at both ends with concrete. One end of the tube was filled on one end with concrete. After several days of curing, moist sand was added to the tube. A concrete cap was placed immediately afterward. Sand was added in a moist condition to prevent concrete bleed water from bleeding excessively into the sand through capillary action.

2.4 Testing Procedure

Cyclic loads were applied to all specimens except 8.D-C, 8.S-C, and 8.R-C. The test was displacement-controlled in the sense that the displacements at the ends of the specimen (including the effects of test setup flexibility) were monitored and controlled during loading. One end of the specimen was arbitrarily chosen as the control for the displacement history. Ideally, symmetry should result in equal and opposite end displacements during testing; however, this did not always occur because of the statically indeterminate nature of the test specimen and setup, and because of the effects of inelastic behavior at advanced stages of the test.

Hydraulic rams were configured to apply equal and opposite pressures to the two rams. Displacements were not chosen based on "story-drifts" as is usually done in test on composite beam-column assemblies. The absence of beams and the flexibility of the test apparatus created a situation in which story-drifts were difficult to define. Instead, a displacement history selected using data from the pilot specimen was used in subsequent tests so that data could be compared.

3. Experimental Results from Panel-Zone Tests

3.1 Panel Zone Tests

Tests were conducted on fifteen half-scale concrete-filled tube (CFT) specimens to determine how forces were transferred through the panel zone of a split-tee though-bolted moment connection. As discussed in Chapter 2, idealized panel zone tests were divided into three tests series: Series A, B, and C. The prime variable for Series A and B was the size of the area of load application against the tube. The specimens of Series C were designed to look at special modes of behavior by cutting sections of steel from the side panels prior to testing. Other variables across series of specimens were: concrete compressive strength and b/t ratio of the steel tube. Test results are reported in this chapter. Analysis and application of the results to the development of a model are included in the following chapter.

3.2 Series A: Specimen 8.4A, 8.6A and 8.8A

Series A specimens consisted of three specimens in which the main variable was the width of load application. Material properties and specimen dimensions were held constant. Specimens 8.4A, 8.6A and 8.8A had loaded widths of 0.5b, 0.75b and b, respectively. The peak deflection was limited by the stroke of the testing equipment; however, peak loads were generally reached before the limiting stroke was reached.

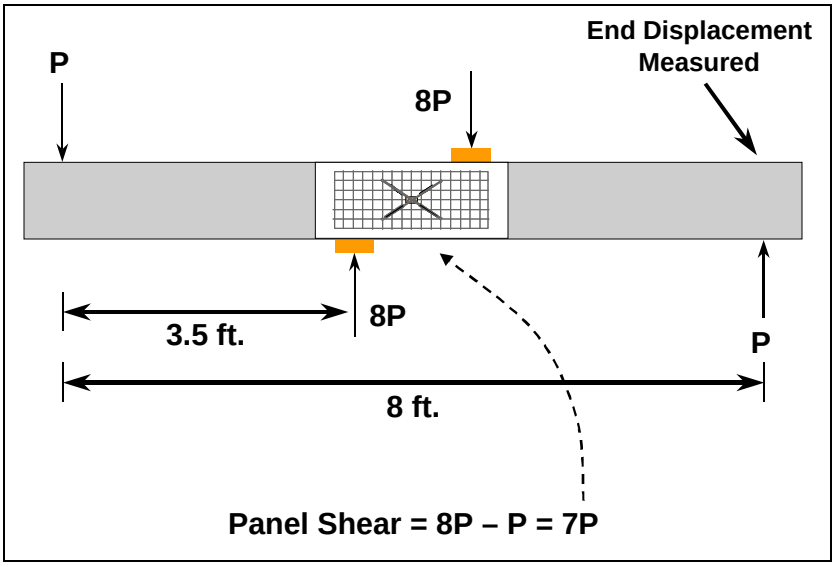

Figure 3.1 - Definition of End Displacement and Panel Shear

Values of displacement are reported as inches corresponding to the actual displacement at one end of the specimen as illustrated in Figure 3.1. Displacement was chosen over story drift ratios because the test setup did not permit conversion of displacements to realistic story drifts. Flexibility in the bolts holding the loading blocks introduced a source of deformation that would not be representative of connections with beams transferring compression to the connection. For comparisons between specimens, specimen end displacements were more appropriate. In Figure 3.2 through Figure 3.4 stable hysteresis is observed in plots of Panel Shear vs. End Displacement. When Figure 3.2 through Figure 3.4 are compared, results are nearly identical.

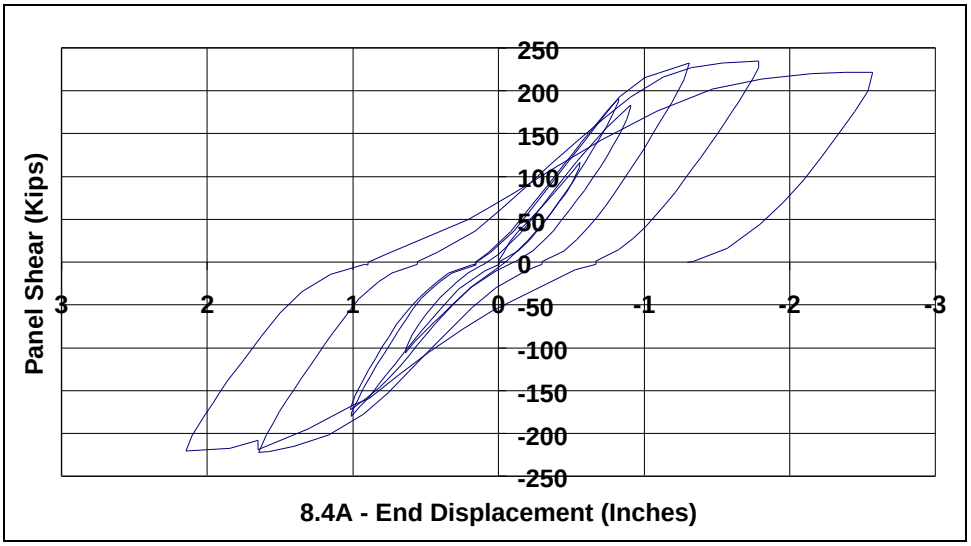

Figure 3.2 – 8.4A Load/Displacement Curve

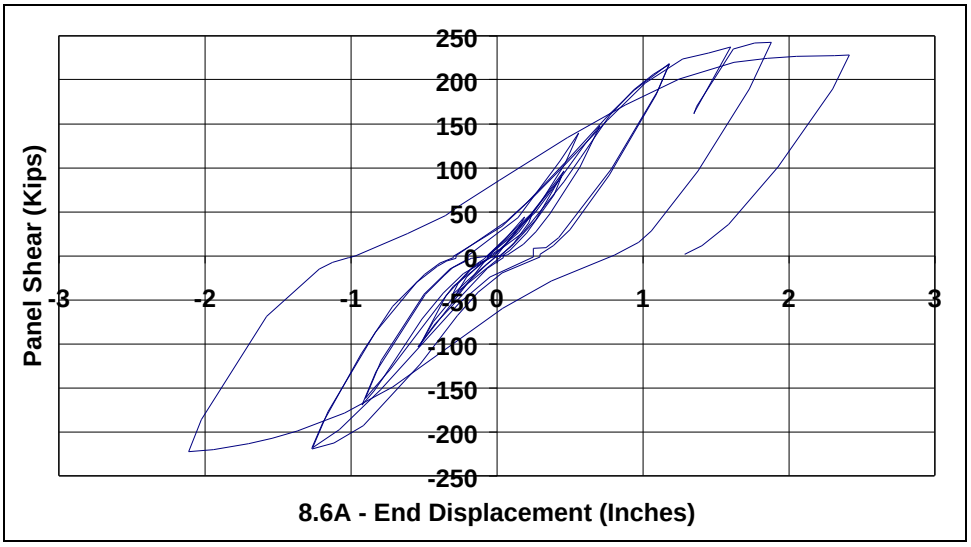

Figure 3.3 - 8.6A Load/Displacement Curve

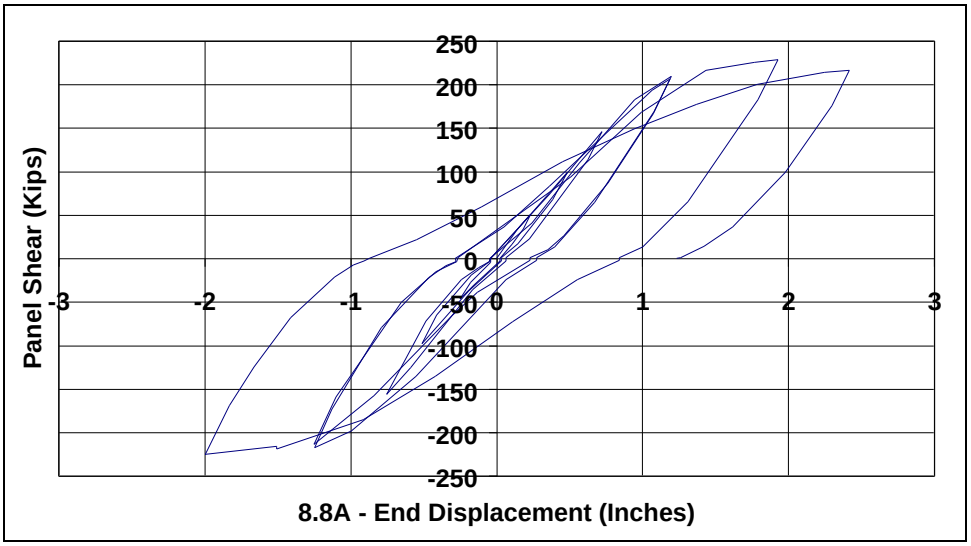

Figure 3.4 - 8.8A Load/Displacement Curve

Results for maximum panel shear and moment for Series A are tabulated and presented in Table 3-1. As seen in the table, there is only a range of about 3% between all three specimens for maximum shear.

Table 3-1 - Series A Results

Specimen	V_{Max} Kips	M_{Max} k-ft
8.4A	233	117
8.6A	241	121
8.8A	237	119

When panel-zone distortions are compared (Figure 3.6 through Figure 3.8), there is little difference between specimen 8.4A, 8.6A and 8.8A; however, specimen 8.8A experienced greater panel zone distortion than 8.4A and 8.6A during the first half of the last cycle, corresponding to an end displacement of 2 inches. Panel zone distortion was determined using crossed linear transducers across the panel-zone region, as illustrated in Figure 3.5. Averaged values of data taken from both sides of the tube specimen were plotted.

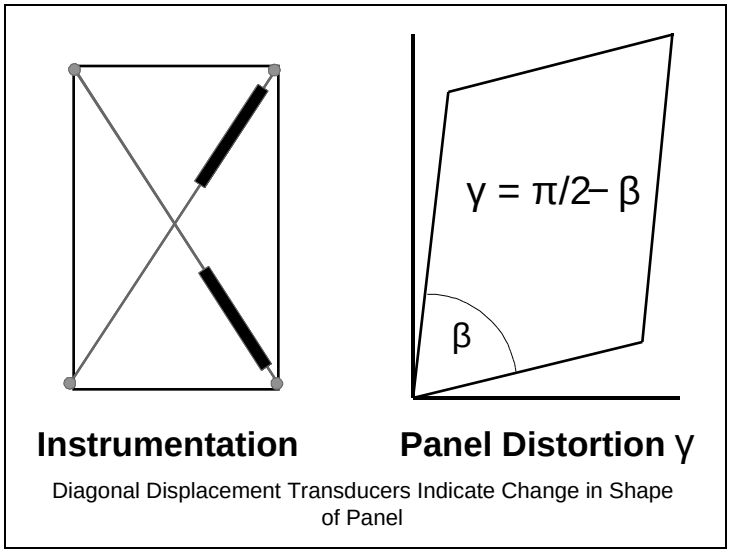

Figure 3.5 - Panel Zone Distortion

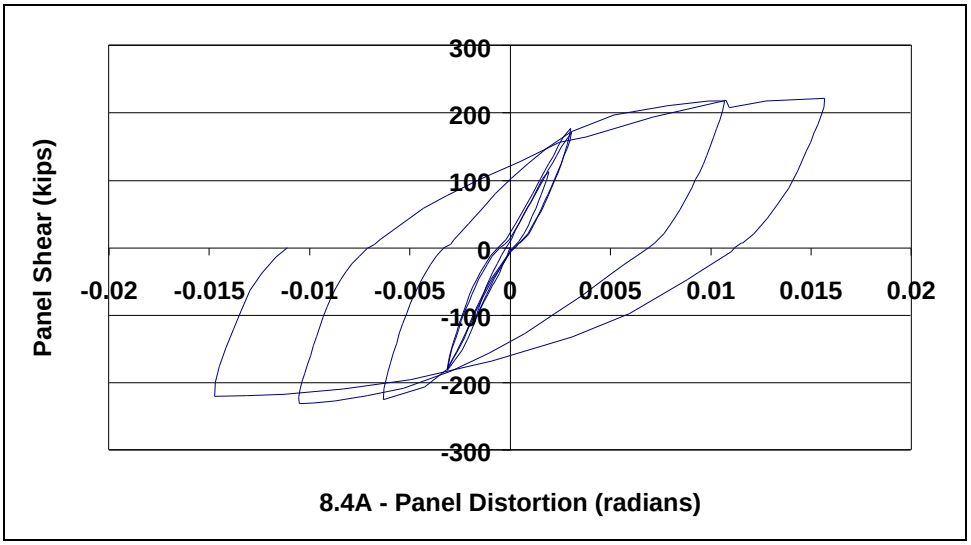

Figure 3.6 – 8.4A Panel Zone Distortion

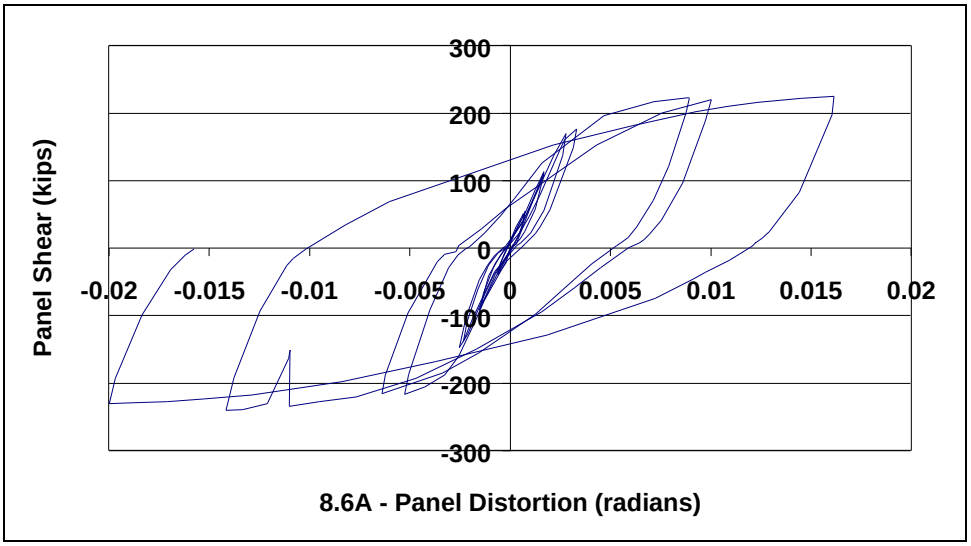

Figure 3.7 – 8.6A Panel Zone Distortion

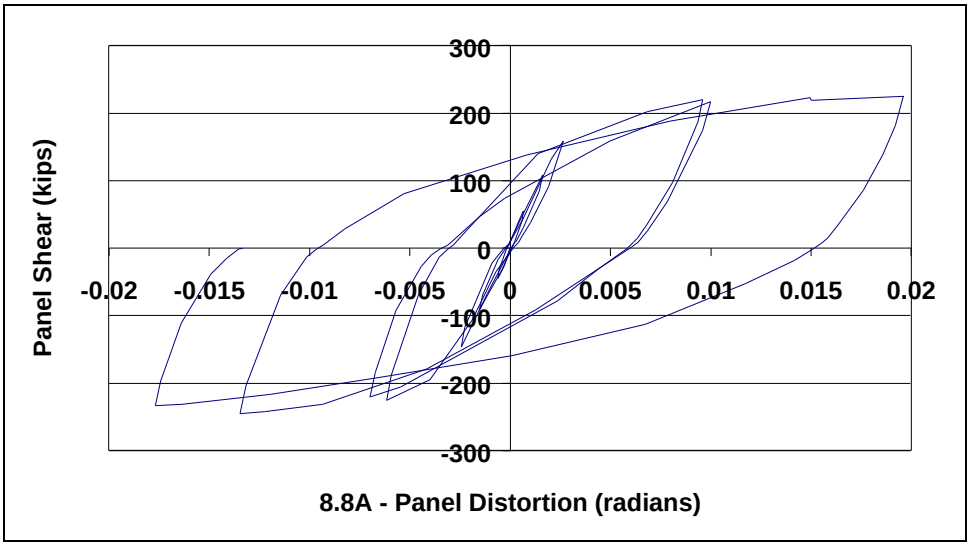

Figure 3.8 – 8.8A Panel Zone Distortion

One-sided strain gauge data were collected to evaluate, if necessary, the influence of out-of-plane bending of the steel panel on distortion measurements collected by the linear displacement transducers. The difference in calculated

strain is illustrated in Figure 3.9 for Specimen 8.4A. Panel strain along the diagonal is computed for the displacement transducer by dividing the displacement change by the diagonal length of 7.2 inches. It should be noted that the one-sided strain gauge measured strain at a point midway between the center of the panel zone and one corner of the defined zone, but it was aligned in the direction of the displacement transducer. According to the data, good agreement between the two instruments was observed for steel in tension. Deviation occurred for steel in compression. Also, it should be noted that values are plotted only for the cycles in which the one-sided gauge maintained bond. For 8.4A, the one-side gauge de-bonded after the 1-inch displacement cycle. Tests continued beyond 2 inches of end displacement for the A Series, so the one-sided gauges were ineffective due to de-bonding.

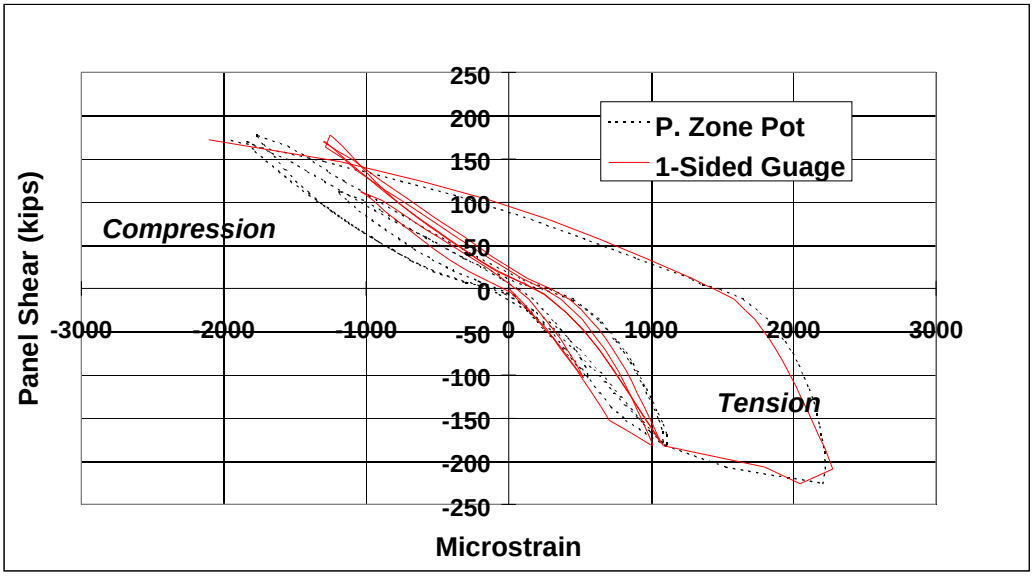

Figure 3.9 - Comparison Between Linear Pot and 1-Sided Strain Gauge – 8.4A

Within Series A, significant panel-zone shear distress was observed in both the steel and concrete, and localized bearing failure at the location of the reaction blocks against the steel tube surface (see Figure 3.10 to Figure 3.12). A well-defined series of crossing diagonal cracks could be seen. The spalled concrete provides an indication of the extent (or area of influence) of the compressive loads applied to the CFT.

Figure 3.10 – Interior Damage to 8.4A

Figure 3.11 – General Crack Direction in 8.4A
(Area of Contact Denoted by 4" x 4" Squares on Side)

Figure 3.12 – Contact Face Exposed

Figure 3.12 is of particular interest because the effects of local bearing action on the concrete can be seen. The square with the "X" identifies the loading block in compression during the final half-cycle of the test. Cracks

through the panel zone from that location and through a diagonal through the joint are more visible than cracks along the opposite diagonal because of the locked-in deformation at the end of the test.

3.3 Series B: Specimens 8.4B, 8.6B, and 8.8B

The specimens of Series B were used to determine the effect of a change in the slenderness ratio of the steel tube. All other variables remained the same as in Series A. The reaction blocks, which were used to simulate the changing "tee width", also varied from 50% to 100% of the tube depth. Nominal concrete strengths were the same in both series. Panel shear vs. end displacement curves for the specimens of Series B are shown in Figure 3.13 through Figure 3.15.

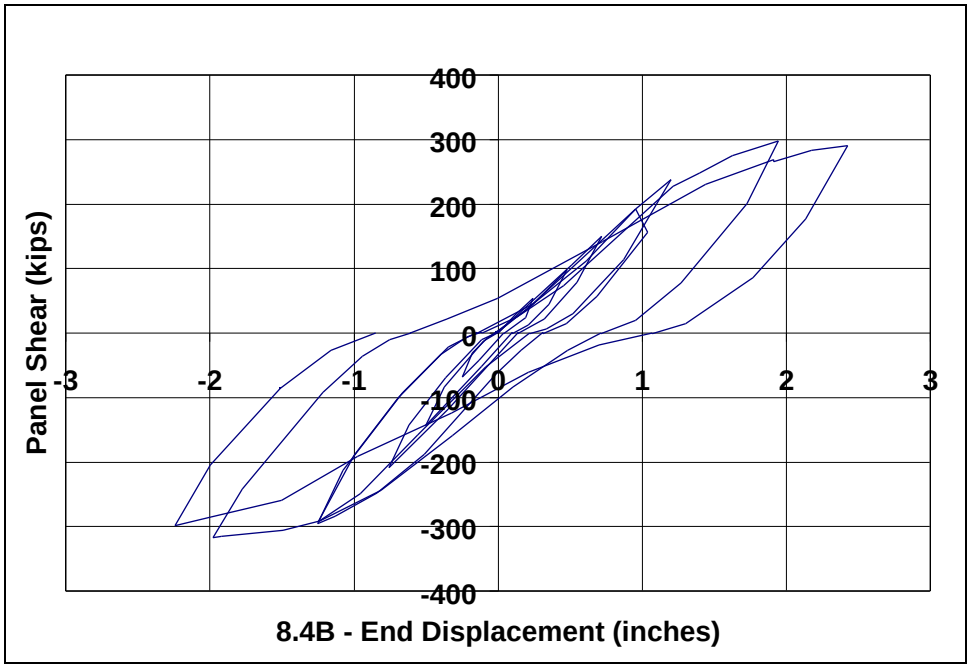

Figure 3.13 – 8.4B Load/Displacement Curve

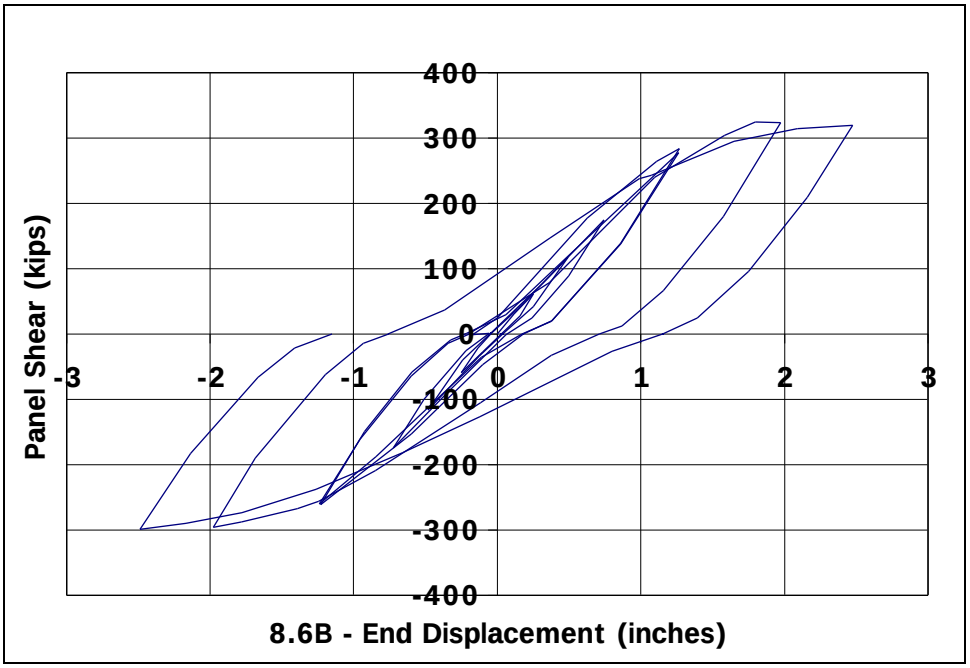

Figure 3.14 – 8.6B Load/Displacement Curve

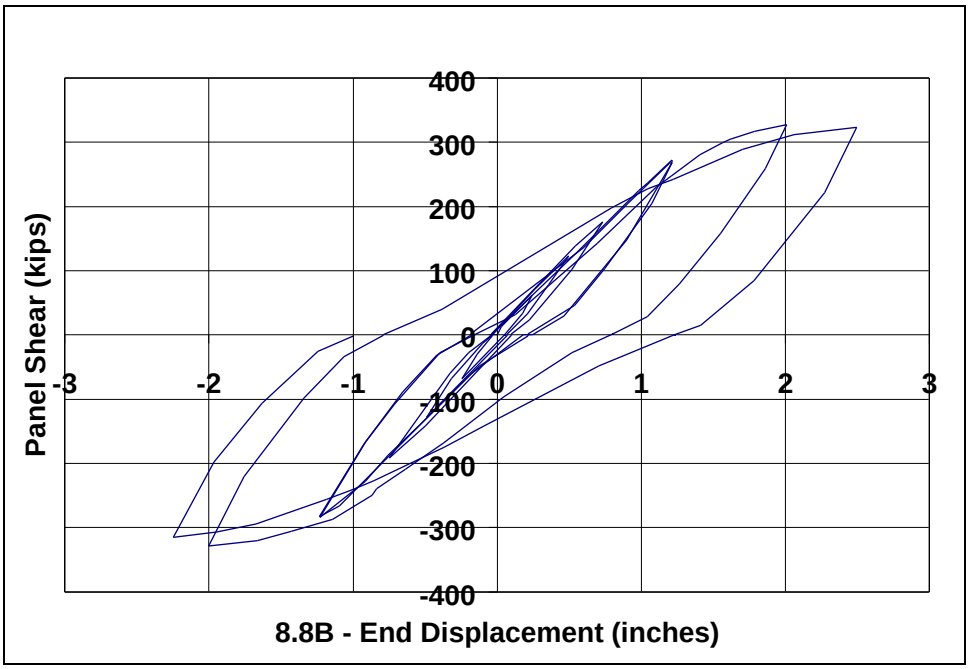

Figure 3.15 – 8.8B Load/Displacement Curve

Plots of panel distortion for Series B are shown in Figure 3.16 through Figure 3.18. The high loads necessary to fail the Series B specimens interrupted the testing of Specimen 8.8B, which was the first specimen tested from the B series. At approximately 270 kips in each forward and reverse cycle, the test apparatus slipped relative to the laboratory floor. When such slip occurred, the test was halted, and the pots corresponding to the end displacement of the specimen were reset to eliminate the shift in the curve. The anchorage of the test setup to the lab floor was strengthened before the remainder of the specimens were tested. After the test set-up was improved, slip did not occur in the remaining specimens 8.4B and 8.6B.

Comparing the panel-zone distortion curves of 8.6B and 8.8B (Figure 3.17 and Figure 3.18), the final hysteresis loop bounds roughly the same area, but with an offset of 0.005 radians between the two. It seems reasonable to assume that direct comparisons between these three tests could be made up to the point of the first load slip, which is indicated by the arrow on the plot for 8.8B (Figure 3.18).

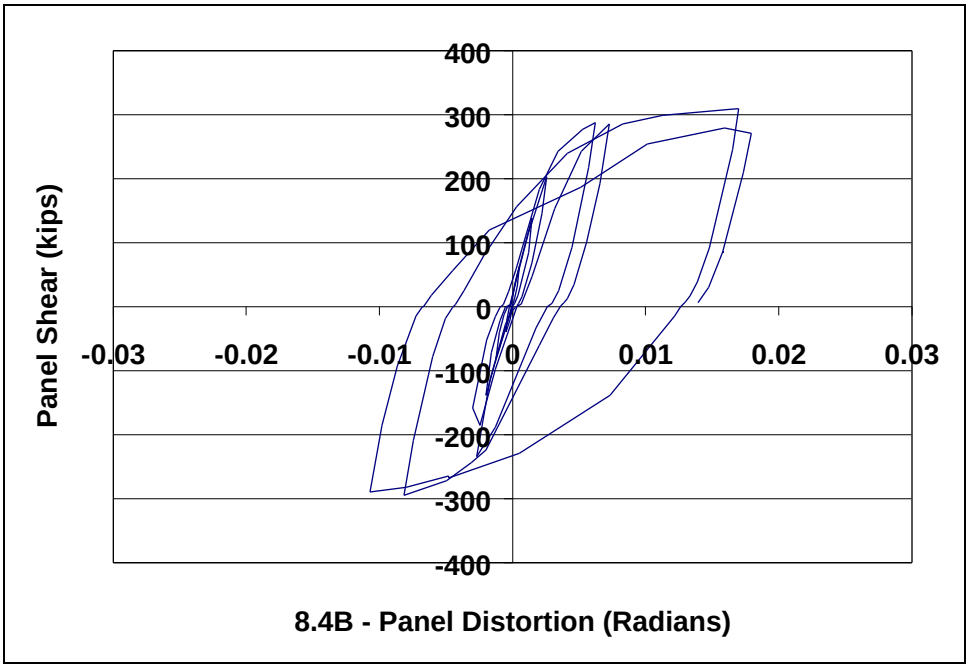

Figure 3.16 - 8.4B Panel Zone Distortion

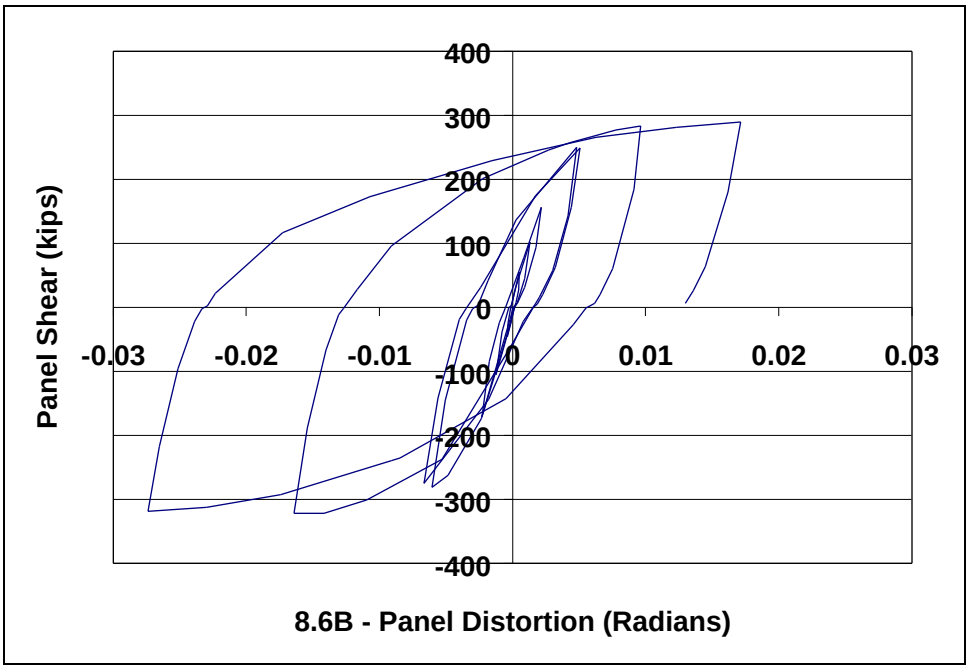

Figure 3.17 – 8.6B Panel Zone Distortion

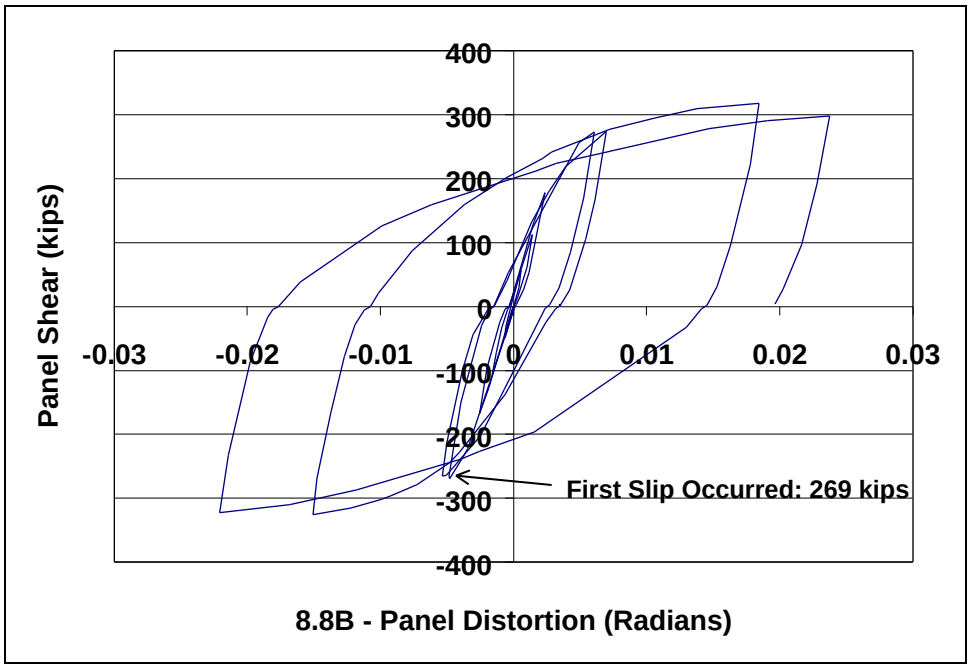

Figure 3.18 – 8.8B Panel Zone Distortion

Results for maximum panel shear and moment for Series B are tabulated and presented in Table 3-2. As with Series A, there is no noticeable difference in test results between the three Series B specimens. The difference in peak panel shear is only on the order of 1%.

Table 3-2 - Series B Results

Specimen	V_{Max} Kips	M_{Max} k-ft
8.4B	313	157
8.6B	313	157
8.8B	316	158

3.4 Specimen 8.MB

Specimen 8.MB was prepared to test the flexural strength of the Series B tubes. Specimen 8.MB had the same material properties as others in Series B, but loaded as a simply-supported beam under a 600 kip testing machine. Center-point loading was applied to force a plastic hinge to form at the mid-span of the specimen. The graph in Figure 3.19 shows the load-displacement of the mid-span. The reduction in the load after peak was due to buckling of the steel tube in the compression flange. The maximum moment was 180 k-ft, a value that is 13% higher than the maximum moment achieved in the panel-zone tests, suggesting that the earlier specimens failed in a combination of shear and flexure. Series B specimens were not controlled by flexure alone. Moment-shear interaction was involved.

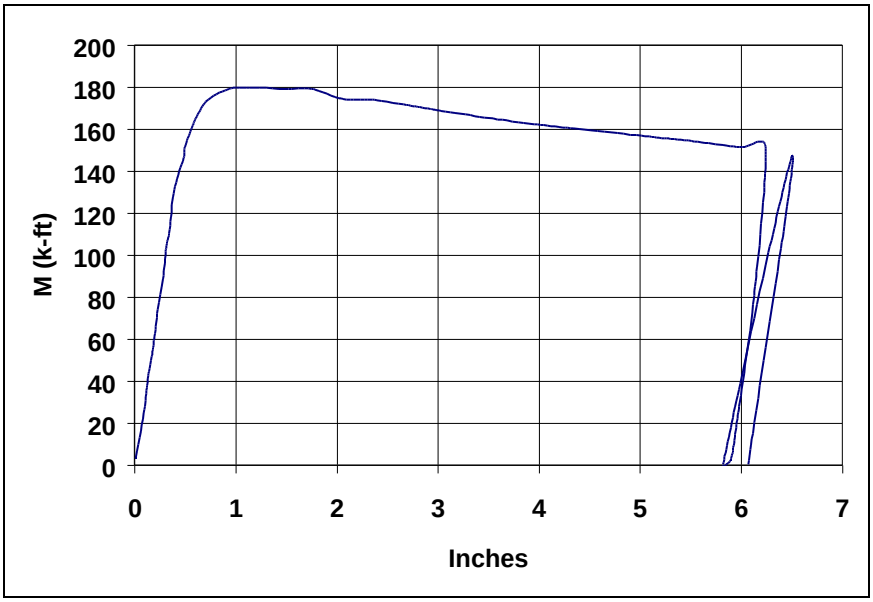

Figure 3.19 - Specimen 8.MB Load-Displacement

3.5 Series C Specimens

There were two objectives to the testing of Specimens in Series C. The first was to examine the effect of changing the concrete strength. Two reference specimens were prepared (8P.C and 8P2.C), using 4.0 ksi and 6.0 ksi concrete, respectively. Both specimens were plain CFT specimens using steel tubes of the same dimensions as in Series A. The second objective was to compare the behavior of some non-typical "cut-out" specimens with 8.PC. The specimens of Series C were designed to isolate various components of the force transfer mechanism in the panel-zone. Parts of the panel zone were removed during fabrication. The two reference specimens of Series C (8P.C and 8P2.C), the rebar enhanced specimen 8.BC, and the sand-filled specimen 8.SAC were loaded cyclically in the same manner as the A and B Series specimens. The three cut-out test specimens of Series C (8D.C, 8R.C, 8S.C) were loaded monotonically. Cyclic loading for the cut-out specimens was not practical because severe damage early in the loading history of all specimens was expected. In addition, specimen 8.DC was non-symmetric.

3.5.1 Reference Specimens 8.PC and 8.P2C

Reference specimens 8P.C and 8P2.C were tested to compare results when using two different concrete strengths. The panel-shear vs. end-displacement curves for the two reference specimens are shown in Figure 3.20 and Figure 3.21. Panel distortion for both specimens is shown in Figure 3.22 and

Figure 3.23. Specimen 8.P2C (6 ksi) reached peak shear at 227 kips, which was a 12% increase in panel shear strength of 203 kips for 8P.C (4 ksi).

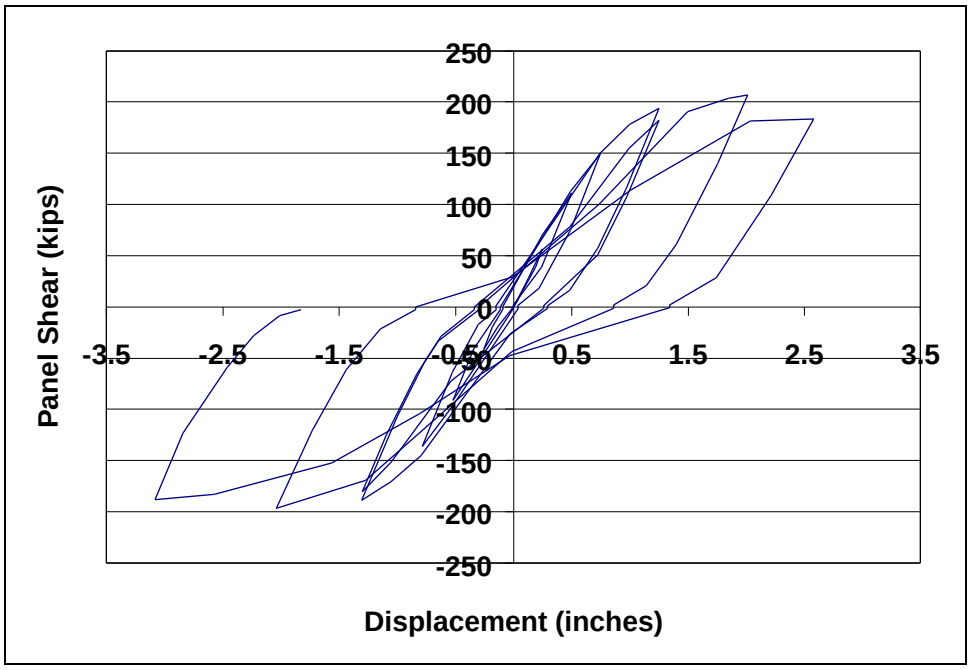

Figure 3.20 - Specimen 8P.C Load -Displacement

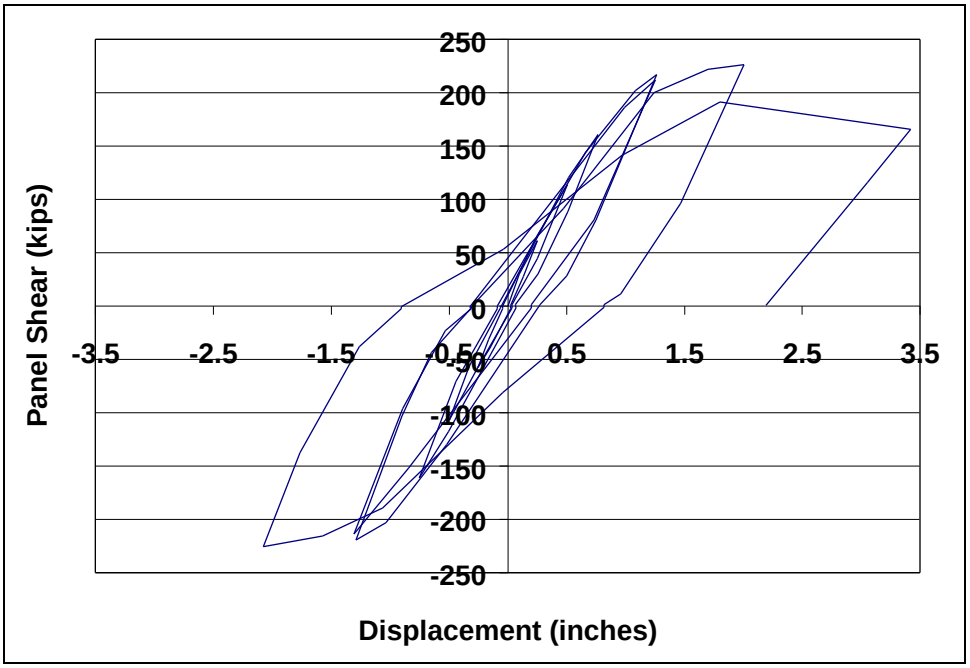

Figure 3.21 - Specimen 8P2.C Load-Displacement

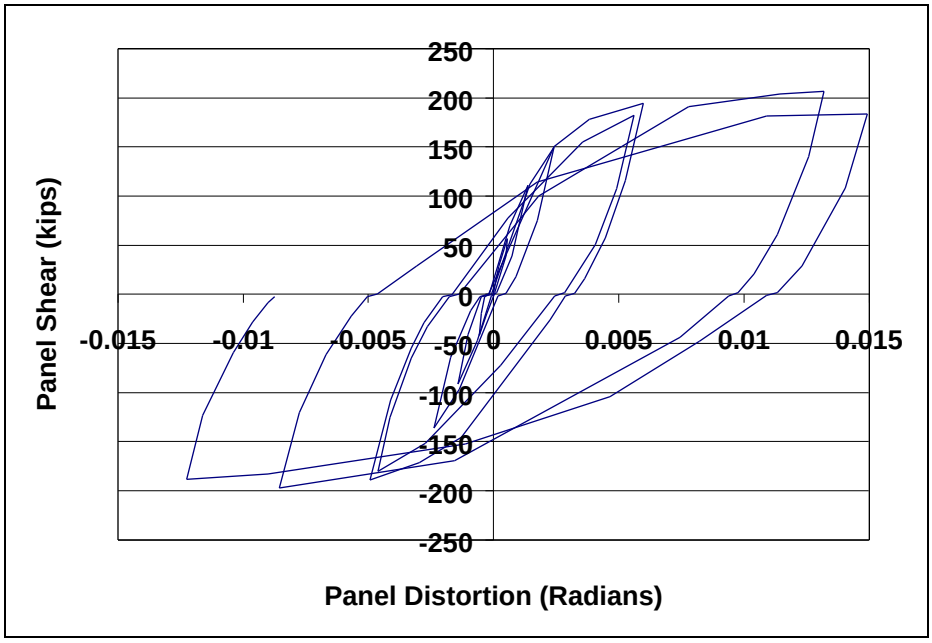

Figure 3.22 - Specimen 8P.C Panel Distortion

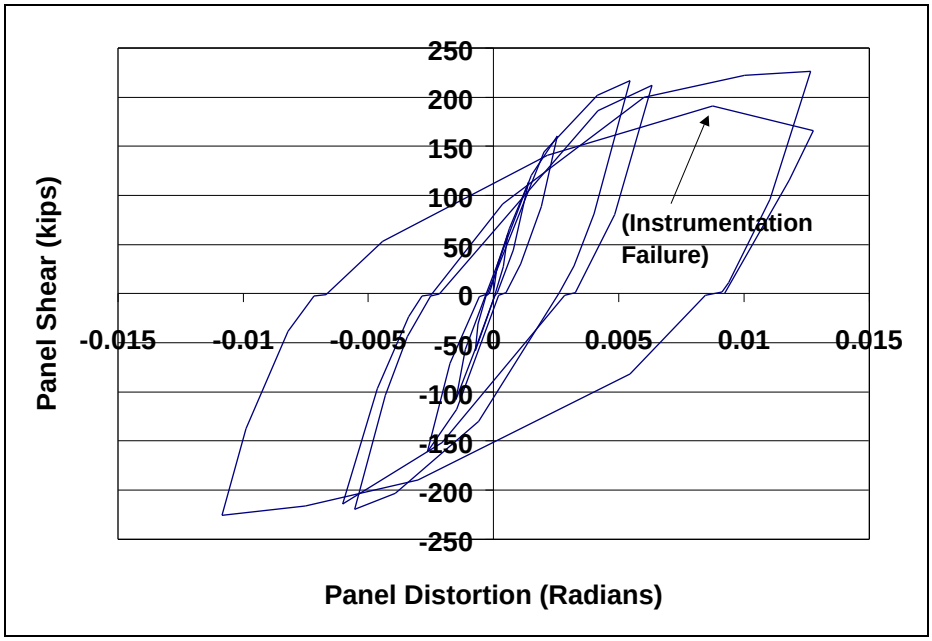

Figure 3.23 - Specimen 8P2.C Panel Distortion

3.5.2 Specimen 8.RC

Specimen 8.RC (Figure 3.24) had rectangles of steel removed from the panel zone, such that concrete was expected to be the primary contribution to force transfer. During testing, the concrete cracked very early. At the second displacement level, 0.5 inches of specimen-end displacement, a large crack progressed diagonally across the concrete core. At the third level of displacement, 0.75 inches, the specimen reach a plateau in which the cracks were widening at increasing levels of displacement with no increase in load. At one inch displacement, the specimen began to pick up load again, and progressed to the limiting stroke of 2.75 inches. Panel zone linear transducers started to debond at 1.75 inches, and all were removed at about 2 inches of displacement.

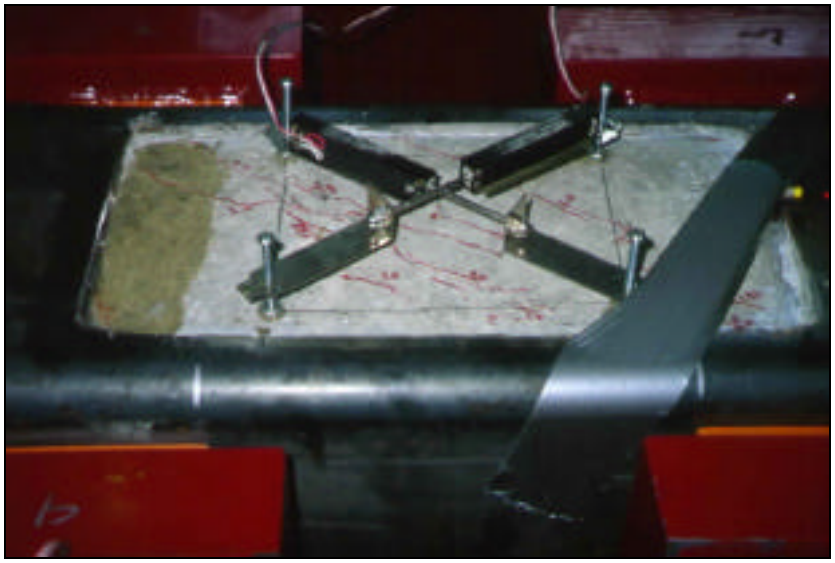

Figure 3.24 - Specimen 8.RC

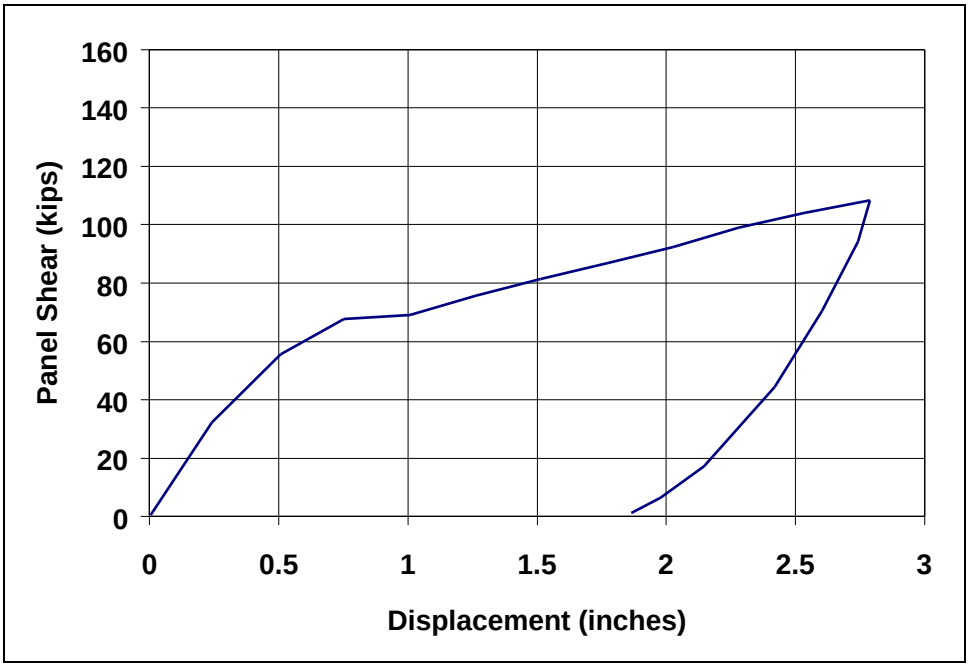

Figure 3.25 - Specimen 8R.C (rectangular cut-out)

Diagonal panel-zone displacement measurements for 8.RC could only be taken from the surface of the exposed concrete within the panel zone (Figure 3.24). Values of average strain along the diagonal, computed using the recorded displacements in tension and compression, were plotted for the panel zone of 8.RC in Figure 3.26 and Figure 3.27. It is important to note that especially in the case of concrete in tension, cracking causes the transducers to indicate large "average" strains. Values of compressive strain in the concrete are more realistically represented than tension strain because of the way cracking influences the measurements.

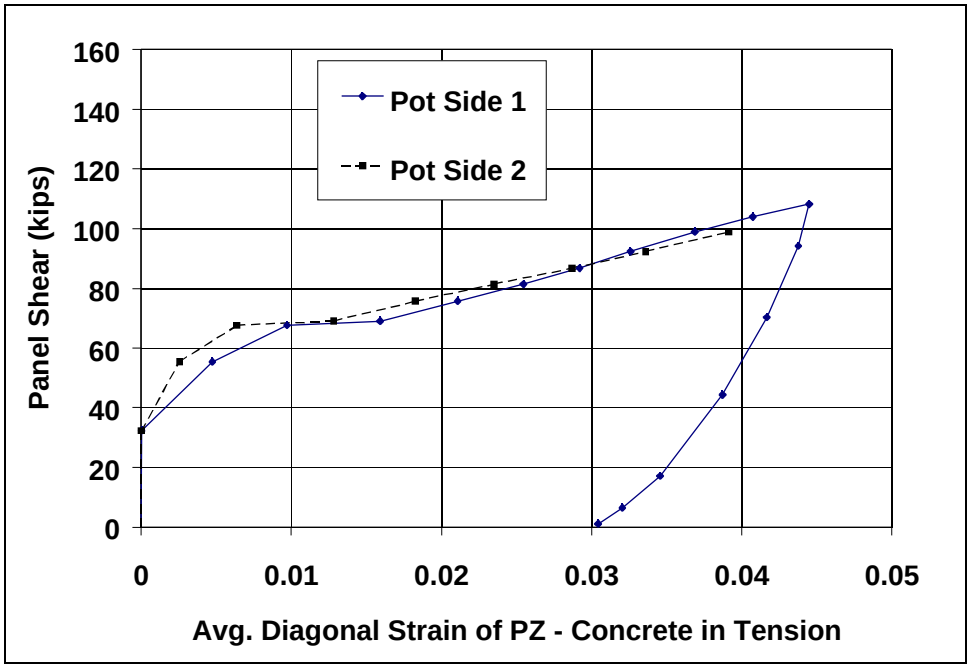

Figure 3.26 - 8.RC Average Diagonal Concrete Strain - Tension

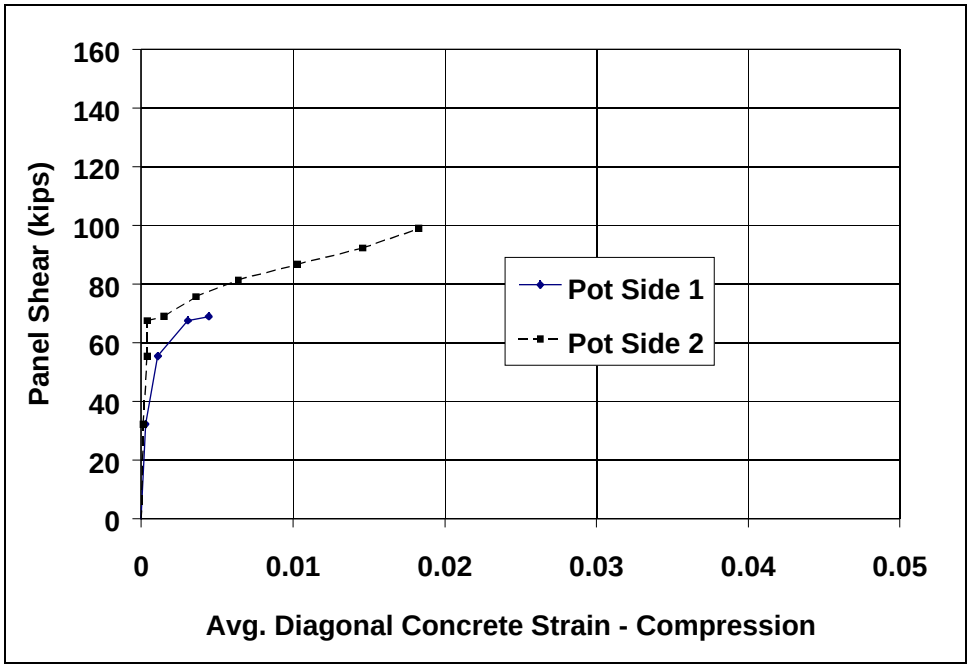

Figure 3.27 - 8.RC Average Concrete Panel Strain – Compression

3.5.3 Specimen 8.DC

Specimen 8.DC (Figure 3.28) had a diagonal strip of the steel left intact, while portions of the steel were removed from the panel zone. Such modification was done to examine the effect of reducing, but not completely eliminating the contribution of steel to the strength of the panel-zone. During testing, transducers mounted to the concrete were removed early due to cracking through the adhesive, and also due to interference with the transducers attached to the steel strap as the concrete began to push upward (out of plane).

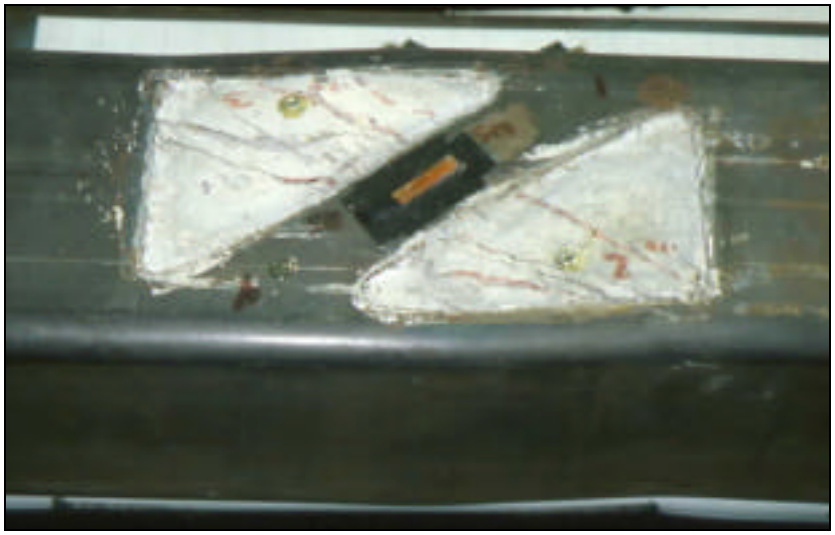

Figure 3.28 - Specimen 8.DC (instrumentation removed)

Values of diagonal strain (based on displacements from the diagonal linear pots) are plotted in Figure 3.30 and Figure 3.31. Diagonal linear transducers were located such that the tension diagonal was placed on the surface of the steel strap, and the compression diagonal pot was adhered to the surface of the exposed concrete of the panel zone. Figure 3.30 shows the relationship of the steel tension strap strain to the panel shear. Values of strain from both sides of the specimen are averaged in this plot. Figure 3.31 shows the plot of panel shear versus the strain in the compression diagonal. In this graph, values from both sides of the specimen are plotted together because one of the transducers disengaged from the specimen early in the test, so the values could not be averaged throughout the course of the test.

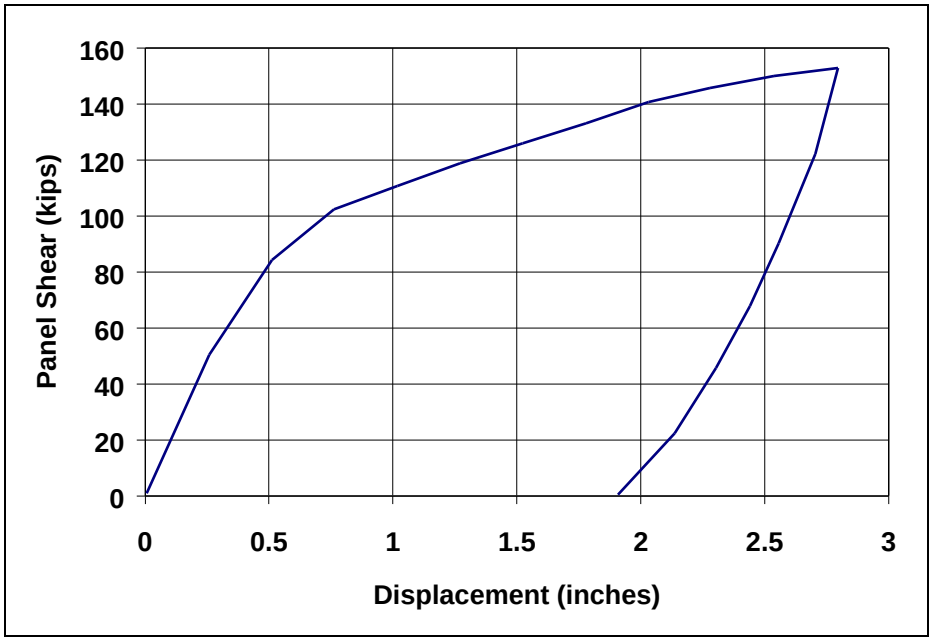

Figure 3.29 - Specimen 8D.C (diagonal steel strap)

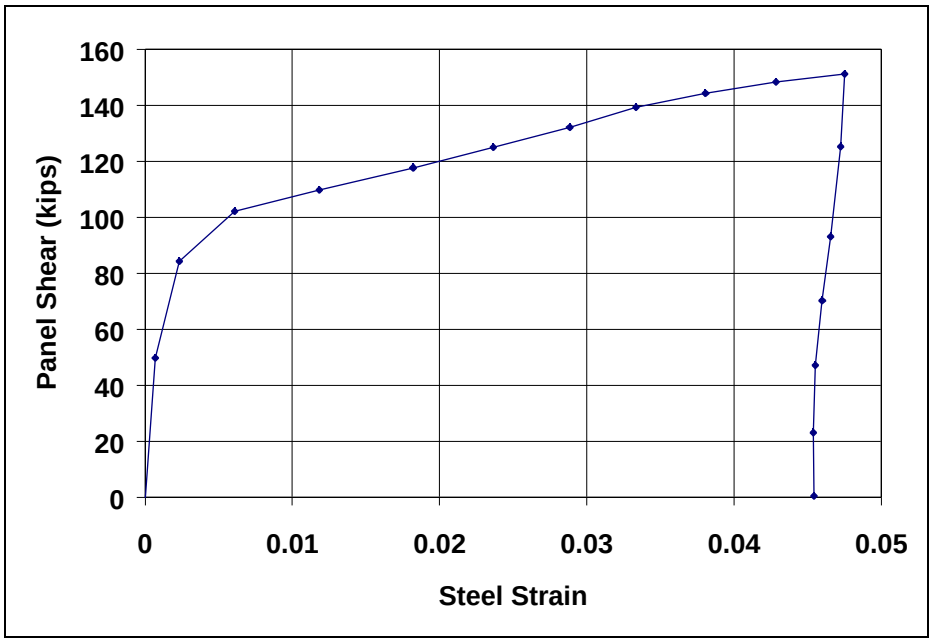

Figure 3.30 - Specimen 8.DC Strain in Steel Tension Strap (average both sides)

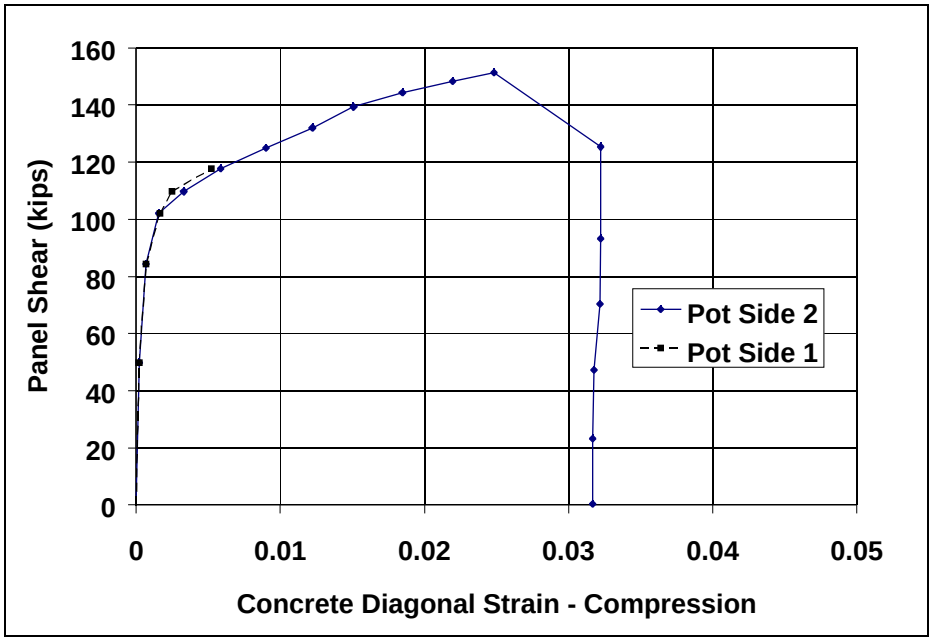

Figure 3.31 - Specimen 8.DC Compression Diagonal Concrete Strain

3.5.4 Specimen 8.SC

Specimen 8.SC had just a narrow slot of steel removed along the center axis of the tube. This was done to retain some of the confining properties of the steel, while severely weakening the ability of the steel to resist shear in the panel-zone. During testing, cracking was audible during the first displacement level. Cracks were visible through the narrow slot during the second displacement cycle. Testing continued until 2.79 inches of end displacement.

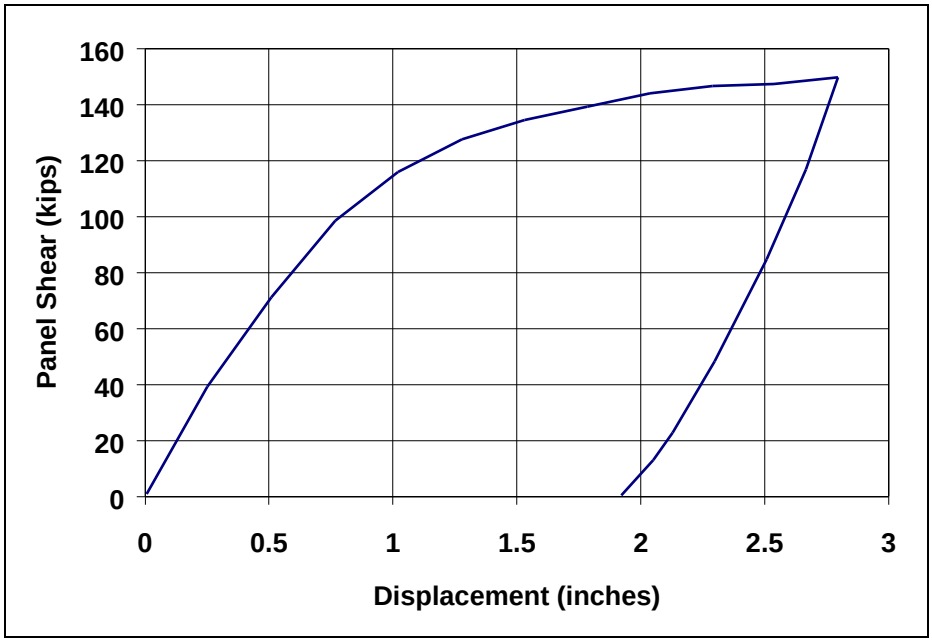

Figure 3.32 - Specimen 8S.C (narrow slot cut-out)

3.5.5 Specimen 8.SAC

Specimen 8.SAC was a special case in which sand occupied the panel-zone of a standard CFT specimen. The remainder of the tube outside the panel-zone was filled with concrete. This specimen was assembled as a limiting case in which the shear would need to be carried by the steel alone because the cohesionless sand would not be able to develop the necessary strut mechanism. Specimen 8.SAC could represent a specimen with very poor concrete in the joint or one in which concrete was not very well consolidated through the joint region. It could also represent badly damaged concrete. Failure consisted of buckling of the tube sides. Sand was unable to form a strut mechanism, so the tube folded at the reaction block locations, and buckling of the tube was apparent near the

corners. The panel shear at the point of limiting stroke was 49.2 kips, a value of 24% of the reference specimen 8.PC.

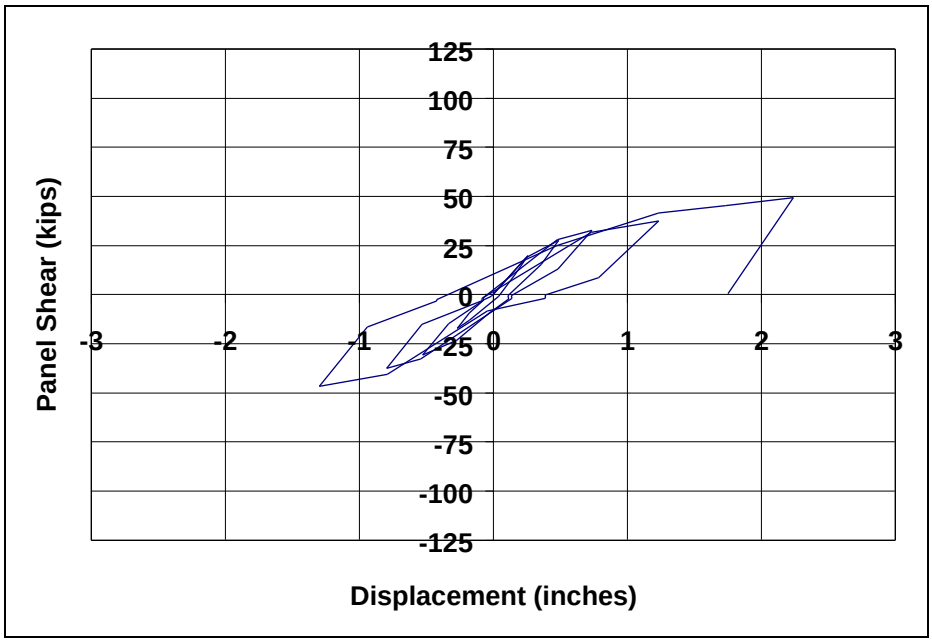

Figure 3.33 - Specimen 8.SAC (Sand in Panel)

It is important to note that the maximum measured value of shear of 49.2 kips is much less than the calculated value of V_{max} of the steel panels in shear. If a conservative estimate of the steel panels in shear is calculated using only the flat portion of the steel tube (6.5 inches), then the shear capacity of the two panels is: 02 x 0.6 x (6.5)(.25)(61.5) = 120 kips, which is much greater than 49.2 kips. This observation is important in defining limits for the applicability of an equation for the shear capacity of the panel zone. If such an equation is a summation of a steel and a concrete term, then theoretically one could neglect the concrete term in the case of very poor concrete, and reach a value that is merely the steel shear term. As shown in the test on 8.SAC, such an analysis would prove to be

unconservative because the steel cannot reach its shear capacity when there is insufficient resistance to buckling of the steel tube.

3.5.6 Specimen 8.BC

The panel shear vs. end displacement behavior for the rebar enhanced specimen 8.BC is shown in Figure 3.34. The shear vs. panel distortion response is plotted in Figure 3.35, and shows that panel shear failure was achieved.

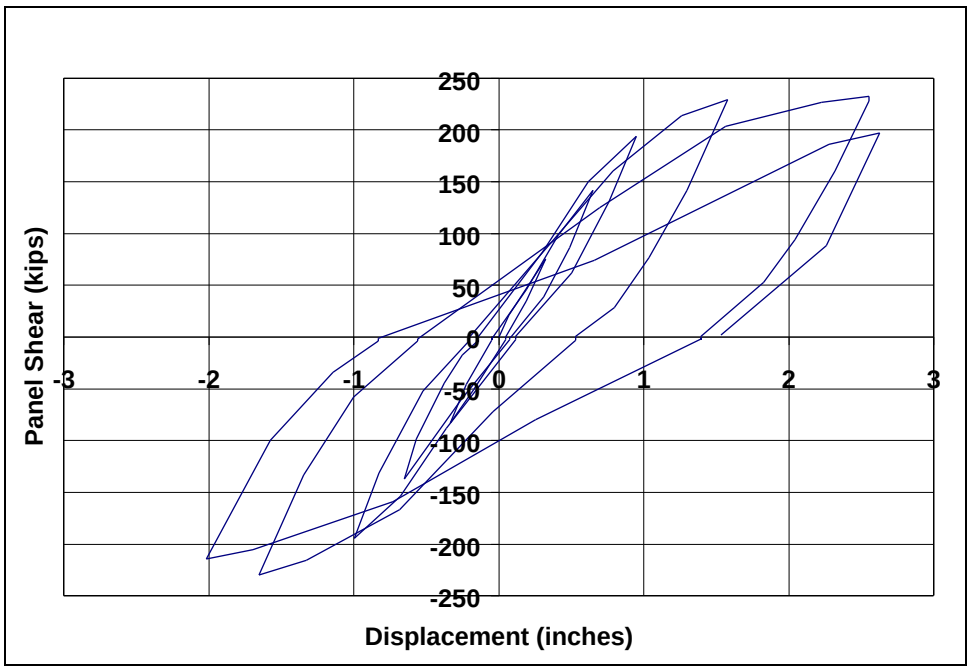

Figure 3.34 - Specimen 8.BC (Rebar-Enhanced)

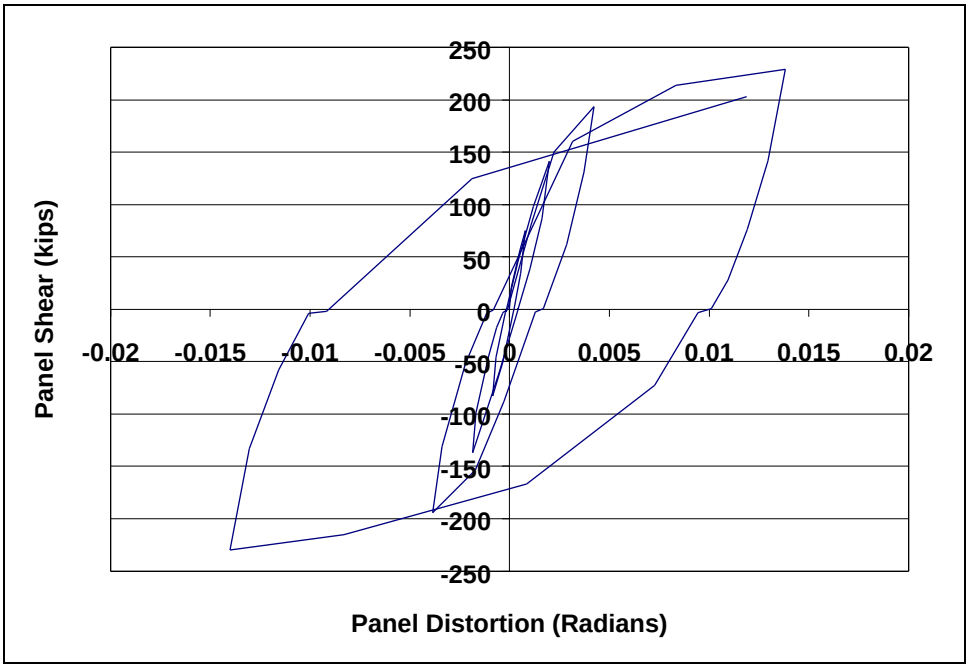

Figure 3.35 - Shear vs. Panel Distortion for 8.BC

3.6 Series C Results Tabulated

Table 3-3 - Series C Measured Capacities

Specimen	Description	Panel Shear (kips)	Compared to 8.P-C
8.P-C	Reference 1	203	1.0
8.R-C	Rectanglar Cut-out	103	0.51
8.D-C	Diagonal Cut-out	150	0.74
8.S-C	Slot Cut-out	146	0.72
8.B-C	Rebar Cage Inside CFT	232	1.14
8.SA-C	Sand within Panel Zone	49.2	0.24
8.P2-C **	Reference 2	227	1.12

3.7 Validity of Panel-Zone Tests

To understand better the correlation between the performance of the panel-zone specimens, Uchida et al (1998) developed a FEM analysis to study the panel zone behavior (See Appendix A for more the complete report). The results of the FEM analysis were compared with data from experimental results of the small panel-zone specimens. After determining that the FEM model satisfactorily represented the test results, the same analytical procedure was used to model a full-scale moment connection tested at Lehigh. The response of the full-scale connection was compared with the results of the small-scale panel-zone analyses to assess how well the panel zone specimens represented the conditions of a complete beam-column joint.

The FEM analysis of Appendix A confirmed that (1) the analytical model could reliably predict panel-zone specimen behavior, and (2) that the panel-zone specimen behavior was similar to that of the full-scale CFT split-tee through-bolted connections. Figure 3.36 shows that two variations of the FEM model produce comparable levels of strength for specimen 8.4A. The panel diagonal displacements computed using the FEM model correlated well with measured values using diagonal linear transducers attached to the steel panel zone surface (Figure 3.37).

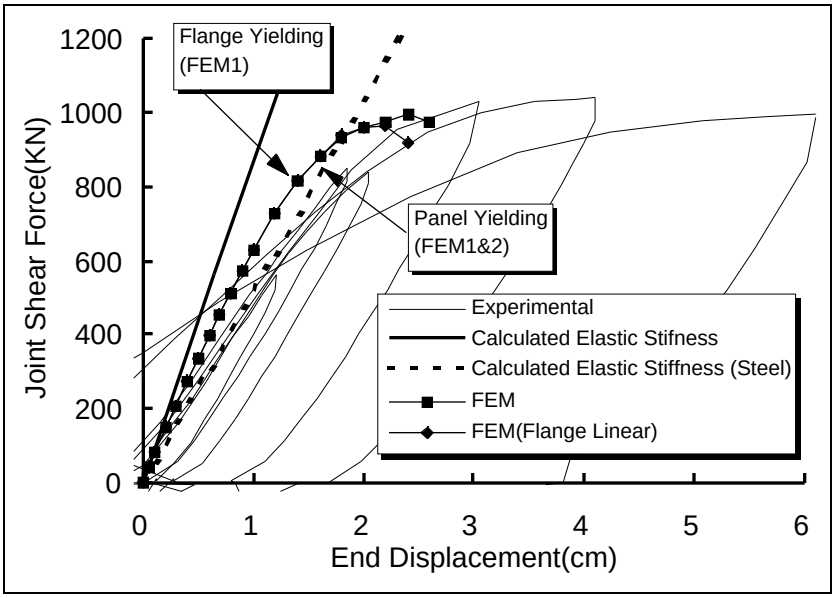

Figure 3.36 – Specimen 8.4A Results Compared to FEM Model (Uchida, et al 1998)

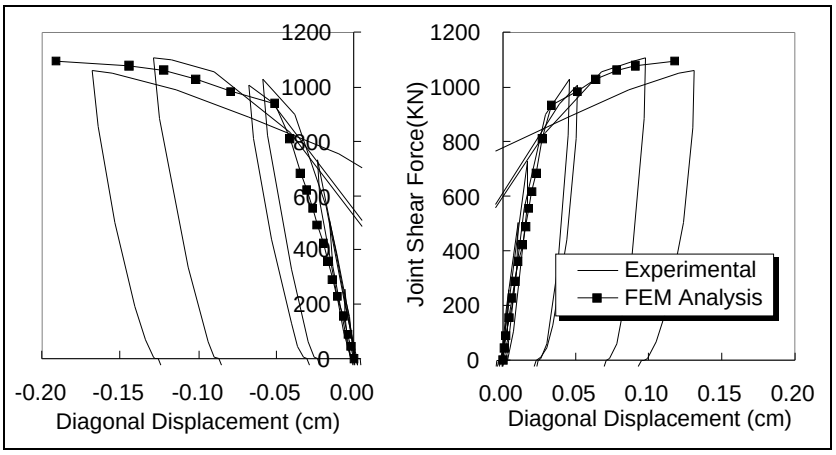

Figure 3.37 – Specimen 8.8A Diagonal Panel Zone Displacement FEM Comparison (Left: Compression, Right: Tension) Uchida et al (1998)

Plots of stress contours on the surface of the steel reveal that similar load paths and stress gradients were obtained from models of both a small-scale panel zone specimen and a full-scale moment connection (Figure 3.38). The notation

"C6" refers to the modeling of Lehigh Specimen C6, which was a CFT split-tee through-bolted connection. The two solutions (PC-bar and Nodal Force) designate the assumptions made regarding the distribution of bearing forces on the face of the tube in the FEM analysis.

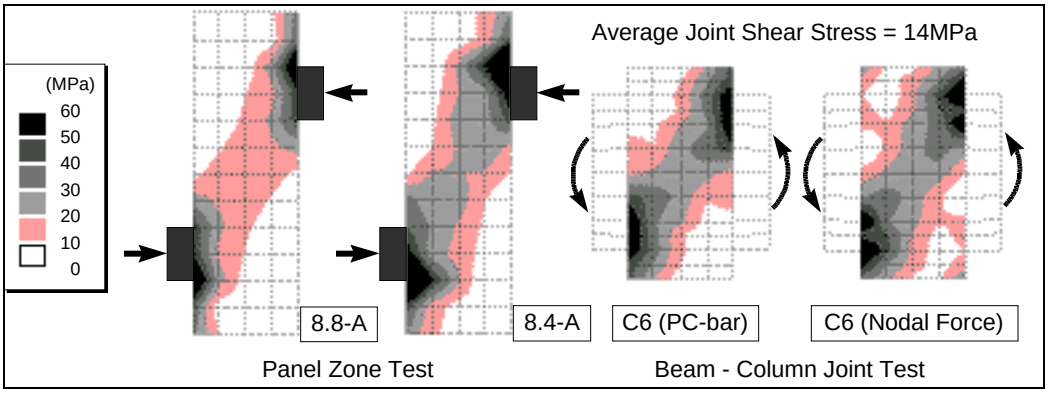

Figure 3.38 - FEM Stress Contour Comparison (Uchida et al, 1998)

4. Analysis of Panel-Zone Tests for the Development a Behavioral Model

4.1 Contributions to Joint Shear Strength

In the study of CFT systems, understanding the role that the concrete plays in the transfer of joint shear forces is needed. If steel behavior is well known and documented, then subtracting the theoretical prediction of its contribution to test results on composite sections should provide a basis for understanding the role of the concrete. The cut-out specimens of Series C were designed to discern if the steel contribution may be simply subtracted out of the test results in this manner, and to provide a stronger case for the superposition of the contributions of concrete and steel to joint strength.

Deierlein (1989) showed that, in the study of joints in SRC composite connections, the panel shear contribution of the steel could reliably be calculated as the shear strength of the steel web, and neglecting the effects of column flange yielding. A CFT system could arguably be considered very similar to the SRC composite system, with the exception that the steel is on the outside, and that the concrete is well confined by the steel tube, and thus does not require reinforcement internally. The steel side panels of the CFT are analogous in this sense to the steel web of an encased W-section. The confinement to the concrete that the steel tube provides is more difficult to assess.

Parsley (1998) showed that the confinement provided by square CFTs had an effect on specimens loaded in axial compression. It is unknown, however,

how well this translates to horizontal joint shear behavior—a situation where the load is not uniform along the longitudinal axis of the specimen as it is with direct axial load. The warping of the steel tube panels during testing would suggest lack of contact with the concrete at some point during the testing. Confinement in this case may be limited to just the corners of the tube, or areas near the contact faces of the tube. Confinement may be present, but in a completely different sense.

4.2 Evaluation of the 8-inch Tube Series

In the analysis that follows, attention will focus initially on the CFT systems in which varying the tee width was not the chief concern. Specimens in all three series of 8-inch tubes had flat tube surface widths that measured just over 6 inches. In particular, Series A and B both had approximately 6.5 inches of flat width, despite the fact that they had different tube wall thicknesses. The panel flat width parameter is discussed later in the analysis. Series C, on the other hand, which had the same nominal dimensions as the tubes of Series A, had approximately 6.25 inches of flat tube width. The proceeding analysis will initially focus only on specimens using 6-inch and 8-inch test setup reaction blocks. All of the Series C specimens were tested using the 6-inch block configuration, which would accurately represent the coverage of a tee bearing only on the flat portion of the steel tube with no overhang. Increasing the block width to 100% of the tube depth (8 inches), which results in the block extending over the side of the curved corners, had no effect on the test results for strength compared to the 6 inch block cases. It is assumed here that the 6 inch loading

width, when considering the effects of the local confinement and stiffness provided by the corners of the tube, would provide nearly full mobilization of the interior concrete despite the fact that the width of direct contact to the face of the tube is less than the actual full width of the tube.

Because the aim of this research is to understand to what extent the concrete contributes to overall shear strength of the panel zone, tests on the cut-out specimens of Series C were conducted to aid in evaluating this aspect. The behavior of steel in panel-zone shear is widely known for steel structures. By separating out the steel contributions from the strength of the specimens in Series C, the contribution of the concrete can be quantified. This concrete contribution can be compared to existing models to try to refine a predictive model.

4.2.1 Series C "Cut-out" Specimen Analysis

The specimens of Series C were designed to isolate various contributors to the shear strength of CFT system. Also within the series were two reference specimens, 8.PC and 8.P2C. Both specimens were plain CFTs with different concrete compressive strengths. Specimen 8.PC is a standard against which the cut-out specimens can be compared because they had identical material properties. 8.P2C was used to evaluate the effect of increasing the concrete strength.

4.2.1.1 Specimen 8.RC Analyzed

A rectangular steel panel was removed from the steel tube of specimen 8.RC prior to the casting of concrete. The missing steel from the panel measured

12 by 5.5 inches, which left only 1.25 inches of steel from the outer edges of the CFT to the exposed region. As seen in the yield zones of Figure 4.1, the remaining steel served as flexural hinges in bending. Deformation of the connection region caused each steel flange to develop a flexural hinge in much the same way that the flange of a steel wide-flange beam develops a flexural hinge while the web develops shear distortion. Figure 4.2 illustrates how this shearing force is related to the moments at the location of the plastic hinges.

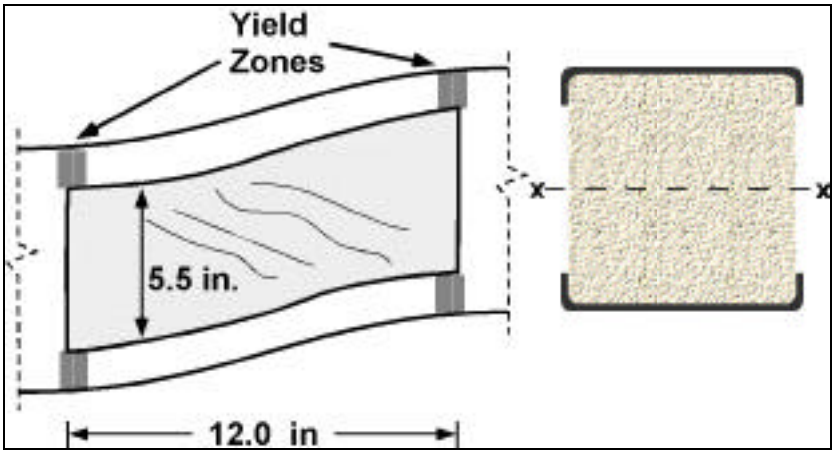

Figure 4.1 – Specimen 8.RC (X-X: Axis of Bending)

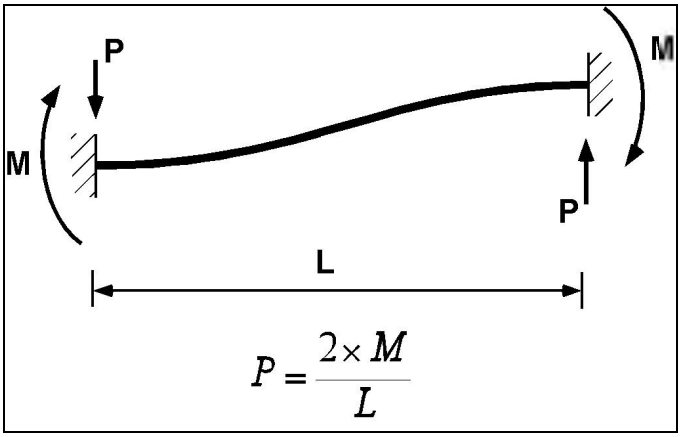

Figure 4.2 – Relationship Between Shearing Force P and Fixed End Moments M

The calculation of the contribution of steel to the maximum shear on specimen 8.RC follows:

$Z = 0.4\ in^3$ (small U-section)

$F_y = 61.5$ ksi

$L = 12$ in.

$M_p = (0.4)(61.5) = 24.8$ k-in.

$V_s = 2 \times 2M_p / L = 8.3$ kips

When 8.3 kips is subtracted from the experimentally obtained 103 kips, the concrete contribution V_c is 95 kips. For the following analyses on the cut-out specimens V_c will be taken as 95 kips.

4.2.1.2 Reference Specimen 8.PC Analyzed

The missing steel rectangle accounted for a shear area having cross sectional dimensions of 5.5 x 0.236 inches. Because the yield value of the steel used in the "C" series was 61.5 ksi, the shear contribution of the missing steel is:

$V_s = 2 \times 0.6(61.5)(5.5 \times 0.236) = 96$ kips.

Adding the theoretical strength of the missing steel (96 kips) to the measured shear strength of 8.RC (103 Kips) gives 199 kips, which is close to the value of reference specimen 8.PC (203 kips), which indicates that the steel panel contribution as discussed by Deierlein (1988) in his study of connections

utilizing concrete encased wide flange beams is applicable here. The concrete is unconfined on the exposed panels specimen 8.RC, and confinement is limited to the corner regions of the remaining steel tube. Additional confinement of the steel side panel seems minimal as discussed by Parsley (1998). Her results showed that the benefits of confinement are most prominent near the corners, and that at the center of the side panels there is little resistance to outward pressure.

4.2.1.3 Specimen 8.DC Analyzed

For specimen 8.DC (Figure 4.3) the theoretical contributions of the steel elements are added to V_c, and then compared to the test results. The contributions to the steel term V_s in the case of Specimen 8.DC are: plastic hinging of the tube flanges, and the interaction of tensile yielding of the steel strap and moment in the steel strap due to rotation (See Figure 4.3). Strain gauge data showed that the center of the strap yielded in tension. Moment / axial-force interaction will be checked to determine the contribution of moment. The final deformed shape of the specimen was complex. It is not clear based on data and physical examination whether the strap rotated enough to develop significant moment, or if the combined action of eccentric shear and bending of the tube flanges primarily (Figure 4.3) resulted in tension in the steel straps. The strap did not appear to deform in flexure, but strain data showed that the strap yielded in tension.

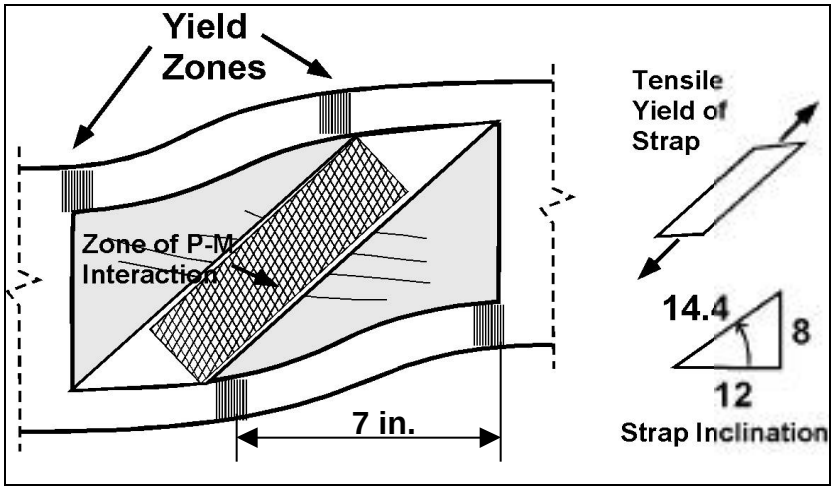

Figure 4.3 - 8.DC Steel Contribution in Shear

Calculations of the steel contributions are as follows:

Yield Zones (tube flanges):

$Z = 0.4\ in^3$

$L_1 = 7.0$ in.

$M_p = (0.4)(61.5) = 24.8$ k-in.

$V_{s1} = 2 \times 2M_p / L = 14.2$ kips

Interaction Check for Strap:

The following interaction equation for tension and moment on the steel strap will be used:

$$\left(\frac{P}{P_y}\right)^2 + \frac{M}{M_p} = 1.0$$

Strain data showed that the steel yielded in tension, so *M=0.* To determine the shear due to the steel strap, only the component of the tensile force in the strap in the direction of shear is necessary:

$A = (2)(0.236) = 0.47\ in^2$

$P_y = (0.47)(61.5) = 28.9$ kips

$V_{s2} = 2 \times (28.9)(8 / 14.4) = 32$ kips (for two steel straps, one on each side)

Concrete (from tests):

$V_c = 95$ kips

Theoretical Shear Strength:

$V = V_c + V_{s1} + V_{s2}$

$V = 95 + 14 + 32 = 141$ kips

The calculated shear strength for specimen 8.DC is 141 kips. Specimen 8.DC reached 150 kips in the test, which is very close.

4.2.1.4 Specimen 8.SC Analyzed

The slot-cut specimen (8.SC – See Figure 4.4) had a rectangular area of steel measuring 1.25 x 12 inches removed from both sides of the pane zone. The failure mode for the steel was plastic flexural hinging, which is similar to the behavior of the remaining steel for 8.RC.

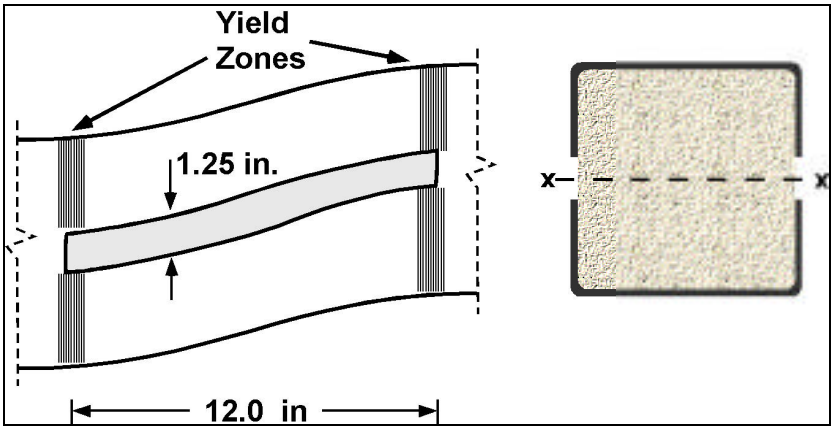

Figure 4.4 - Specimen 8.SC

Calculation of Shear:

$Z = 2.54\ in^3$

$F_y = 61.5\ ksi$

$L = 12\ in.$

$M_p = (2.54)(61.5) = 156\ k\text{-}in.$

$V_s = 2 \times 2M_p / L = 52\ kips$

The computed contribution of the remaining steel for 8.SC is 52 kips. When this 52 kips is added to the V_c of 95 kips, the theoretical value of 147 kips closely matches the experimentally obtained value of shear of 146 kips.

4.2.2 Summary of Cut-out Series

From comparison of the three cut-out specimens with reference specimen 8.PC, V_c appeared to be a nearly constant quantity. A value of V_c=95 kips was subtracted from the measured capacity of reference specimen 8.PC to obtain a

contribution of 108 kips as the steel panel in shear. Based on the yield value of the steel and the actual thickness of the tube, and also neglecting the shear required to yield the tube flange in bending, the width of the steel panel mobilized in shear is 6.2 inches. Plastic hinging of the remaining steel flanges contribute only an additional 3% and was neglected. The calculated panel width of 6.2 inches corresponds approximately to the width of the flat portion of the steel tube away from the corners. The actual flat panel width was measured to be 6.25 inches for the tubes of Series C. Based on the analysis of the cut-out specimens, the theoretically obtained V_c from tests seems reasonable.

4.3 Development of Behavioral Model

The main variables in the test program were concrete compressive strength (f'_c) and the b/t ratio of the steel tubes. The effects of the influence of both variables on the term V_c will be studied further. In Table 4-1, values for V_c are calculated by subtracting the contribution of the flat width of the steel panels for specimens.

Table 4-1 – Estimated Vc for Selected Specimens

Specimen	f'c (ksi)	Vs (kips)	Vmax (kips) From Tests	Vc = Vmax - Vs
8.PC	3.9	109	203	94
8.P2C	5.9	109	227	118
8.6A	6.2	96	241	145
8.8A	6.2	96	237	141
8.6B	6.1	140	306	166
8.8B	5.9	140	322	182

The values for *Vc*, the contribution of the concrete to the shear strength, provide a foundation for developing a model for the shear strength of the composite connection studied in this project. Data from full-scale connections (Chapter 6) will be used to calibrate the model. Existing models for concrete strength within joints will be used for comparison, and also to examine variables that have been found to be important in the prediction of concrete shear strength.

Models exist for the analysis of the strength of concrete within the panel zone of moment connections. Two existing models for concrete strength will be discussed and used to compare with the experimentally obtained V_c. The first model is the Kanatani model for the split-tee through-bolted connection. The second model is the V_c term proposed by the ASCE Task Committee on Design Recommendations for composite joints.

4.3.1 Shear Strength by the Kanatani Model

In order to detail the specimens for this test series, and to provide a benchmark for values of maximum CFT shear strength, a formula developed by Kanatani, *et al* (1985) was used initially to predict the failure load of specimens tested. The Kanatani model is shown in Figure 4.5. This shear strength model is a superposition of the shear strength of the steel panels, and the crushing strength of the assumed compression strut within the interior of the panel zone. The assumed connection zone is of the split-tee through-bolted type. The tension flange of the beam only transfers load to the connection through the bolts passing through the interior of the joint. The bolts are unbonded throughout the connection, so the tees are only transferring forces to the tube through compression. Variables S and α depend entirely on the geometry of the connection and its elements, so the model yields different results as the connection geometry varies.

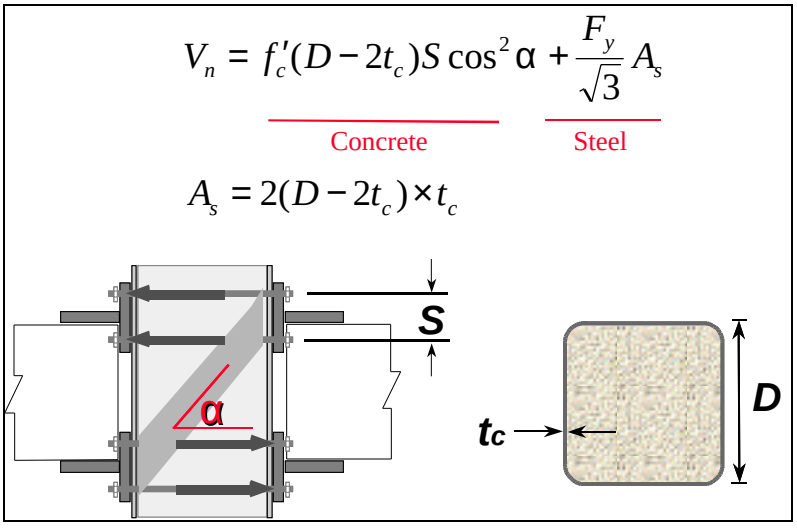

Figure 4.5 - Kanatani Model for Predicting Shear Strength of Square CFT Section

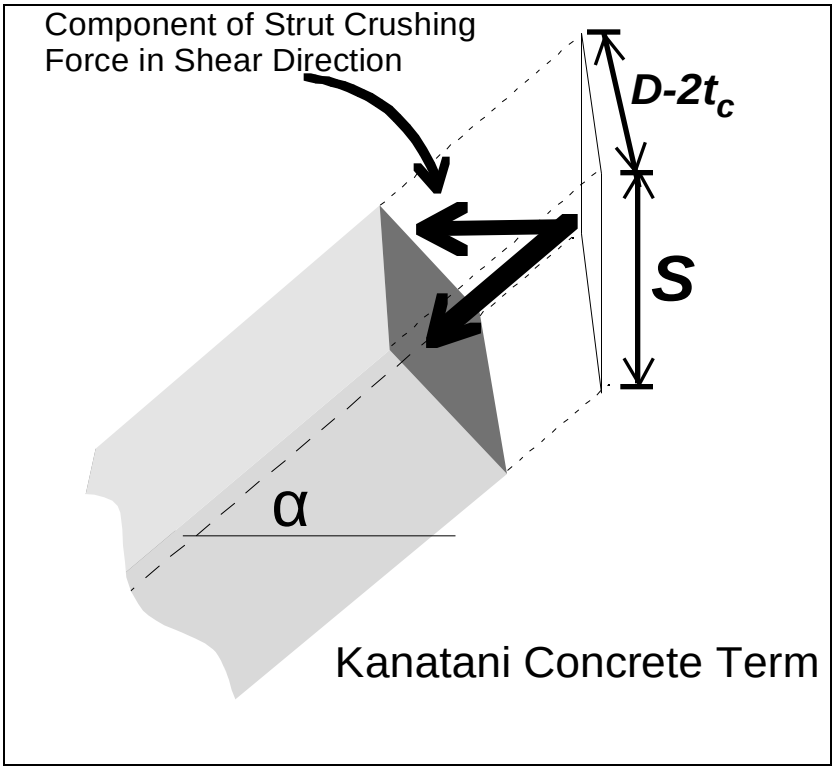

Figure 4.6 - Illustration of Kanatani Concrete Term

It is important to note that the steel contribution in this case is based on the full depth of the steel tube minus the thickness of the flanges. In terms of the shear strength due to the steel, this term alone is likely to be unconservative based on the results of Series C, from which only the flat portion of the tube was assumed to carry the required shear.

The concrete term in the Kanatani model is based on a strut-and-tie analysis within the core of the joint. This approach seems reasonable because the geometry of the split-tee through-bolted connection suggests a very clean and well-defined load path for the tension through-bolts, with the resulting

compression along a diagonal path though the joint. A compression strut forms, and is relied upon to carry shear through the joint until it reaches its ultimate capacity. Crushing in compression would be expected at an angle inclined in the direction of the diagonal through the panel zone. Cracking would be expected along the diagonal as well.

Also important to note is that the concrete term used by Kanatani is proportional to the concrete cylinder crushing strength f'_c, as it is in the design of compression zones in reinforced concrete. Kanatani's concrete capacity is expressed as an (area) x (crushing strength) equation in which the area term represents the area of the strut in a plane perpendicular to the load path diagonally through the joint (Figure 4.6). The shear term for concrete is based on resolving the components of tee contact against the tube into the direction of the strut.

4.3.2 ACI-ASCE Committee 352 Term for V_c

In reinforced concrete joint construction, the joint type defined for use in situations prone to high load and displacement cycles in the inelastic range is referred to as a type 2 joint. According to ACI-ASCE Committee 352, the concrete contribution to shear strength within the panel zone of a reinforced concrete connection with a well confined core, is taken as V_c, as seen in Equation 4.1. Meinheit and Jirsa (1981) concluded that connection geometry had no influence on the shear strength of the joint as long as the shear area remained constant, so the term V_c includes only the shear area with no geometric parameters. The coefficient C in the V_c term is to be taken as 20 for interior type

2 joints, and this assumes units of: lbs, psi, and inches. If kips and ksi are the units used, the coefficient C is taken to be 0.63.

$$V_c = C\sqrt{f_c'}b_e h \qquad (4.1)$$

$C = 0.63$ when units are: kips, ksi, and in^2

$C = 20$ when units are: lbs, psi, and in^2

In Equation 4.1, the terms b_e and h refer to the cross sectional dimensions of the square concrete interior. This concrete term was also adopted by the ASCE Task group for composite connections, so it is used here as a benchmark. In contrast to the Kanatani model, the concrete contribution is proportional to the square root of the concrete strength. The methodology used in the development of this equation was based on the average shear stress on the plane when peak shear capacity of the joint is reached. Shear strength of concrete has been shown to vary with the square root of the concrete strength because of its relationship to the tensile strength of concrete, so this forms the basis for the joint strength recommendations presented by both ACI/ASCE 352 and the ASCE Task group for composite connections.

4.3.3 Relationship Between V_c and f'_c for CFTs

The CFT system studied in this research presents a situation where the relationship between f'_c and the concrete contribution to strength is not so evident. For composite joints, the ACSE Task Group proposed that the term *Vc*

is directly proportional to the square root of f'_c and the horizontal shear area within the joint. Kanatani's research was based on a strut model for the concrete, in which the effective strut is based on known exterior geometrical properties of the joint and area of tee contact. The idealization of the strut depends on the loaded area dimensions and the inclination of the formed strut. In effect, both models assume that a strut mechanism has formed at failure, but use different equations to represent the capacity of the joint in which the strut forms. Finding an appropriate relationship between concrete strength and the shear strength of the joint is the primary concern. Adjustments for additional variables, such as slenderness (b/t) of the steel tube, will be addressed in a following chapter after the consideration of additional test data from full-scale connections.

The concrete terms from the ASCE and Kanatani models are presented for comparison in Table 4-2. The concrete contribution predicted by the two models is vastly different. Both models significantly underestimate the amount that the concrete contributes to the joint shear strength in the specimens in this program. Kanatani underestimates the role of the concrete by a factor of over 3 in some cases. The ASCE model underestimates the concrete contribution by as much as a factor of 2 in some cases. The cases with the largest difference are the Series B tubes, which had a lower steel tube slenderness compared to the other specimens.

Table 4-2 - Comparison of Concrete Predicted Strength

Specimen	$V_c = V_{max} - V_s$ (tests)	V_c (Kanatani)	V_c (ASCE)	f'_c (ksi)
8.6A	143	58	89	6.2
8.8A	139	58	89	6.2
8.6B	174	54	83	6.1
8.8B	177	54	83	5.9
8.PC	90	37	72	3.9
8.P2C	114	56	88	5.9

To understand the relationship between the concrete term V_c derived from experiments and varying powers of f'_c, a log-log plot of V_c versus f'_c is shown in Figure 4.7. In this plot, data points for 8.8A, 8.PC, and 8.P2C were used. They represent specimens of constant b/t=32, using three different concrete compressive strengths of 6.2, 3.9 and 5.9 ksi, respectively. Specimen 8.6A was not added to the data because it was nearly identical in its test results to 8.8A, and its addition would have unfairly weighted the results for the 6.2 ksi case.

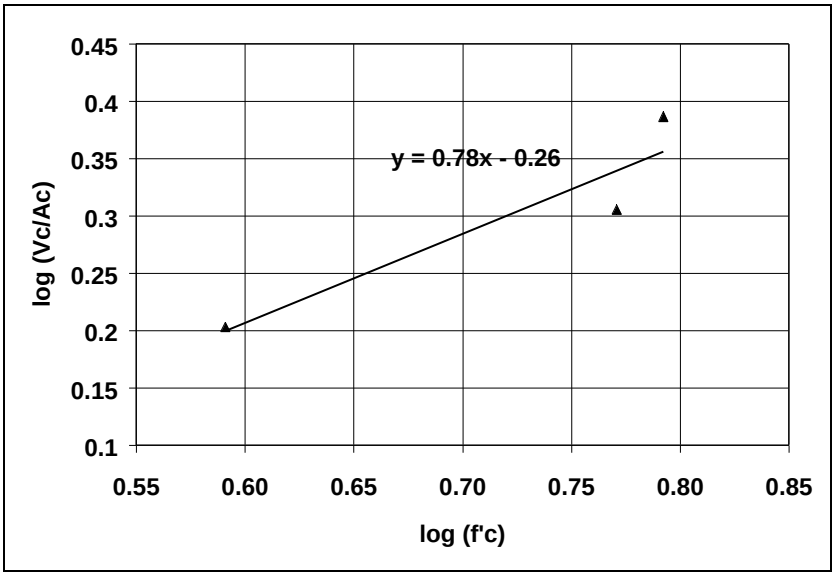

Figure 4.7 – Log-Log Plot of Vc Versus f'c for Specimens with Constant b/t=32.

From the slope of the regression line through the small sample of data of tubes with the same b/t=32, the power of 0.78 would be applied to f'_c in the calculation of shear strength of the concrete within the CFT panel zone. For simplicity, a power of 0.8 will be used initially on the term f'_c in the subsequent analysis.

4.3.4 Trial Models

In the preceding analysis, a power of 0.8 for f'_c was obtained based on the data, but the three data points used to arrive at a power of 0.8 are insufficient to extrapolate with confidence the range of possible cases. As a starting point in the development of a useful model, a few equations will be used and compared for the cases of CFT specimens presented above. The equations that will be tested are: the Kanatani model, the ACI concrete term V_c added to a proposed steel

term V_s (Eq. 4.2), and two newly proposed equations (4.3 and 4.4) that are based on results gathered so far.

Equation 4.3 is based on $f_c'^{0.8}$. A coefficient of 0.54 for units of ksi, and 2.1 for units psi, was calibrated to the test data by averaging the results of the Series A and Series C concrete terms to arrive at $V_{calc} / V_{test} = 1$. The curve fit was done only for three specimens of varying concrete strength, but with the same b/t. Because there were only two specimens in series C with different concrete strengths (the two reference specimens), using more than one of the series A specimens in the curve fit would have unfairly weighted the results toward the series A case, and all three tube in series A had the same results. For the purposes of this initial analysis, d_{fl} is defined based on the actual measured flat steel panel width of the test specimens. This could be further refined to relate the effective tube web depth to the tube thickness for the purpose of design.

$$V_s = 2 \times 0.6 d_{fl} t F_y \tag{4.2}$$

where d_{fl} is the depth of the flat portion of the steel tube.

$$V_n = V_s + 0.54 A_c f_c'^{0.8} \tag{4.3}$$

where f_c' is in units of ksi,

and $A_c = (d - 2t)^2$, or

$$V_n = V_s + 2.1 A_c f_c'^{0.8}$$

when units of psi are used

Equation 4.4 is based on the square root of f'_c., a formulation similar that used in the ASCE Task Group composite joint recommendations. By fitting test data in a similar manner to that done for 4.3, coefficients of 0.9 (for ksi) and 28 (for psi) are used.

$$V_n = V_s + 0.9A_c\sqrt{f'_c} \qquad (4.4)$$

where f'_c is in units of ksi, or

$$V_n = V_s + 28A_c\sqrt{f'_c}$$

when units of psi are used.

Figure 4.8 shows the comparison between the four equations to the test data. The bar chart is normalized by the maximum value of shear obtained for each specimen in the tests. There appears to be little difference between the results of equations 4.3 and 4.4 based on the sample of tests. It is interesting to note that although the terms for V_c between the Kanatani model and the ASCE model vary significantly (refer back to Table 4-2), similar joint shear strengths are obtained. Although Kanatani's equation underestimates V_c, his equation overestimates V_s (by using the full depth of the tube minus the flange thicknesses for the steel shear contribution).

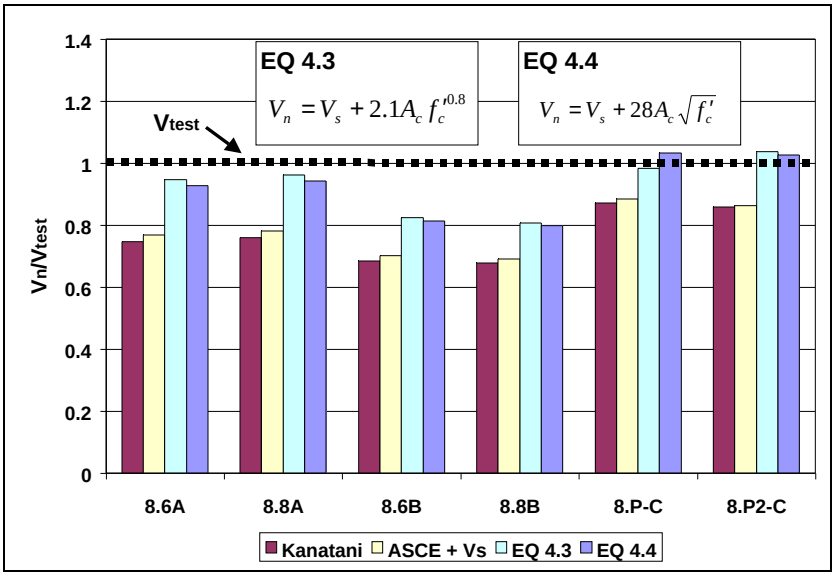

Figure 4.8 - Equations Compared to Normalized Test Data

Table 4-3 - Four Equations Normalized to Test Data (NORM=V_{calc}/V_{test})

Specimen (actual V_{max})	**Kanatani V_{max}**	**NORM**	**ACI V_c (4.1) + V_s (4.2)**	**NORM**	**EQ 4.3**	**NORM**	**EQ 4.4**	**NORM**
8.6A (**241 k**)	180	0.75	185	0.77	213	0.95	209	0.93
8.8A (**237 k**)	180	0.76	185	0.78	213	0.96	209	0.94
8.6B (**319 k**)	218	0.68	224	0.70	249	0.82	246	0.81
8.8B (**322 k**)	218	0.68	222	0.69	247	0.81	244	0.80
8.PC (**203 k**)	177	0.87	179	0.88	190	0.98	198	1.03
8.P2C (**227 k**)	195	0.86	196	0.86	221	1.04	219	1.03
Average		**0.77**		**0.78**		**0.93**		**0.92**

The results are also tabulated and presented in Table 4-3. Equations 4.3 and 4.4 appear to best fit the data. The same models will be tested on full-scale connection specimens to determine the validity of the model across the entire range of the testing program to-date. All four models are notably more conservative when analyzing the Series B tubes, which had the lowest of the two *b/t* ratios in the testing of the panel-zone specimens.

4.3.5 Effect of *b/t* Ratio

Questions remain, then, as to the effect of a relatively lower *b/t* ratio on the ability to enlarge the effective strut, and/or to aid in confining the concrete. The *b/t* ratio and its possible effects on confinement must now be looked at in order to address the issue of the variation between the tubes of Series B and the others. It is suggested that *b/t* has an effect on the term V_c because when the specimens in the A series are compared against specimens in the B series (refer back to Table 4-2), in which similar strength concrete was used, there was a significant difference in the contribution of the concrete interior. Series B had a 30% increase in V_c over that of Series A when only the b/t had changed. Because the same nominal strength concrete was used in both series, the *b/t* of the steel must have had some beneficial effect on the concrete.

It was observed in the tests on the specimens of Series B, that localized bearing distress was not as evident as it was for the specimens of Series A. Series A specimens, and most notably specimen 8.4A, had a pronounced indentation into the side of the steel tube. If the mechanism of joint shear failure is characterized by the formation of a strut through the core, then a widening of the

effective loaded area on the concrete due to the added stiffness of a stockier steel tube may explain an increase in the overall strut strength within the column. Due to the limited amount of data available, namely only two b/t ratios to choose from, and only one concrete strength used in that comparison, a study of the *b/t* will be handled in the subsequent chapter where additional data from the full-scale connection tests may be incorporated into the analysis.

One more important observation regarding the effects of slenderness on the shear carrying capacity of the steel tube is that the tubes of Series A and C experienced some buckling toward the end of the test, but this buckling did not appear to result in any reduction in the strength of the CFT system. Buckling was limited by the stiffening effect of the encased concrete. High slenderness (*b/t* ratio) does not appear to reduce the stability of joints in the CFT systems studied here.

4.3.6 Variation of the Tee Width Against the Tube

Within Series A and B, tests were conducted to examine how changing the "tee width" changed the failure mechanism or load carrying capacity. Although localized distress was most severe for the smallest loading area (8.4-A, *b*=50%), the ultimate load carrying capacity was virtually unchanged between specimens. For specimens in Series A, B and C (with the exception of the "cut-out" specimens), failure was observed to include a combination of significant panel-zone shear distress in both the steel and concrete, and localized bearing failure at the location of the reaction blocks against the steel tube surface. Bearing distress was less severe in the Series B specimens, in which the b/t ratio

of the tube wall was 21 compared to the Series A b/t ratio of 32. This supports the theory that the *b/t* ratio had an effect on the widening of the loaded area, and thus widened the effective strut. Flexural yielding of the tube just outside of the panel zone was observed in all of the above specimens. In addition to visual inspection of the exterior, specimen 8.4-A was carefully examined by removing the steel from around the joint region. Concrete crushing due to flexural compression was not apparent or obvious. Most of the concrete was left intact, with small diagonal crack patterns and localized indentations in the concrete due to high bearing stresses from the reaction blocks.

Within series A and B, changing the area of the reaction blocks did very little to change the ultimate load at failure (Table 4-4). Although bearing distress was more severe with the smaller area, the load carrying capacity was not changed. Specimens 8.4B and 8.6B carried the same load, and 8.8B was only 1% higher than the two. Confinement likely helped limit degradation due to crushing at the bearing location in Series B. The panel zone tests within series A and B did not develop full plastic hinging outside of the panel zone. Specimen 8.MB, which was tested in center point flexural loading to determine the plastic moment capacity of the Series B specimens, reached a maximum moment of 180 k-ft. The maximum moment carried by the specimens of Series B was 158 k-ft, which is 88% of the measured flexural capacity of 8.MB. All specimens of Series B were deformed to reach peak loads. The load dropped in subsequent cycles at larger deformations indicating that peak load was not limited by the stroke of the test apparatus.

Obvious visible distress around the panel zone, accompanied by large indentations near the points of loading also showed that panel-zone shear was contributing to inelastic deformation. Failure of the panel zone specimens was due to a combination of shear and bearing, and not by plastic hinging.

Table 4-4 - Series A and Series B Results

Specimen	V_{Max} Kips	M_{Max} k-ft
8.4-A	233	117
8.6-A	241	121
8.8-A	237	119
8.4-B	313	157
8.6-B	313	157
8.8-B	316	158

4.4 Summary of Panel-Zone Analysis

The panel zone tests provided the opportunity to isolate a few key variables. Based on the results so far, Equations 4.3 and 4.4 work equally well, so it is proposed that equation 4.4 be used for the basis of further analysis on the panel zone. Of the two equations, Equation 4.4 uses a V_c term that closely resembles that used in practice for composite joints, so it resembles something already familiar to engineers. The only difference is a slight increase in the coefficient *C*. As with the AISC treatment of the shear panel, the flanges of the steel tube are neglected in the equation. Krawinkler (1975) noted that, in the AISC treatment of structural steel columns with varying flange thicknesses, relatively large beam flanges can contribute noticeably to the horizontal shear strength of the column. Rectangular steel tube columns, by virtue of their

geometry, have the same relative flange thickness in all cases. Analysis of the cross-section of a steel tube shows that including the shear due to flange yielding in design calculations will add only 3% to the calculated shear strength of the steel. It is for this reason that the the flange contribution to the steel term is omitted.

The panel zone tests showed that:

1. Varying the contact width of the reacting blocks against the CFT from 50% to 100% of the tube depth had no effect on the capacity of the panel-zone.
2. Varying the *b/t* ratio of the steel tubes served to reduce the bearing stress against the concrete behind the tube wall. The beneficial effects of *b/t* need further study.
3. The failure of the panel-zone was the result of a combination of shear yielding in the steel, bearing failure at the location of the reacting blocks, and some cracking within the concrete core.
4. Failure was not governed by the plastic moment capacity of the section.

The panel-zone specimens were scaled by 50% compared to the actual connection specimens. It is important to note that the linear scaling of the tee dimensions actually resulted in a more severe bearing stress condition against the face of the column for the half-scale specimens because stress is related to area. The area of contact was reduced by the square of the linear scaling of the contact width. Bearing crushing was evident, but it is safe to assume that the extent of crushing, if any, would be not as severe with the full-scale specimens

because the stress of contact would be _ of that experienced in the half-scale panel-zone specimens.

5. Tests on Full-Scale Connections

5.1 Description of Tests

The purpose of the remaining full-scale connection tests was to calibrate information gathered from the panel zone tests using large scale moment connections. Split-tee through-bolted moment connections with no shear tabs or diaphragm-like stiffeners were tested (See Figure 5.1). The moment connections in this series of tests were cruciform type beam-to-column specimens, in which the assumed inflection points for the beams and columns of an actual building were the basis for choosing the width and height of the specimens (Figure 5.2).

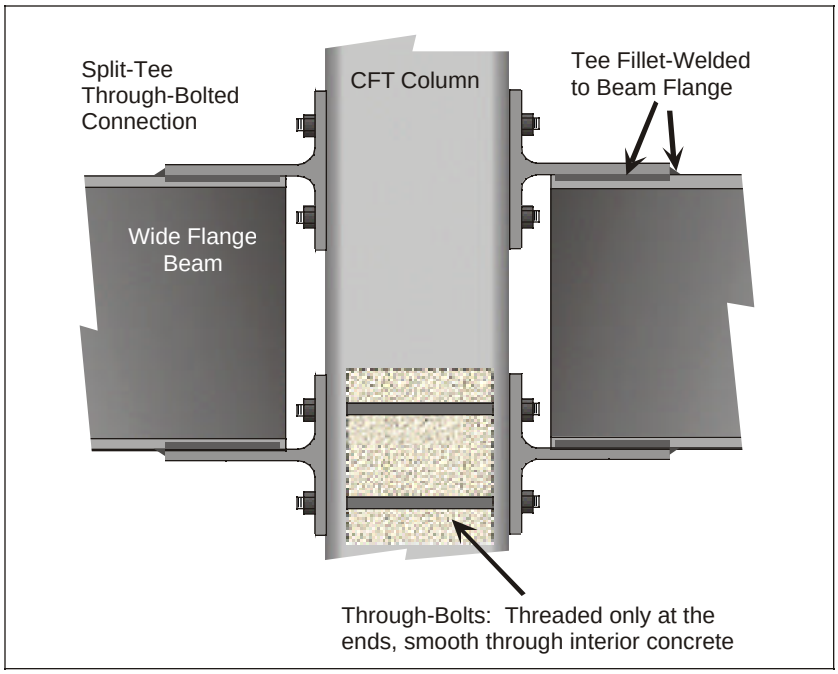

Figure 5.1 - Split-Tee Through-Bolted Connection

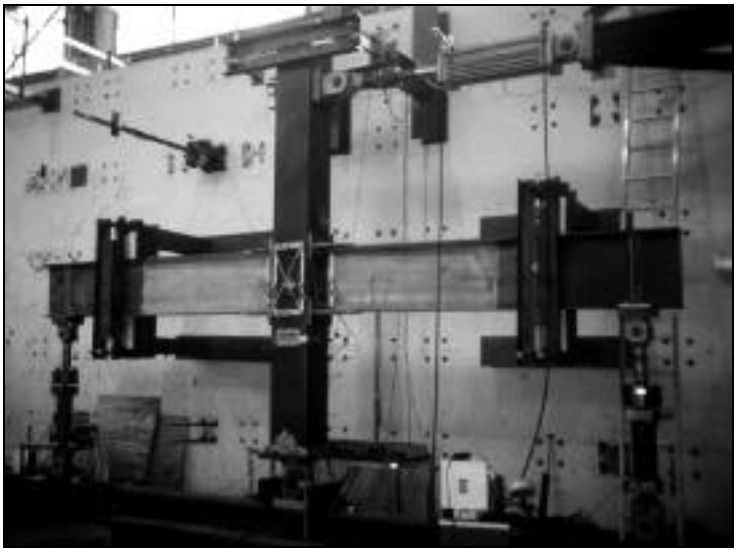

Figure 5.2 - Cruciform Shaped Specimen in Test Setup

The contact loading area of the beam flange forces against the tube walls (tee width) was the primary variable. Two specimens were designed to develop panel-zone failures. Although panel-zone failure is not the design objective for moment connections in an actual structure, the results were useful in understanding how well joint strength would be predicted using the equation developed in Chapter 4. Knowledge gained from such an investigation will help quantify the panel zone strength, which in turn will provide valuable guidance in the drafting of design guidelines and building code recommendations.

5.2 Specimen Descriptions and Details

The test series of six CFT moment connection specimens is comprised of four 12 inch square CFT connections, and two 16 in. CFT connections. All six specimens utilize the same connection design, but vary in their connection

component dimensions. Specimens CFT.5 and CFT.6 more closely resemble the Lehigh specimens in their overall dimensions. The column height used for all six specimens was held constant at 12 ft so that the same test setup could be used for all six tests. The beam spans for CFT.1 through CFT.4 were based on their scale relative to the full-scale specimens CFT.5 and CFT.6. Thus the beam span for CFT.1 through CFT.4 was 15 ft., and 20 ft. for CFT.5 and CFT.6. The dimensions and material properties of the full-scale CFT specimens are shown in Table 5-1.

Table 5-1 – Measured Properties of Concrete-Filled Tube Sections

Specimen	Square CFT (in.)	Concrete f'_c (ksi)	Steel Tube Properties		
			Fy (ksi)	*Fu* (ksi)	% Elongation
CFT.1	b = 12 t = 0.45	7.2	53.1	60.4	25.8
CFT.2		7.2			
CFT.3		7.3			
CFT.4		7.4			
CFT.5	b = 16 t = 0.472	7.14	57.6	70.3	41.0
CFT.6		7.14			

5.2.1 12” x 12” CFT Connections

The four 12 in. square CFT specimens were designed based on scaling the 16 in. CFT specimens by _. The beam depths were also appropriately scaled. The 12 in. tubes were used because they were donated to the project. Four 12 ft. sections were cut from the same steel tube stock.

5.2.2 16” x 16” CFT Connections

Two full-scale CFT moment connections were designed and constructed similar to specimens tested at Lehigh University (Ricles et al, 1997). Specimen CFT.5 is based on Lehigh specimen number 6, and has similar dimensions for the

CFT and all of the connection components. Specimen CFT.6 was designed with a smaller tee width on the face of the column. CFT.6 was designed to examine the effect of narrowing the tee width, while preserving the same beam and column properties as those used in CFT.5.

5.2.3 Beam Sizes

Beam sizes used for all six specimens are shown in Table 5-2. Beam sizes used for the 12 in. CFT specimens were W18s. W18 x 46 beams were used in specimens CFT.1 and CFT.2 to allow the beams to form plastic hinges. W18 x 65 beams were chosen to produce panel-zone failures in specimens CFT.3 and CFT.4. The amount of over-strength in the design choice of the W18 x 65 beams assured that minimal inelastic deformation would occur in the beams, and that the connection would develop inelastic deformations at locations other than the beams. Deformation of the panel-zone and connecting elements is the assumed method of energy dissipation. Typical design requires a strong-column / weak-beam failure mechanism; however, testing the converse provides insight into the strength of the components that should remain robust.

For CFT.5 and CFT.6, W24 x 68 beams were used. These beams were chosen based on their ability to achieve plastic hinges during earlier tests at Lehigh University. Both specimens were designed to fail through inelastic beam rotation near the face of the column, a failure mode consistent with current practical design methods.

Table 5-2 - Wide-Flange Beam Properties

Specimen	Beam Size (AISC)	Beam Flange Properties		
		F_y (ksi)	F_u (ksi)	% Elongation
CFT.1	W 18 x 46	55.0	74.4	25.0
CFT.2				
CFT.3	W 18 x 65	53.2	74.9	21.2
CFT.4				
CFT.5	W 24 x 62	56.4	72.9	25.3
CFT.6				

5.2.4 Structural Tees Used

Structural tees and tee-to-beam details are presented in Appendix C along with as-built dimensions and hole patterns. The dimensions of the structural tees are shown in

Table 5-3. Structural tees were torch-cut and surface prepped with a grinder. Holes were drilled using a drill press. The tees for specimens CFT.1 through CFT.4 were over-designed to ensure that failure would not occur in the tee. For all specimens except for specimen CFT.5, the tees were cut rectangular such that the full width of the tee extended to the end of the tee stub. The entire stub was welded to the beam flange (Refer back to Figure 5.1). For CFT.5 the tee stub was cut such that the width tapered in size from the 15 in. width against the column face to the 7 in. flange with of the beam. This was done to maintain a similar design between CFT.5 and Lehigh specimen number 6.

Table 5-3 – Measured Dimensions of Split Tees

Specimen	h (in.)	w (in.)	w (%b)	t_f (in.)	t_w	L	taper to	# of bolts
CFT.1	11.25	10	83	1.19	0.75	12	n/a	4
CFT.2	11	8	67	1.38	0.88	12		
CFT.3								
CFT.4	11	9	75	1.38	0.88	11.5		
CFT.5	9.25	15	94	1.19	0.69	16	7	7
CFT.6	9.5	9	56	1.88	1.06	13.5	n/a	5

5.2.5 Through Bolts

Through-bolts used in the moment connections were made from Grade B7 (ASTM A193) smooth stud stock, and were threaded only at the ends. Threading the bars only at the ends allowed slip between the rods and the inner concrete. This also allowed for a more direct transfer of bar tensile forces through the joint. Providing this mode of force transfer (minus interlock between the bar and concrete) was necessary for the development of the concrete compressive strut idealized in the theoretical model. Properties of the rods used for through bolts are listed in Table 5-4.

Table 5-4 - Through-Bolts Used and Tensile Strength of the Group Based on AISC LRFD Tables

Specimen	# of Bolts per Tee	Bolt Size (in.)	ΦF_t (kips)
CFT.1	4	1-1/8	336
CFT.2	4	1-1/8	336
CFT.3	4	1-1/4	416
CFT.4	4	1-1/4	416
CFT.5	7	1-1/8	587
CFT.6	5	1-1/4	520

5.3 Specimen Fabrication

Construction of the CFT moment connection specimens was completed in a series of steps that included: drilling of the tube sections, placement of either rods or PVC tubes into the holes in the bare steel tubes, placing and consolidating concrete, fastening tees to the tubes and beams, post-tensioning through-bolts, and welding tee stubs to the beam flanges.

5.3.1 Drilling of Tube Sections and Insertion of Placeholders

Prior to placing concrete into the steel tubes, holes had to be drilled for the through bolts. Rods (or placeholders) had to be inserted to leave a space in the concrete for the through bolts. A large stationary drill press was used to cut holes into the sides of the steel tube sections.

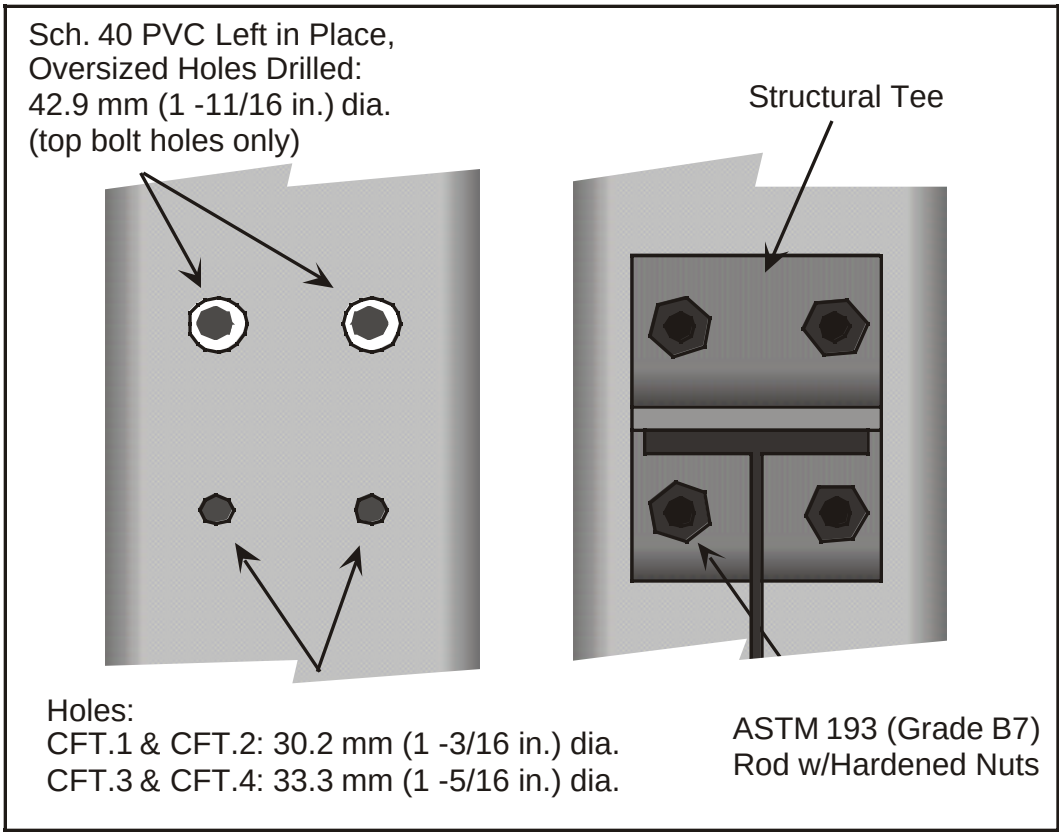

Figure 5.3 - Hole Pattern for Specimens CFT.1 through CFT.4

5.3.1.1 CFT.1 Through CFT.4

For the first four specimens, two methods of hole placement were used: (1) inserting PVC into oversized holes -- to be left in place during specimen assembly, and (2) casting the actual through bolts in place without using sleeves of any kind. It was decided to use a combination of these placement methods for all of the first four specimens (See Figure 5.3).

For the bottom tee bolt holes, the through rods were cast in place. For those hole locations, appropriately sized holes for the through bolts were drilled in the tube.

For the top tee hole locations, Schedule 40 PVC pipes were inserted into the bolt hole locations, and were intended to be left in place. The PVC had to have an inner diameter larger than the threaded rods used for through bolts. This required that the holes cut into the tubes at the upper tee location had to be large enough to accommodate the outer diameter of the PVC. For the top holes of all four specimens, holes measuring 1 11/16 in. were drilled into place. The holes for the top tees were oversized. The larger holes reduced the net-section, and led to a different failure mode during the testing of CFT.1. For subsequent tests, an additional plate was welded to the tee bearing surface of the CFT to prevent net section failures.

To prevent bending of the PVC due to the force of falling concrete, the rods for the upper tees were threaded through the PVC and tightened against the tube. O-ring seals were placed on all rods to create a water-tight seal between the holes in the steel tube wall and the rods or PVC pipes.

5.3.1.2 CFT.5 and CFT.6

For the full scale connections (CFT.5 and CFT.6), it was decided to use the same hole design used by Lehigh. In these specimens, PVC was placed prior to the concrete pour, but the PVC was removed after the concrete cured. To facilitate this, each PVC pipe was greased with axle grease, which had the proper consistency and high viscosity required to prevent its removal during concreting operations. Because this PVC would be removed after curing, the PVC outer diameter only needed to be slightly larger than the rods. A 1 in. Schedule 40 PVC, which had an outer diameter of approximately 1 5/16 in., was adequate to

provide ample, but not excessive holes for the bolts. Holes drilled in the tube were 1 3/8 in. in diameter. To prevent bending of the PVC rods due to the force of falling concrete, small temporary rods were placed through the PVC and tightened against the tube wall. Small rubber o-rings were placed to seal against water leakage from the fresh concrete between the PVC and the hole in the steel tube. The temporary rods were tightened against the steel tube, providing a tight seal with the o-rings.

5.3.2 Concrete

The CFT specimens were cast vertically, which required that the concrete be vibrated from the top, and down into the specimen as shown in Figure 5.4. Concrete was placed in lifts of just under 2 to 3 ft. at a time. A conventional concrete spud vibrator was used to consolidate the concrete, although it was impossible with the equipment available to adequately vibrate the lowest 3 ft. of concrete in the column. The panel zone and an adequate distance below it were well consolidated, even in the presence of through-rods. The vibrator was narrow enough to penetrate between the bars, and past the panel zone to the column below in all cases. After the concrete cured, the temporary PVC pipes of CFT.5 and CFT.6 were driven out with a sledgehammer.

Figure 5.4 - Filling the tubes with concrete (left), and vibrating (right).

5.3.3 Specimen Assembly

5.3.3.1 CFT.1 Through CFT.4

Because the rods for the lower tees were already cast in place, the lower tees were fastened to the columns first. The column was then placed into the test setup. The top tees were held in place to the top flanges of the beams using clamps. The beams were seated onto the bottom tees, which were already fastened to the CFT. Next, the top tee bolts were threaded through the connection and tightened into place. At that point, the specimen was in place, and final adjustments were made prior to welding the beams to the tees.

5.3.3.2 CFT.5 and CFT.6

Rods were threaded into the bottom tee holes of the CFT column, and the lower tees were fastened. The column was then placed into the test setup. The top tees were held in place using clamps to the top flanges of the beams, and then the beams were seated onto the bottom tees, which were already fastened to the CFT. Next, the top tee bolts were threaded through the connection and tightened prior to welding.

5.3.4 Post-tensioning

The through-bolts were post-tensioned with a pneumatic impact wrench, and were tightened using a turn-of-the-nut approach. The through-bolts were tightened to 2/3 turn each.

5.3.5 Welding

Beams were welded to the tee stubs using E7018 shielded metal arc welding. Placement detail of the welds is shown in Appendix C. The throat thickness of the welds varied between 3/8 in. and 5/8 in., depending on the available material thicknesses of the tee stubs, but the welds were very conservative in design, and were over designed in most cases.

5.4 Test Setup

The test set-up is shown schematically in Figure 5.5. The base of the test setup was anchored to the rigid reaction floor, and the hydraulic ram was anchored into the adjacent reaction wall. Cyclic loads were applied to the top of the column, while the base of the column was allowed to rotate about a pin

support that was anchored to the floor. Beams were attached to rigid links, which were allowed to rotate in-plane at their ends. The rigid links used for the beam-end supports were constructed as turnbuckles, which allowed for fine adjustments during the placement of specimens into the setup, and also allowed a change in height when the beam sizes changed.

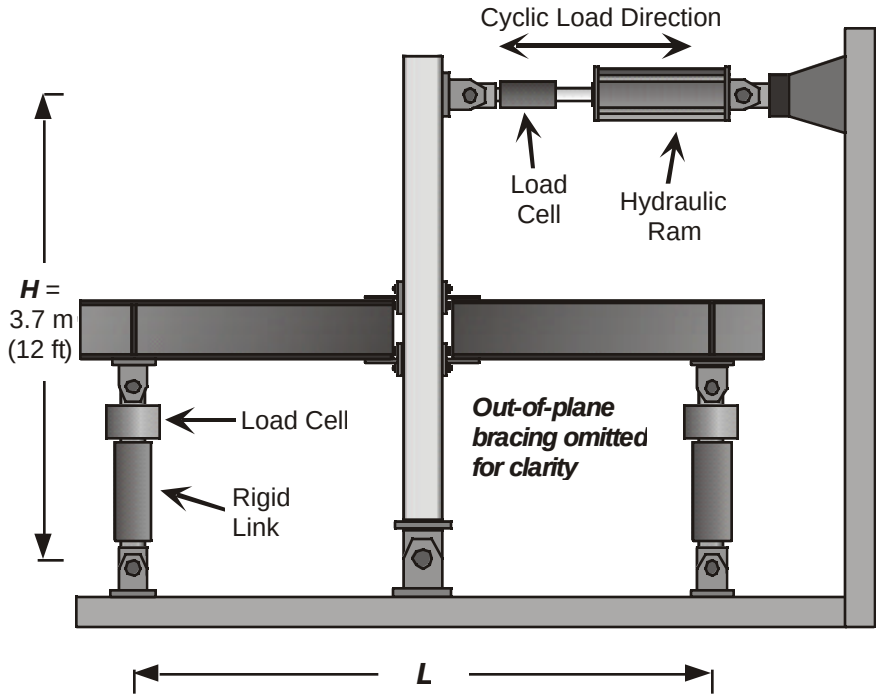

Figure 5.5 - Test Setup for Full-Scale Specimens

5.4.1 Loading System

Load was applied to the top of the CFT column using a 300 kip hydraulic ram (see Figure 5.6). An electric motorized pump with a handheld control for both advancement and retraction of the ram was used to drive the loading

system. Loading was done in both tension and compression with the ability to hold constant load at each load increment, and to quickly reverse loading direction.

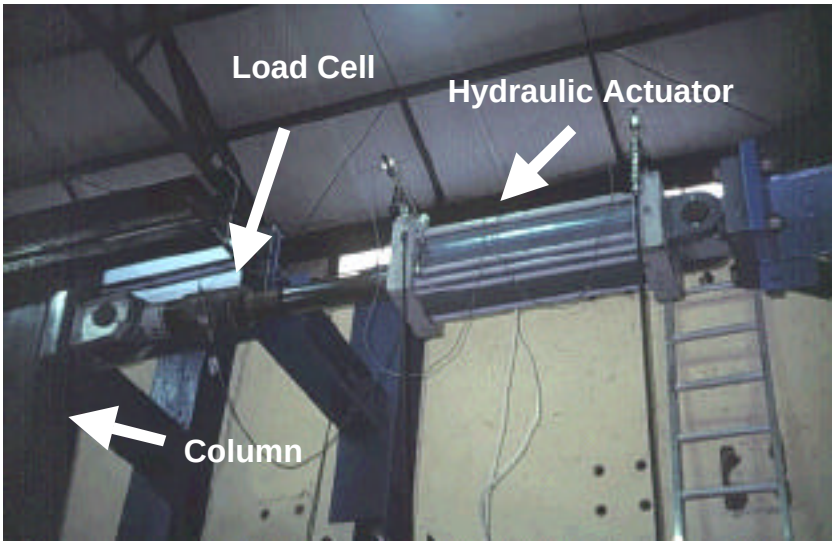

Figure 5.6 - Loading System: Ram Applied to Column Top

5.4.2 Measurements and Data Acquisition

Data were recorded for both loads and displacements, and stored in a PC using data acquisition software. Data channels were scanned at predefined displacement increments throughout the loading history (for Displacement History, see Section 5.5).

5.4.2.1 Load Data

Load cells and pressure transducers were used to monitor load, with the exception of specimen 6, in which only load cells were used. Three load cells were used to capture load data for each specimen. One load cell was positioned in-line with the hydraulic ram, which was positioned perpendicular to the

specimen (see Figure 5.5). The remaining two load cells were positioned in-line with the rigid links that supported the beam-ends.

Two pressure transducers were attached to the hydraulic ram near the point of entry into the ram. The pressure transducers measured pressure for each direction of loading.

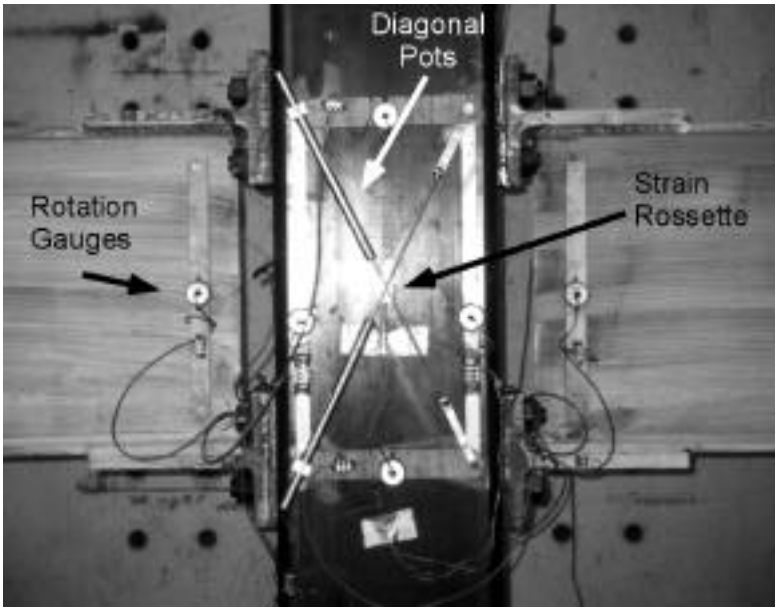

Figure 5.7 - Panel Zone Instruments

5.4.2.2 Displacement Measurements

Measurements were obtained for both the distortion of the panel zone, and for the global member displacements of each specimen. Within the panel zone, three types of measurements were taken: (a) linear displacement transducers along the panel-zone diagonal, (b) rotational gauges along all four edges of the panel zone boundaries, and (c) strain rosettes. Linear pots were used in conjunction with rotational gauges for the purposes of comparison, and

for data redundancy. Data from both types of instruments can be used to obtain the angle change, or shearing distortion, of the panel zone. This angle change was measured as the deviation from its original rectangular shape. Strain rosettes were used to obtain the strain within the center of the panel zone at the surface of the steel.

The linear pots and the strain rosettes were placed on both sides of each specimen. Rotation gauge measurements were only taken one side of each specimen. Readings from all panel zone measurements of differing specimens were used to compare the degree to which the steel was mobilized when the panel zone was subject to severe loading. Other measurements included: drift measurement of the column tip, rotations at the base and tip of the column, beam-end displacements, and rotations of the beams.

5.5 Testing Procedure

Testing of the CFT specimens was displacement controlled. The displacement history shown in Figure 5.8 was based on values of inter-story drift (% ISD), and was used consistently throughout the testing of all six CFT specimens. An identical displacement history was used at Lehigh University for the purposes of comparing test results. The displacement measurement of the top of the column was used to determine inter-story drift. The load actuator (ram) was controlled by hydraulic pressure, and load was held at each load increment momentarily prior to data collection to reduce dynamic effects.

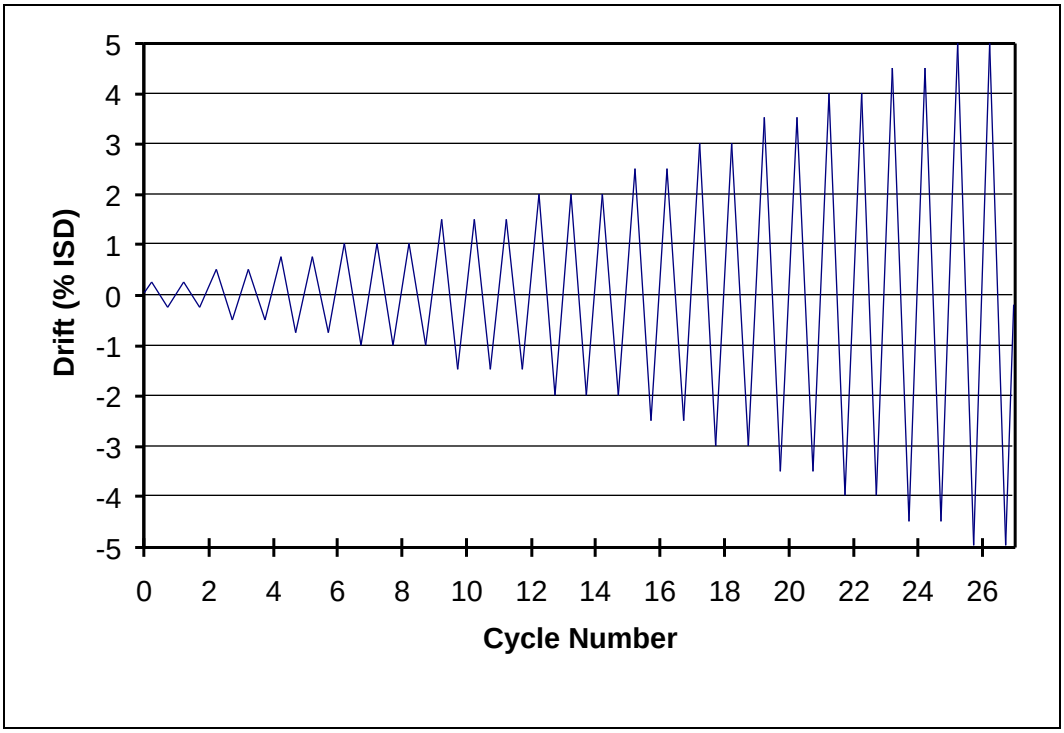

Figure 5.8 - Displacement History

Drift levels used were: 0.25, 0.5, 0.75, 1.0, 1.5, 2.0, 2.5, 3.0, 3.5, 4.0, 4.5, and 5.0 percent inter-story drift. To determine the stability of the hysteresis curves, cycles were repeated at each cycle. Cycles 0.25% through 0.75%, and 2.5% through 5.0% were conducted twice each. Cycles 1.0% through 2.0%, the cycles in which the onset of inelastic behavior was observed, were run three times each.

6. Application of Model to Full-Scale Connection Tests

6.1 Description of Tests

Test were conducted on six full-scale CFT moment connection specimens, four 12 inch CFTs and two 16 inch CFTs. Steel wide flange beams were connected to square concrete-filled tube columns using the split-tee through-bolted connection. The cruciform-shaped specimens were tested using quasi-static reverse cyclic loading under displacement-controlled conditions. Specimens were progressively loaded to increasing levels of drift until either: (a) significant failure made it necessary to halt the test, or (b) the specimens reached a level of 5.0% inter-story drift. The sections that follow will document the behavior during each test, and test data will be discussed.

6.2 12 inch CFT – Results

The first four specimens of the full-scale moment connection tests consisted of square CFTs measuring 12 inches on each side. The first two of these specimens were designed to fail primarily with the hinging of beams just outside of the connection region. The remaining two specimens were designed to fail within the panel-zone, with only minor yielding in the beams near the connection.

6.3 CFT.1

Test specimen CFT.1 was designed to fail by plastic beam rotation near the connection, just outside of the tees. Up to 4.5% drift, the connection of CFT.1

was able to maintain integrity. Prying of the tees from the face of the CFT was observed at around 1.5% to 2% drift. From that point forward, elongation of the bolts due to this prying action was observed. Due to unexpected over-strength of the beam sections used in the actual specimens, complete plastic hinging of the beams was not achieved, although a significant amount of plastic deformation was observed in the beam flanges and a small portion of the web. Test specimen CFT.1 was taken to 4.5% drift (Figure 6.1), and then testing was halted when the steel tube failed at a section through the top bolt holes (see Figure 6.2).

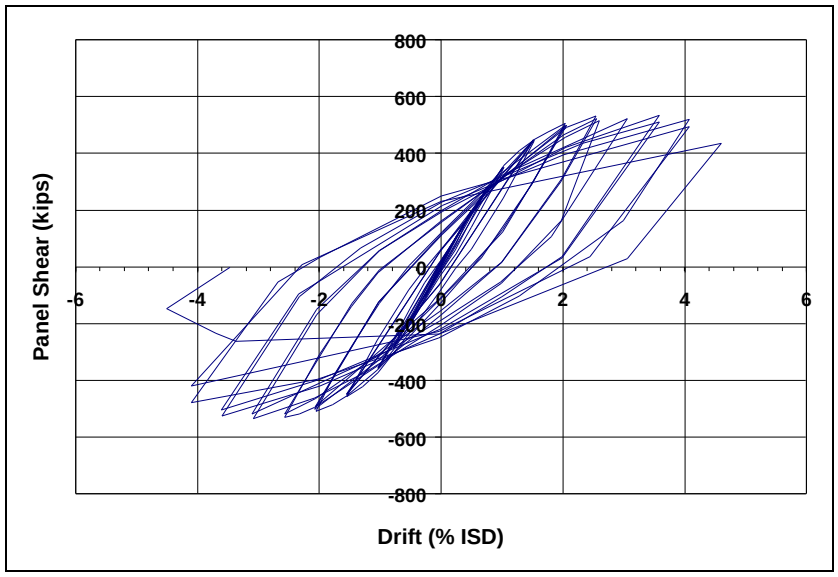

Figure 6.1 – Specimen CFT.1 Load-Displacement Curve

Shear vs. Panel Distortion for CFT.1 is not presented because of problems with the instrumentation. In addition, the placement of panel displacement transducers was modified for subsequent tests.

6.3.1 Net-section Fracture

Fracture on the net section of the steel tube section near the upper-bolt holes of the connection occurred because of an error in strength calculations. The upper-bolt holes were oversized significantly, compared to the lower-bolt holes because two different bolt thread schemes were used (refer back to Figure 5.3). The larger bolt holes reduced the section enough to cause fracture of the net section when the column was subjected to moment. It was apparent after inspection that the failure mode for CFT.1 transitioned from inelastic beam deformation to yielding and fracture of the CFT net section near the upper-bolt holes (Figure 6.2 and Figure 6.3).

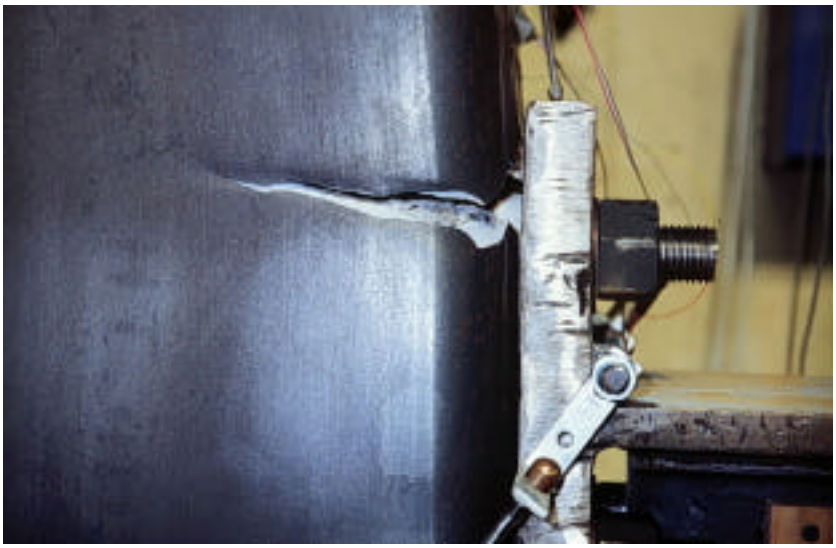

Figure 6.2 – Net Section Fracture on Top Tee Bolt Line

Figure 6.3 – Fractured Column with Beams Removed

6.3.2 Increase in net-section for remaining 12 inch CFTs

Because identical bolt hole schemes were used in the production of specimens CFT.1 through CFT.4, it was necessary to devise a strengthening scheme to prevent the same kind of failure from occurring in subsequent tests on the remaining 12 inch CFT specimens. Failure of the net section of the steel tube is a mode associated with flexure, so the aim was to devise a fix that would enhance the flexural properties of the specimen, but to not interfere with the shear properties of the panel zone. It was decided to add 3/16" (4.76 mm) thick steel plates to the flange area of the CFT tube wall, and to extend the plates from the top of the top tee to the bottom of the bottom tee. Adding such plates would increase the flexural capacity in the zone of the large bolts holes to a value just above the flexural capacity of the zone around the standard smaller bolt holes. Because the yielding of the tube flange in flexure only requires a value of shear between 3 and 4% of the shear needed to deform the panel, and since this

additional thickness represents an additional 38% added to the thickness of the tube flange, the effect of this addition on the behavior of the panel in shear could be neglected.

6.4 CFT.2

After enhancing the net-section of the remaining three 12" CFT specimens, testing of CFT.2 progressed all the way to 5.0% Inter-Story Drift (ISD) (the planned termination point of the test) without net section failure (Figure 6.7).

6.4.1 Beam Behavior

Flange yielding of the beams initiated near 1.0 % drift. At 2.0% drift, flange yielding near the beam / tee junction was most noticeable (Figure 6.4). Yielding of the beam sections continued throughout the remainder of the test, until approximately 80% of the beam web had yielded (Figure 6.5). Buckling of the beam web accompanied beam yielding by the end of the test.

Figure 6.4 – Specimen 2 Beam Yield Pattern at 2.0% Drift

Figure 6.5 – Specimen CFT-2, Beam Web at 4.5% Drift

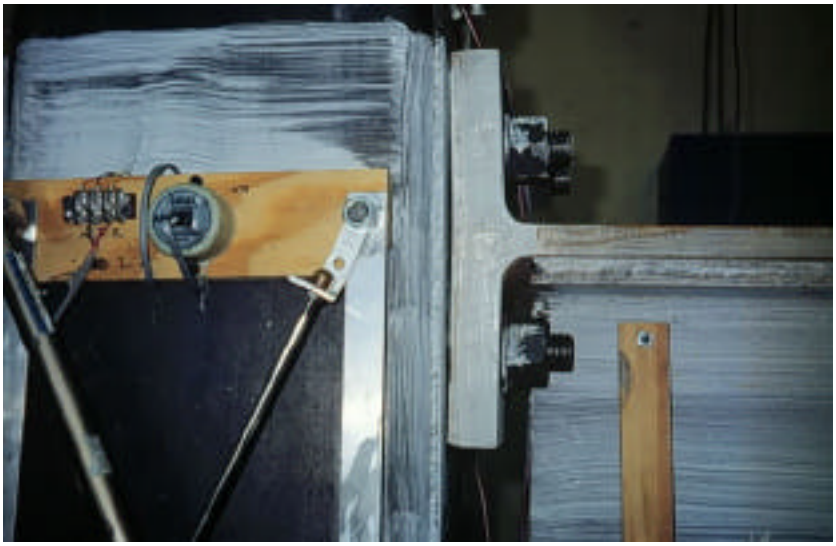

Figure 6.6 – Initiation of Tee Prying around 2.0% Drift

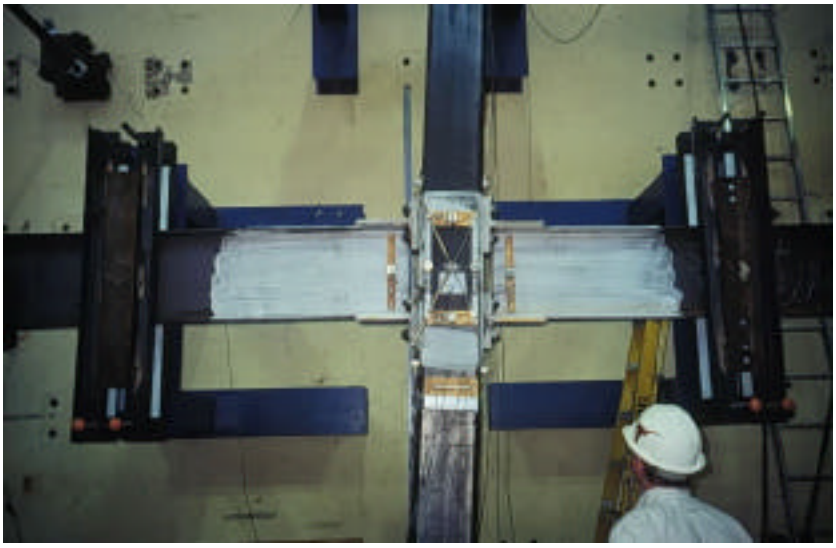

Figure 6.7 – Specimen CFT-2 at conclusion of test: 5.0% Drift

6.4.2 Bolt/Tee Behavior

At 2.0% drift, the tees began to pry away from the column face (Figure 6.6). At increasing levels of story drift, tee prying progressed to the point of complete separation of the tee surface from the column face. It should be noted that this behavior was observed for the top-flange tees only, and occurred above 3.0% drift. The addition prying of the top tee can be attributed to the geometry of the test setup as shown in Figure 6.8. The top beam flanges and tees experienced larger tensile forces than the bottom flanges and tees because rotation of the beam supports caused significant additional tension to develop in the top beam flanges. When the tensile force in the beam support is added to the tensile force "T" due to beam moments, the result is greater tension to develop in the upper tees than in the lower tees.

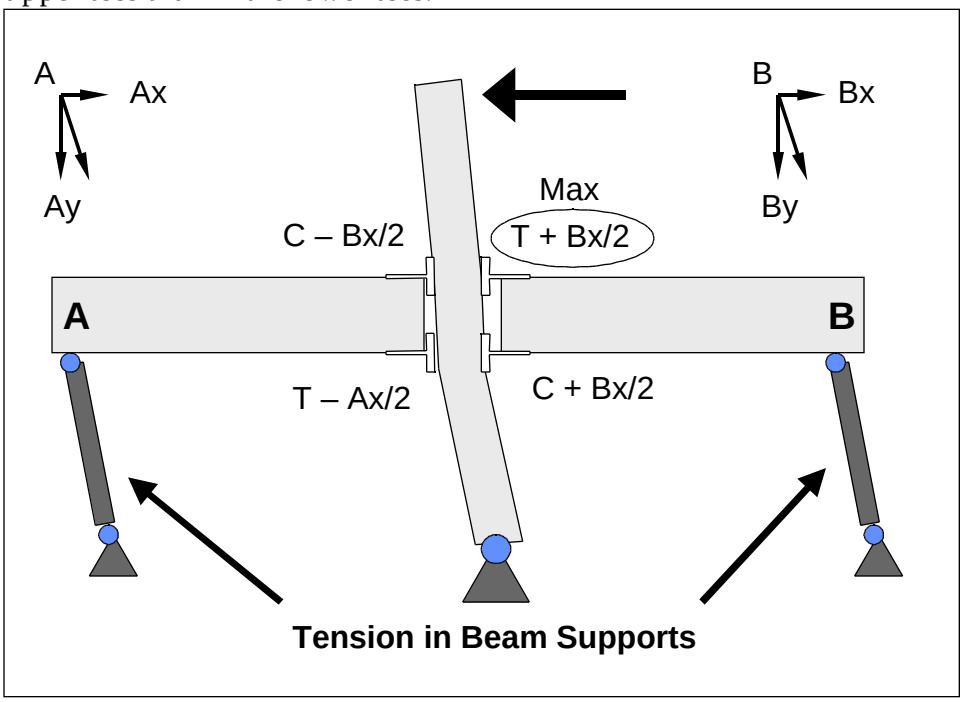

Figure 6.8 - Influence of Test Setup Geometry on Top-Tee Prying

6.4.3 System Performance and Panel Zone

Figure 6.9 shows that stable hysteretic behavior was observed for specimen CFT.2 until the conclusion of the test at 5.0% inter-story drift. Peak load was achieved between 3.0 and 3.5 % drift. At 5.0% drift, there was only a 9% decrease in the peak load compared to that at 3.5% drift.

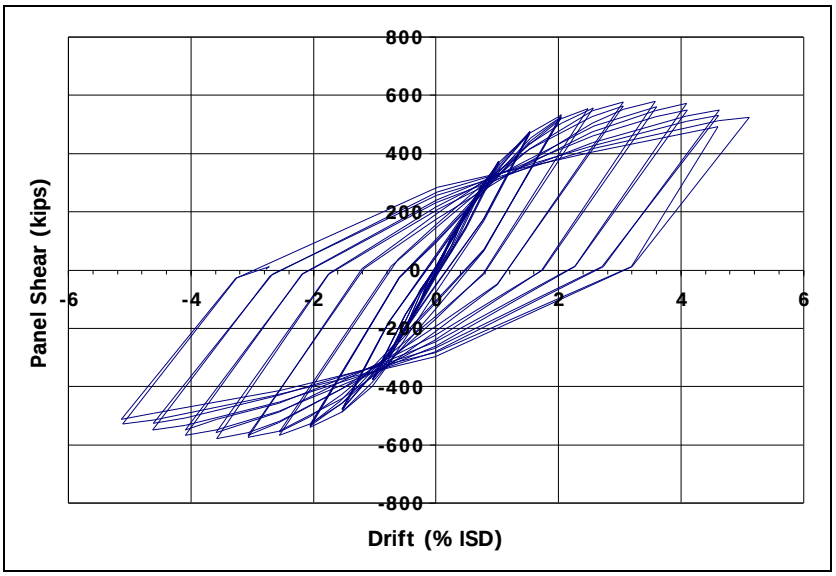

Figure 6.9 – Specimen CFT.2 Load-Displacement Curve

The behavior of the panel zone in shear is shown in Figure 6.10. Although not originally designed to fail in the panel zone, specimen CFT.2 exhibited an appreciable amount of permanent panel-zone deformation. Beam strengths were greater than anticipated, so the mode of failure for CFT.2 was a combination of beam yielding and panel-zone plastic deformation. The maximum panel-zone distortion observed was 3.2% at 5% drift.

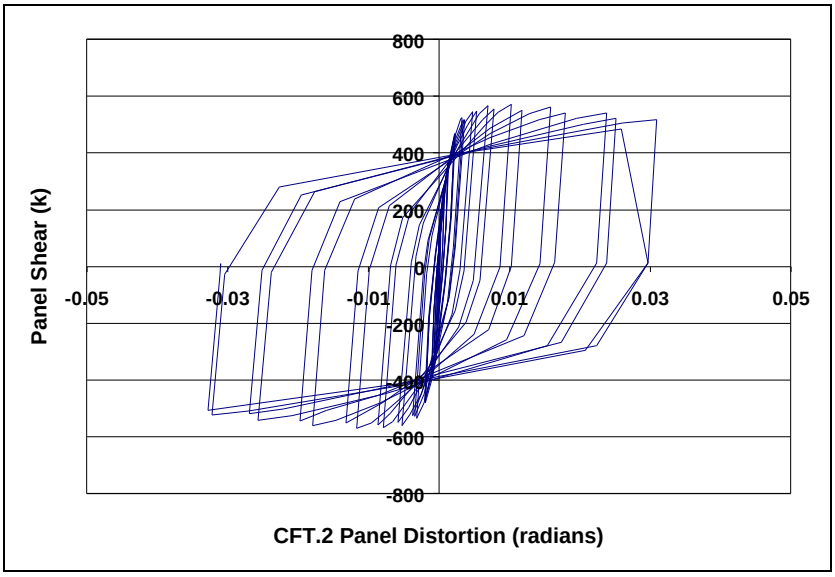

Figure 6.10 – CFT.2 Shear vs. Panel Distortion

In addition to visible permanent distortion in the steel outer panel of specimen CFT.2, severe internal damage to the concrete core was evident after the steel panel was removed (Figure 6.11). Because of locked-in permanent deformation of the steel tube after testing, loose material was diagonally oriented in the direction of the strut during the last half-cycle. The depth of material loose enough to remove by hand was approximately one inch.

Figure 6.11 – Excavation of CFT.2 Concrete – Removal of Loose Material

6.5 CFT.3 and CFT.4

For the remaining two 12 inch specimens, an increased beam section of W 18X65, compared to the W 18X46 sections used for CFT.1 and CFT.2, was used. This increase in beam size was chosen to allow greater damage to the panel-zone, with the goal of creating and observing a panel-zone failure. In addition to the beam size increase, the nominal diameters of the tee bolts increased from 1-1/8 inch to 1-1/4 inch to handle the forces necessary to damage the panel-zone. Specimen CFT.4 differed from CFT.3 only in the choice of tee width against the

column. Whereas the tees in CFT.3 covered only 67% of the column face width, the tees of CFT.4 covered 75%. This increase in tee width was chosen to observe the effects of the change of the tee width on the load path through the joint section. Plots of Panel Shear vs. Drift and Shear vs. Panel Distortion for CFT.3 and CFT.4 are shown in Figure 6.12 through Figure 6.15.

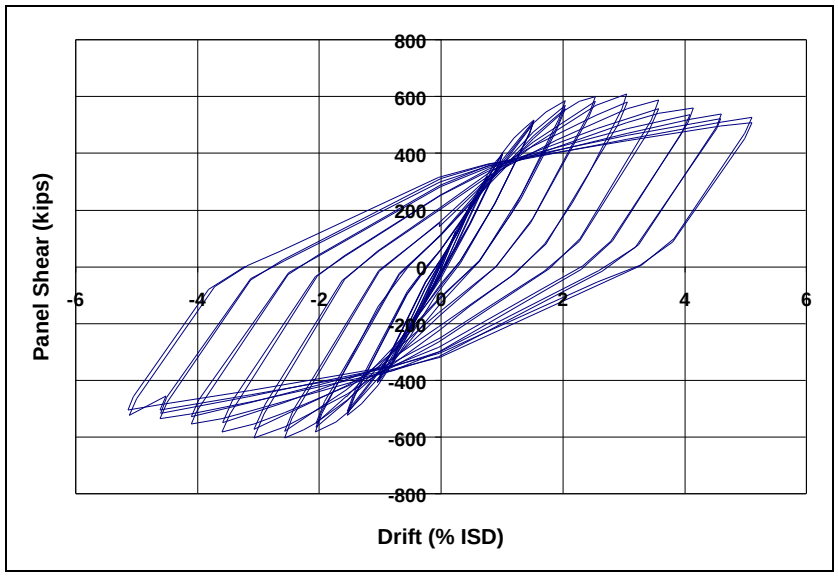

Figure 6.12 – Specimen CFT.3 Load-Displacement Curve

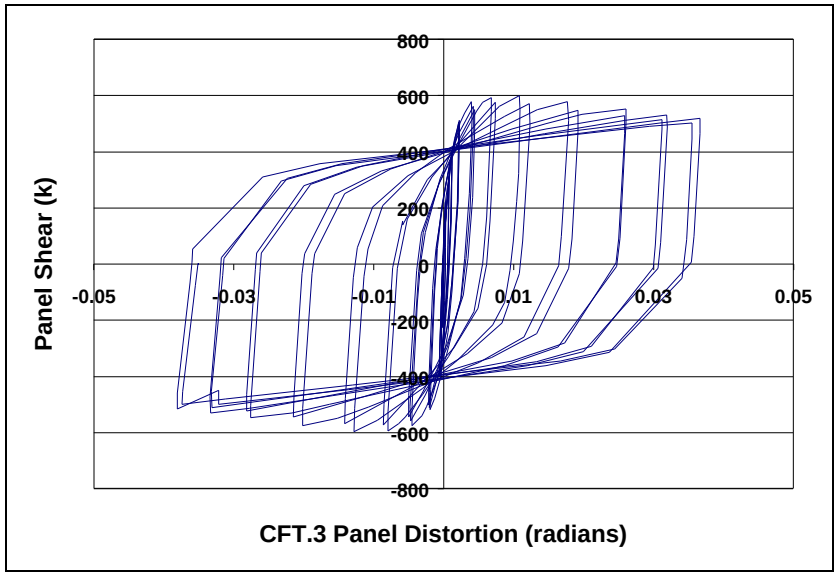

Figure 6.13 – CFT.3 Shear vs. Panel Distortion

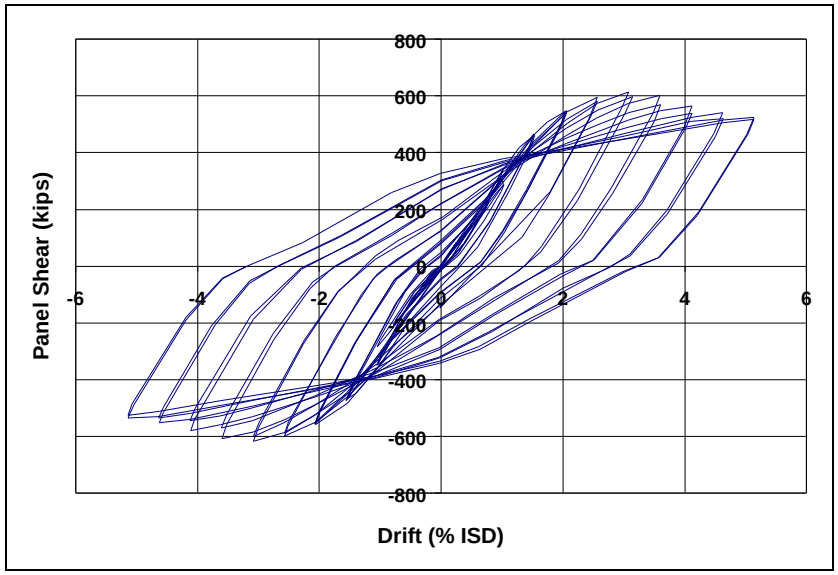

Figure 6.14 – Specimen CFT.4 Load-Displacement Curve

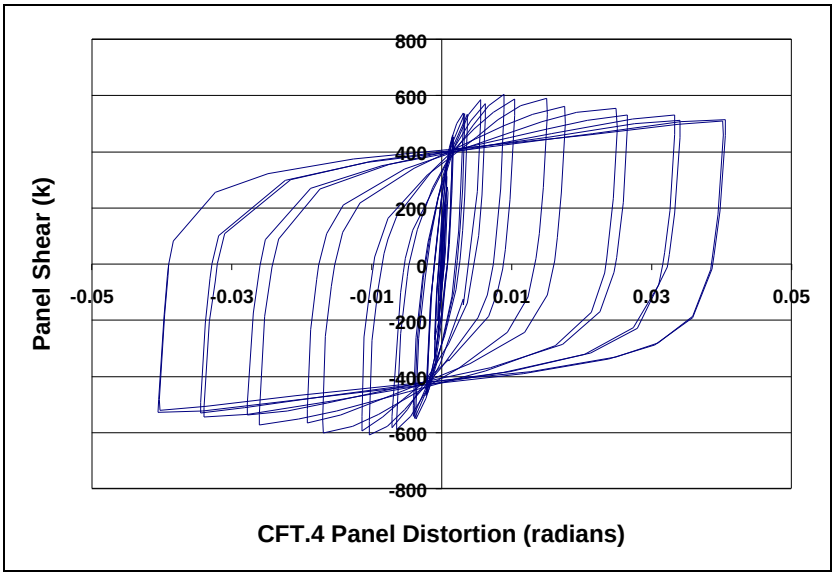

Figure 6.15 – CFT.4 Shear vs. Panel Distortion

6.5.1 Comparisons between CFT.2, CFT.3 and CFT.4

The envelope of Panel Shear vs. Drift is shown in Figure 6.16. When compared, CFT.3 and CFT.4 attained higher peak loads than CFT.2, and had greater energy dissipation. Whereas CFT.2 held peak load from 3.0 to 3.5% drift, CFT.3 peaked at around 3.0% drift, and then dropped off shortly thereafter. At 5.0% drift, the strength of CFT.3 and CFT.4 dropped to 90% of the peak load achieved at 3.0% drift. All three specimens converged to the same level of panel shear at 5% drift. Because CFT.1 experienced problems during testing that prevent direct comparison with the other 12 inch CFTs, it is not included in the comparisons.

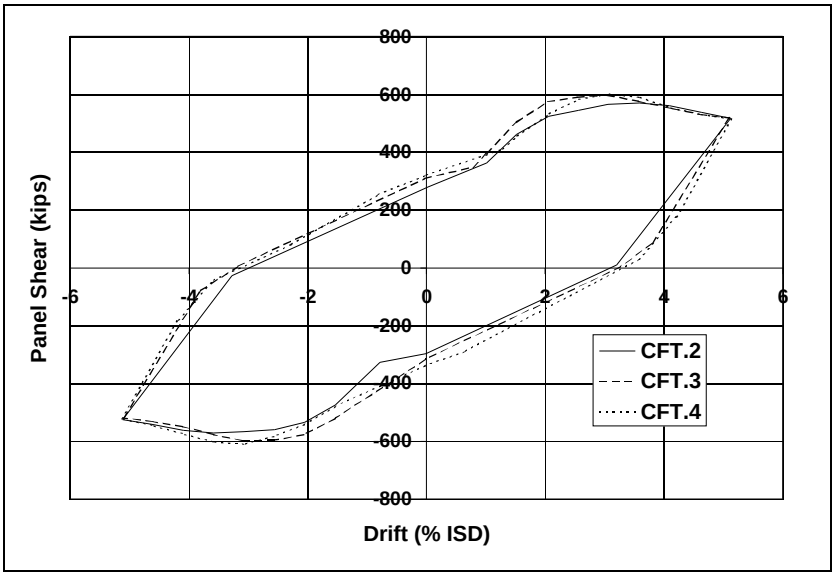

Figure 6.16 - Shear vs. Drift Envelope for 12 inch Series

As seen in Figure 6.17, the panel zones of CFT.3 and CFT.4 had greater energy dissipation than CFT.2. Specimen CFT.3 had maximum distortion of around 0.038 radians, which represents an 18% increase in distortion compared to specimen CFT.2. The increase in panel-zone distortion is consistent with the increase in beam size, and thus the increased demand on the panel zone. It should be noted that, although CFT.2 was not originally designed for panel-zone failure, the over-strength of the beams allowed inelastic panel-zone distortion to occur.

When compared with CFT.3, specimen CFT.4 exhibited nearly identical load-displacement characteristics (Figure 6.16). Because both specimens are very similar, the only difference being a small increase in the tee width, the similarity in overall shear vs. drift behavior was expected. Both specimens peaked at 3.0% drift. CFT.4 peaked at a load only 2% greater than that of CFT.3.

The only noticeable difference in behavior from CFT.3 to CFT.4 was with the panel-zone distortion. Specimen CFT.4 reached maximum panel-zone distortion at 0.04 radians, which is a 5% increase over that of CFT.3. The increase is consistent with the fact that CFT.4 had a larger tee width bearing on the face of the column, pushing more force into the steel side panels where the panel distortion measurements were taken. Peak shear strength of CFT.3 and CFT.4 were essentially the same.

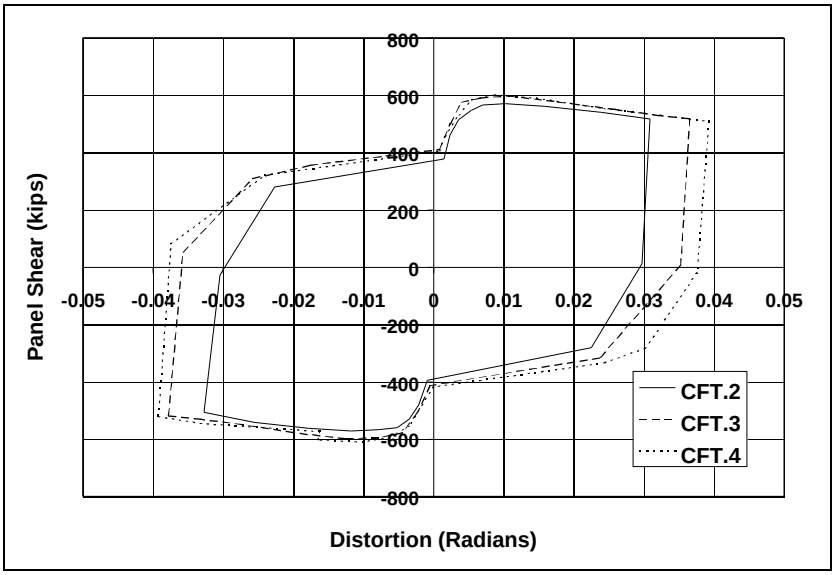

Figure 6.17 - Panel Distortion Envelope, 12 inch Series

Table 6-1 – Tabulated Results for 12" Tube Series

Specimen	Vmax (kips)	Panel Zone Distortion (radians)	Tee w (%b)
CFT.1	529 *	--	83
CFT.2	571	0.032	67
CFT.3	598	0.038	67
CFT.4	610 (2.0 % incr.)	0.04 (5% incr.)	75
* CFT.1 Failed Prematurely			

6.5.2 Common Behavior in the 12 inch CFTs

During the testing of CFT.1 through CFT.4, some observations were common to all tests. Beam flange yielding was observed at or above 1.0% drift. In the case of CFT.1 and CFT.2, beam flange yielding took place at about 1.0% drift. In the case of specimens CFT.3 and CFT.4, which were designed to force failure into the panel zone by using stronger beams, beam flange yielding took place around 1.5% drift. In all cases, tees experienced prying from the face of the columns after 2.0% drift, and, in all cases, the prying was more significant for top tees than for bottom tees for reasons explained earlier in section 6.4.2.

6.6 Application of Panel Shear Equations to 12 inch Square CFT Specimens

The design formula considered in Chapter 4 will now be applied to the 12 inch CFT series specimens. The 12 inch tubes, with the exception of CFT.1, had reliable panel-distortion data. Because peak loads are indicated in the plots of shear vs. steel panel distortion (Figure 6.17), steel panel-zone failure had occurred. Initially, only specimens CFT.3 and CFT.4 were proportioned for panel zone failure. Specimen CFT.2 also experienced panel-zone failure because the beams were stronger than anticipated.

Observations from the small-scale CFT tests (Series A, B, and C from the 8" CFT tests) helped guide the development of the full-scale moment connection specimens. The first notable observation was that changes in the width of load application made insignificant changes to the overall strength and performance of the CFT system. Concrete that is confined by the square tube can only deform in a way that is compatible with the deformation of the steel tube. After observing the specimens tested, it is unlikely that damage to the concrete would be severe enough to destabilize the steel panel, and any changes to the tee width would be unlikely to dramatically change the load path. With a very strong diagonal compression field acting through the joint during one direction of loading, there is a tension field in the steel tube acting in the cross direction. This tension field would act to increase the amount of confinement provided by the steel tube, if it were to have any effect at all on the behavior of the connection during loading.

6.7 A Simplified Model

In chapter 4, a modified equation for the joint shear strength of the split-tee, through-bolted CFT connection (Equation 4.4) was introduced. The equation is a summation of the two material contributions, and is calibrated by the test data for the 8 inch panel-zone specimens. Although CFT.2 experienced panel zone failure, specimen strength was governed by plastic beam rotation. The full strength of the steel panel zone of CFT.2 was not achieved; therefore, in comparing equation 4.4 with test results, only CFT.3 and CFT.4 will be used. In Figure 6.18, theoretical strengths of specimens CFT.3 and CFT.4 normalized by measured shear strength are compared to the panel-zone specimens. Equation 4.4 produces theoretical to test ratios of 0.96 and 0.94, respectively, for CFT.3 and CFT.4.

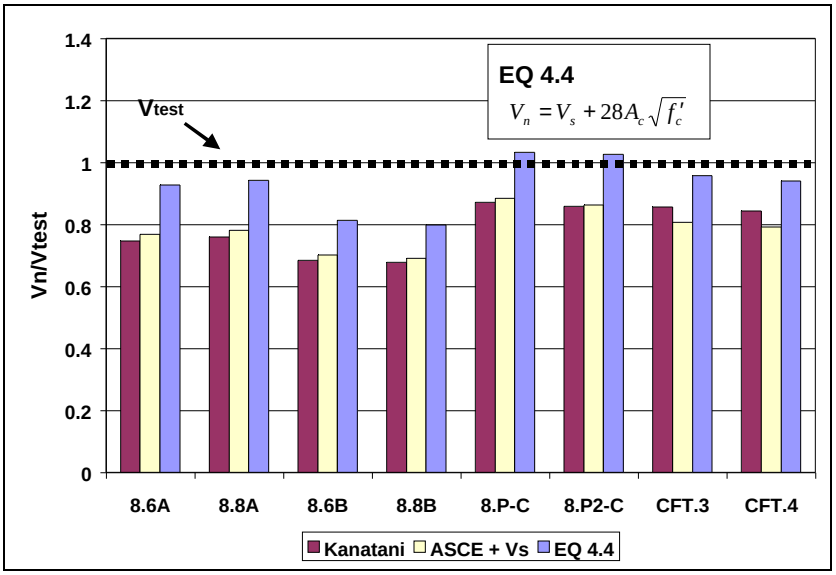

Figure 6.18 – Equations Compared Against Normalized Test Results

The notable variation in results is with regard to Series B. Assuming the variable of concrete strength has been adequately addressed in the development of the equation, *b/t* should be addressed to account for variations in theoretical results of the steel tube. Theoretical results for Series B (*b/t*=21) were more conservative than the rest of the specimens. The lower slenderness ratio may be the reason; however, the level of accuracy of Equation 4.4 for CFT.3 and CFT.4 (*b/t* = 24) is similar to Series A and C (*b/t*=32). The reduction of *b/t* from 32 to 24 in that case did not result in conservative predictions.

6.7.1 Significance of *b/t* and Confinement

Confinement of concrete can increase the compressive strength significantly. Research by Park, et al (1982) showed that the compressive strength of concrete is increased because confinement increases the crushing strain. In that research, tests on square columns with adequate hoop steel showed that the concrete core reached strains as high as 0.026, compared to the typical unconfined concrete crushing strain of 0.003, after the cover had cracked and spalled. Of the type of columns tested, curvature ductilities of 20 and displacement ductilities of 10 could be reached. Square steel tubes could be analogous to steel hoops in reinforced concrete construction. The concrete of the CFT is analogous to the confined concrete core of a square reinforced concrete column. Theoretically, the steel tube is similar to a continuously wound, very closely spaced, hoop.

Parsley (1998) showed that in axial compression, confinement in square tubes was only effective near the corners. Knowles and Park (1969) tested short

square tubes in axial compression and found that the increase in strength was not significant. Round tubes tend to provide the most confining benefits in longitudinal compression because of the hoop stresses that can develop. Within the panel zone of the split-tee CFT connection, however, longitudinal compression is not modeled, so the effects of confinement on the joint shear strength is an area worthy of further study.

6.7.2 Observed Effects Related to b/t and tube thickness

Two important observations were made during the testing of the panel zone specimens. First, the Series B steel tubes did not warp out-of-plane visibly, but the Series A and Series C tubes did warp. Warping out of plane is a buckling phenomenon, and this is related to the b/t of the steel tubes. The Series A specimens were also prone to local bearing crushing near the "tee-contact" area. Bearing crushing is related to the bending stiffness of the tube near the contact point, and the punching shear stresses around the area of contact. Bearing stresses in the panel zone tests were greater than those for the full-scale specimens due to scale effects of the test specimens.

The 12 inch tube specimens CFT.3 and CFT.4, whose panel-zones were designed to fail, exhibiting warping of the steel panel. For those, it would be safe to agree with the notion that confinement is only effective near the corners of the tube. The CFTs of series C support this conclusion because the addition and subtraction of material could be accounted for theoretically disregarding any effects of confinement.

The test results of Series B demonstrate the need for more research on the slenderness ratio *b/t*. Perhaps there is a lower *b/t* limit at which the side panels do in fact contribute to the confinement of the joint—in a manner more effective than just near the corners. Series B specimens had an increase in concrete shear strength of approximately 30% over the tubes of Series A. Further research should be conducted to relate the *b/t* parameter to concrete strength enhancement.

6.8 16 inch CFT – Results

The remaining two specimens of the large-scale test program utilized 16 inch square CFTs. Both specimens were designed to compare the difference in elastic panel-zone behavior with varying tee width. The difference in tee width between the remaining two specimens is more significant than that of the 12 inch specimens because there was less range of tee width that could be used on the smaller 12 inch specimens. For CFT.5 and CFT.6, the tee widths were 15 inches and 9 inches, respectively, and represented 94% and 56% of the column width. This greater range could provide a greater contrast in panel-zone behavior.

Figure 6.19 – Specimen CFT.5

6.9 CFT.5

Specimen CFT.5 (Figure 6.19) was modeled after Lehigh Specimen number 6 (Ricles et al 1997) in terms of beam, column and tee size. Failure was expected to consist of plastic beam rotation. The connection itself was designed to remain robust and functional throughout the duration of the test.

6.9.1 System Performance and Panel Zone

The panel-zone of CFT.5 performed as expected. The plot of load vs. top displacement (Figure 6.20) shows stable hysteresis throughout the duration of the test. The connection dissipated energy through plastic beam rotation just outside of the connection. Yielding of the beam flanges was complete around 2.0% drift (Figure 6.21). Prying of the tees was significant at 3.0% drift (Figure 6.22).

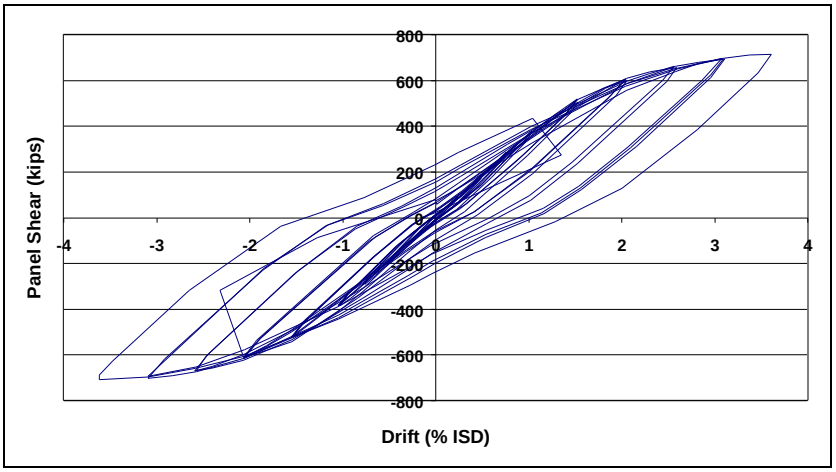

Figure 6.20 – Specimen CFT.5 Joint Shear vs. Drift Curve

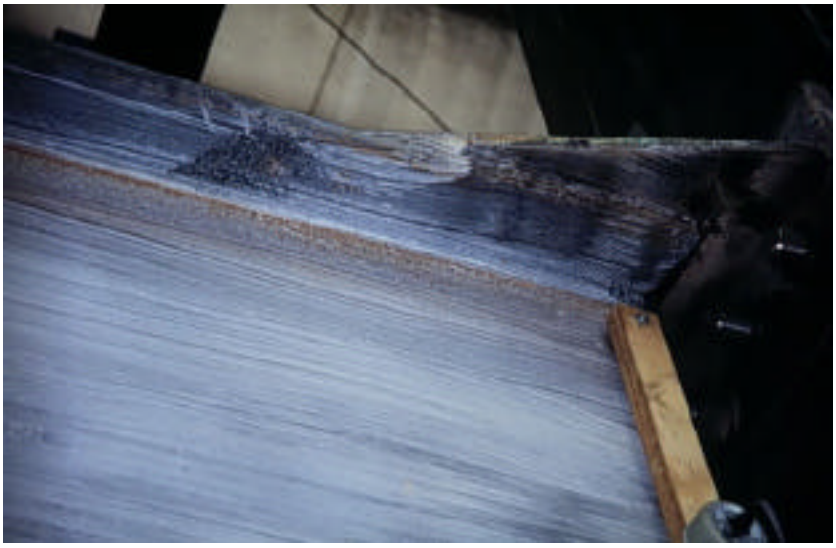

Figure 6.21 – CFT.5 Extent of Beam Flange Yield at 2.0% Drift

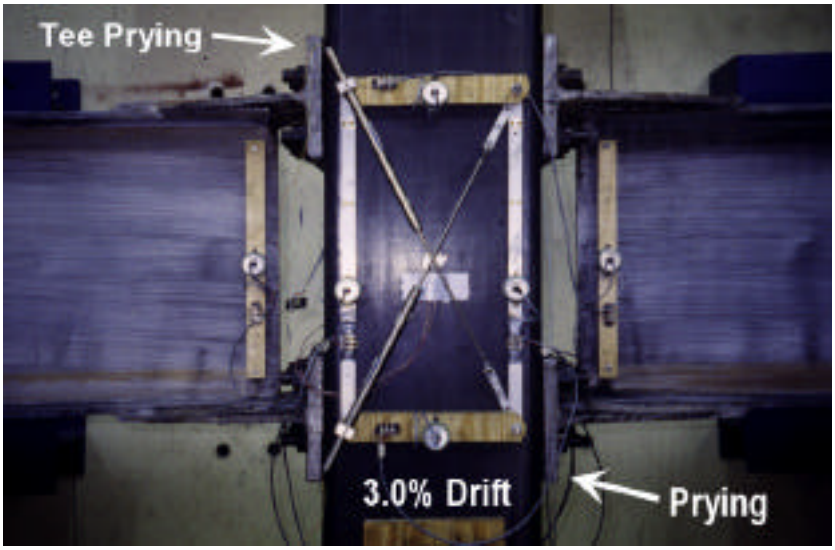

Figure 6.22 – CFT.5 at 3.0% Drift: Tee Prying, Panel Zone Undamaged

The panel-zone experienced some distortion, but did not result in observable permanent distortion after the conclusion of the test. Beams had yielded sufficiently to demonstrate that the connection was able to support plastic beam hinging as the primary mode of energy dissipation (Figure 6.24). A plot of panel shear vs. panel distortion (Figure 6.23) shows energy dissipation, but no loss in panel strength. Because there is no discernable peak during this test, values at 3.0% drift will be used for comparisons between CFT.5 and CFT.6. At 3.0% drift, panel-zone distortion was 0.0033 radians. The hysteresis suggests that some damping and energy dissipation took place, but it was most likely due to internal cracking and damage to the interior concrete.

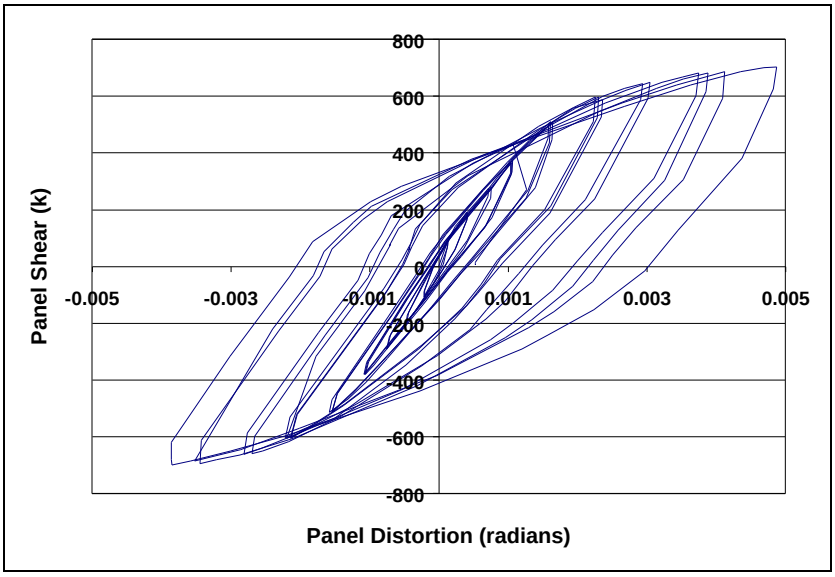

Figure 6.23 – CFT.5 Shear vs. Steel Panel Distortion

Figure 6.24 – Extent of Beam Yield at 3.5% Drift

The initial plan was to take specimen CFT.5 to 5.0% drift, but two problems necessitated conclusion at 3.5% drift. First, a threaded coupler on the right beam support strut pulled out at 3.0% drift. The test had to be temporarily

interrupted in order to fix the support. The test was quickly resumed, and carried to conclusion at 3.5% drift. Unexpectedly, the left-beam split-tee fractured along the K-line at 3.5% drift, so the test ended prematurely (Figure 6.25). The brittle fracture initiated at the toe of a fillet weld termination point. A fillet weld was used to attach a small stiffener plate to the tee stub. Stiffening was used because a fabrication error in the beams resulted in beams that were two inches too short, so there was a larger than desired unsupported length of tee between the beam and the column face.

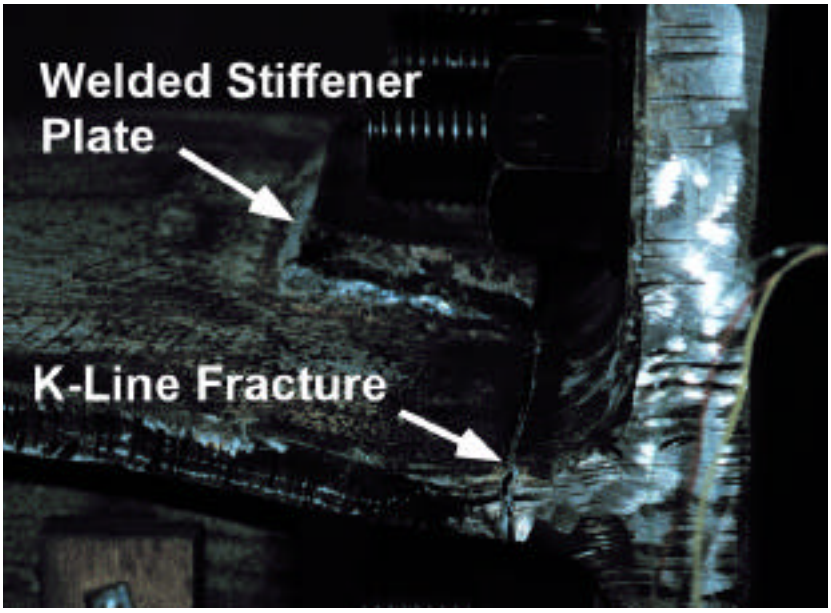

Figure 6.25 – K-Line Fracture of Tee

The fracture of the tee occurred at a nominal tensile stress of 26 ksi while attempting to repeat the 3.5% drift cycle. Nominal shear stress on the tee stub was 2.6 ksi. The abrupt change in the shape in the first quadrant of the curve plotted in Figure 6.20 is the point at which the failure occurred (panel shear = 426

kips). Prior to failure, the tee had been stressed to 41 ksi (tensile) at 3.5% drift. There were a total of twelve previous cycles in which the nominal tensile stress on the tee was greater than the failure stress of 26 ksi.

6.10 CFT.6

Specimen CFT.6 was used to demonstrate the effect of narrowing the tee width against the face of the column, compared to CFT.5. In order to use a narrower tee for CFT.6, a section of tee material was chosen with a tee stub sufficiently thick to carry beam flange tensile forces over the shorter width, and with enough flange thickness to minimize prying from the face of the column. Narrowing of the tee width represented a reduction of the tee width from 94% to 56% of the width of the column face. The reduction would cause the load path of shear forces through the joint to take a more direct path through the concrete core, lessening the degree to which the steel side panels of the CFT would be mobilized. Such a change in the connection details of CFT.6, and thus a change in the load path, would cause less distortion in the steel panel, and would conceivably result in more damage to the core concrete than in CFT.5.

6.10.1 System Performance and Panel Zone

Specimen CFT.6 was tested without any major problems. Testing was halted at 3.5% drift, but not because of unexpected failures or complications. At 3.5% drift, there was sufficient plastic beam hinging and lateral-torsional buckling to stop the test before causing any damage to the testing apparatus.

The joint shear vs. story displacement curve for CFT.6 is shown in Figure 6.26, and the steel panel zone distortion is shown in Figure 6.27.

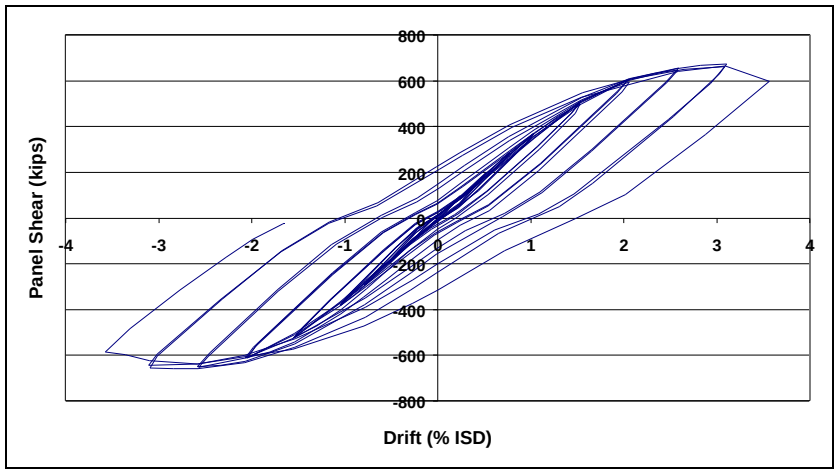

Figure 6.26 – Specimen CFT.6 Joint Shear vs. Drift Curve

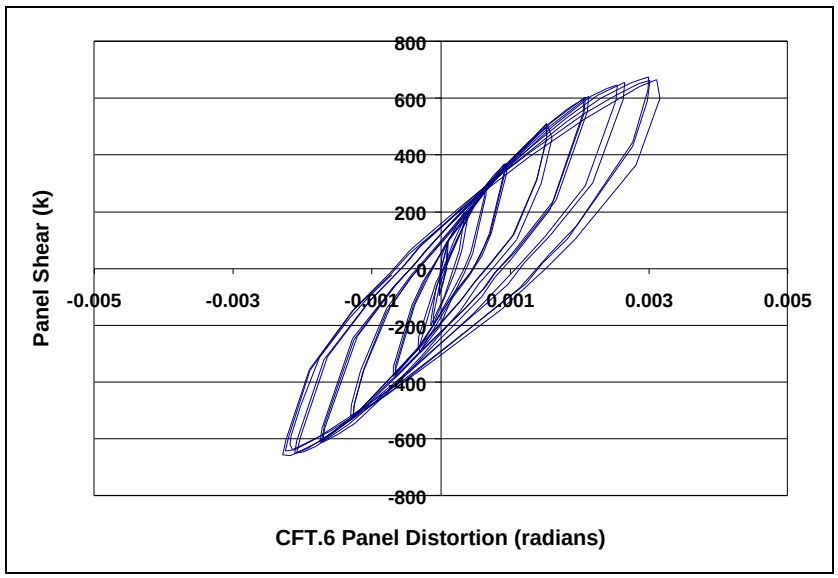

Figure 6.27 – CFT.6 Shear vs. Steel Panel Distortion

The failure mode of CFT.6 was plastic rotation of the beams as planned. Specimen CFT.6 exhibited similar overall behavior to that of CFT.5 when

compared to the load-displacement response of the overall specimen (See Figure 6.28). CFT.5 and CFT.6 reached peak panel zone shear values of 699 and 672 kips, respectively, showing essentially no significant change in overall strength (4% decrease) considering the large difference in the tee width against the column (from 96% down to 56% of the tube depth).

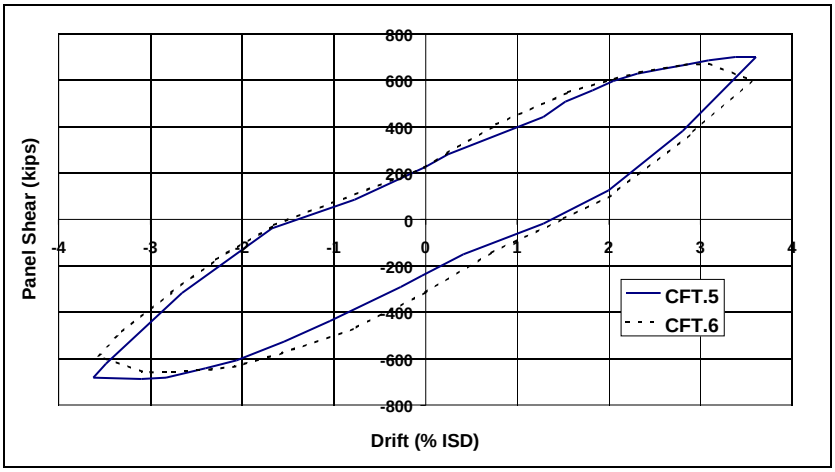

Figure 6.28 - Joint Shear vs. Story Drift Envelope for CFT.5 and CFT.6

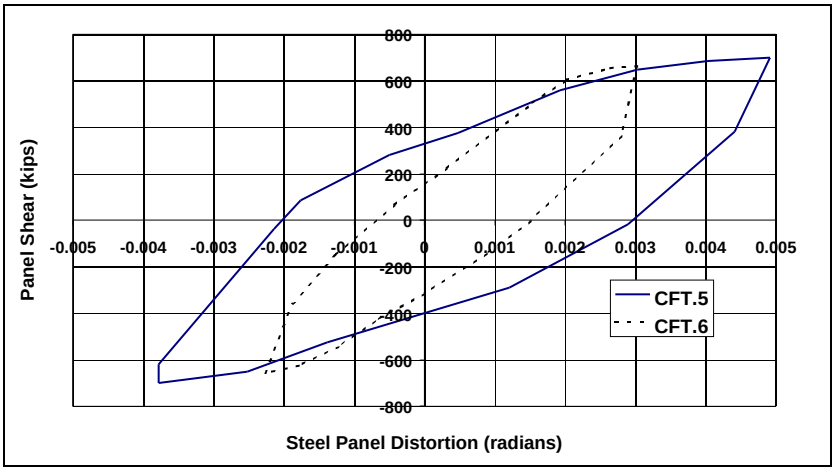

Figure 6.29 - Joint Shear vs. Steel Panel Distortion Envelope

The envelope of shear vs. steel panel distortion is shown in Figure 6.29. Significantly greater energy dissipation in the steel panel of CFT.5 is observed compared to CFT.6; however, overall energy dissipation of the specimens when looking at joint shear vs. story drift (Figure 6.28) appears to be similar. When compared at the same benchmark level of drift (3.5%), the steel outer panel of CFT.6 only reached a distortion level of 0.0031 radians, which is 63% of the level of distortion observed in CFT.5. This data supports the theory that the concrete must be responsible for carrying more of the joint shear forces when the tee is narrower. Results for Maximum Panel Shear and Distortion are shown in Table 6-2. It is noted that since these specimens were not designed for panel-zone damage, the value of V_{max} does not imply that the shear strength of the two specimens was reached.

Table 6-2 - Tabulated Results for 16" Tube Series

Specimen	$V_{measured}$ (kips)	Steel Panel Zone Distortion (radians)	Tee w (%b)
CFT.5	699	0.0049	94
CFT.6	672 (96% of CFT.5)	0.0031 (63% of CFT.5)	56
Specimens not designed for panel-zone failure. Beam hinge was failure mode.			

Upon visual inspection of the interior concrete of Specimen CFT.6 after testing, there appeared to be no significant damage to the core other than a very small crack pattern that consisted of two distinct diagonal cracks through the panel-zone, oriented in the direction of the concrete compression strut (Figure 6.30 and Figure 6.31).

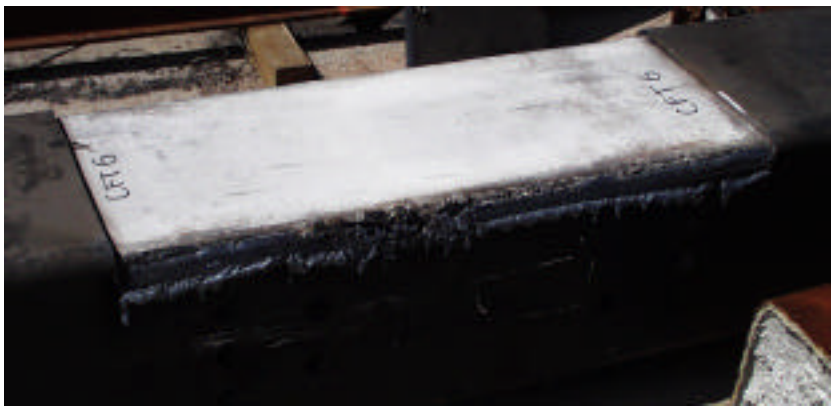

Figure 6.30 – CFT.6 with Panel-Zone Exposed and Intact

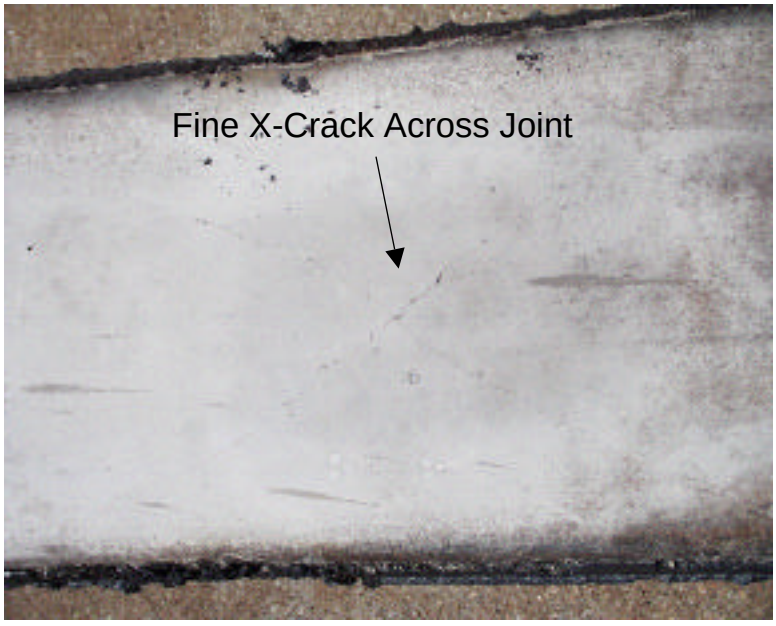

Figure 6.31 – CFT.6 Extent of Interior Concrete Panel-Zone Distress – Hairline Diagonal Cracking

6.11 Behavior of 16 inch CFT Moment Connection Specimens

The main difference between CFT.5 and CFT.6 is that CFT.6 had a tee that did not cover the entire width of the face of the tube. The difference between the testing history of the two 16 inch CFT specimens (CFT.5 and CFT.6) and the 12 inch specimens (CFT.1 through CFT.4) is that CFT.5 and CFT.6 were only tested to 3.5% inter-story drift. Both specimens were to be tested to 5.0% drift, but CFT.5 suffered a K-line fracture through the structural tee, and CFT.6 had experienced sufficient beam plastic hinging and out-of-plane deformations to threaten the stability of the test setup.

Test data for both specimens is normalized by the theoretical value of V_n. Figure 6.32, shows that by the completion of the testing of specimen CFT.5, the steel panel did not reach a peak value. Panel shear at the limiting event of beam plastic rotation peaked at a value of just above 70% of the theoretical prediction of maximum shear for that specimen. Visual inspection after testing revealed no permanent distress to the steel panel, but strain data indicated the onset of yielding. Also, in contrast to the 12 inch specimens, CFT.5 and CFT.6 did not exhibit any visible out-of-plane bending of the steel panel. The hysteresis shown in Figure 6.32 can be attributed to internal shifting and minor cracking of the concrete interior, friction in the testing apparatus, or the onset of yield of the steel panel.

Figure 6.33 shows elastic behavior of the steel panel of CFT.6. This is consistent with the significantly smaller tee-width against the column of CFT.6

compared to CFT.5, which resulted in load transfer to the concrete core. Any hysteresis, minor as it may be, could be attributed to friction between the setup and the specimen, as well as any minor cracking internally.

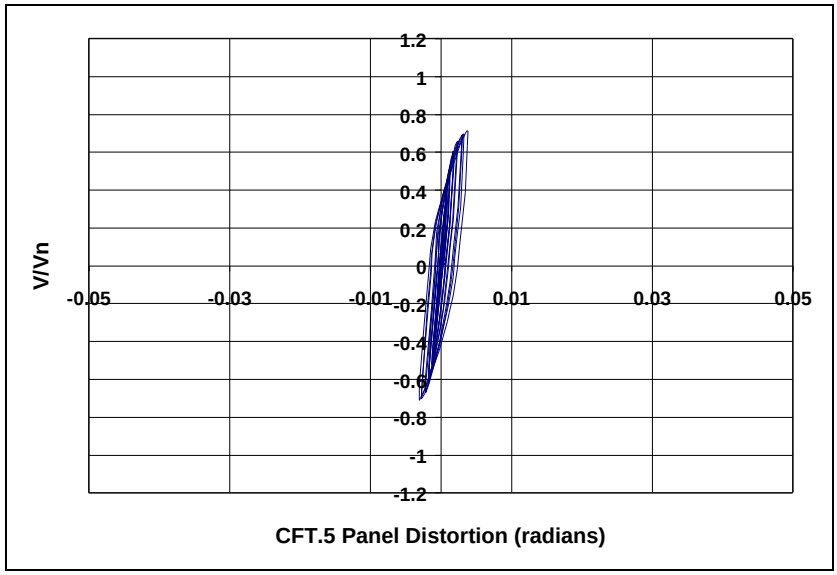

Figure 6.32 - CFT.5 Normalized Shear vs. Distortion

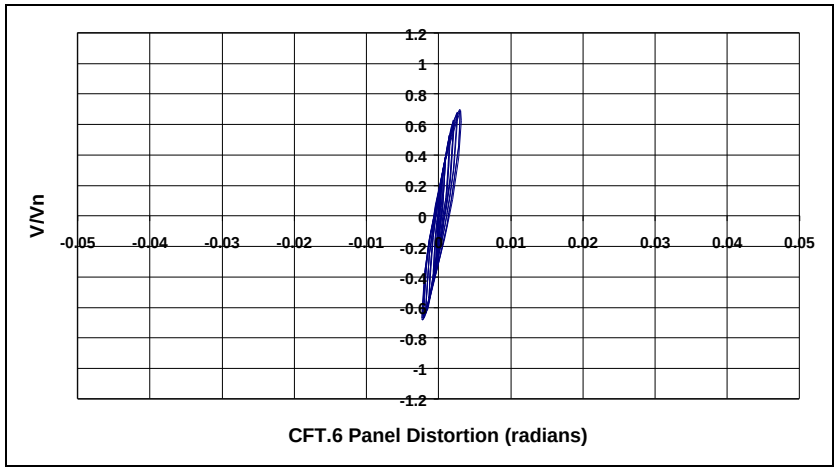

Figure 6.33 - CFT.6 Normalized Shear vs. Distortion

6.12 Contributions of Steel and Concrete, Compared

When joint shear vs. story drift curves up to 1% drift for CFT.5 and CFT.6 are superimposed, near identical joint shear / drift response is observed (See Figure 6.34). The joint shear response shown in the figure includes the effects of both steel and concrete in the joint. Linear regression of the loops in Figure 6.34 reveals joint shear force / story drift stiffnesses of 357 kips and 355 kips for CFT.5 and CFT.6, respectively.

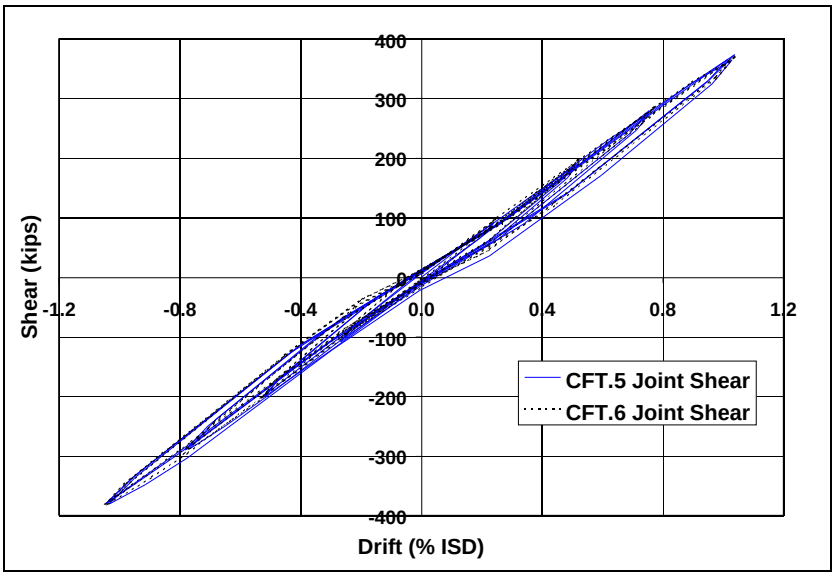

Figure 6.34 - Joint Shear vs. Story Drift for CFT.5 and CFT.6

Strain rosette data is used to evaluate the contributions of steel and concrete. The horizontal shear stress at the center of the panel zone is reduced from rosette data and extrapolated to obtain values of shear force through the steel panels. The calculated shear stress is multiplied by the shear area of the steel. The shear area is defined as the thickness times the flat width of the steel

tube. Figure 6.35 and Figure 6.36 show the steel panel contribution to joint shear for CFT.5 and CFT.6, respectively. Regression through the curves reveals the steel contribution to joint stiffness. According to the extrapolated strain rosette data, the shear force in the steel panel of CFT.5 accounts for approximately 75% of the total joint shear force, whereas CFT.6 accounts for only 50% of the joint shear force. Since the difference between the joint shear and the steel panel shear is the shear contribution of the concrete, the concrete of CFT.6 is participating more than the concrete of CFT.5.

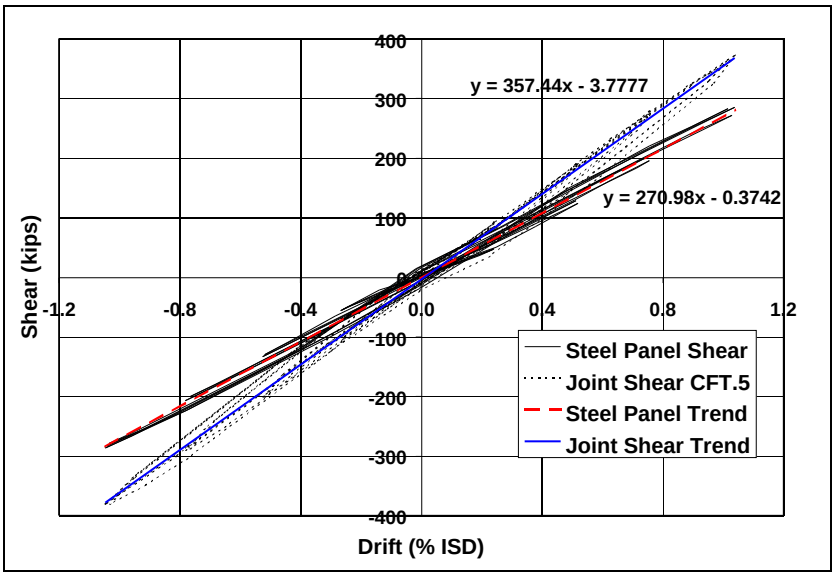

Figure 6.35 - Steel Panel Shear Contribution for CFT.5

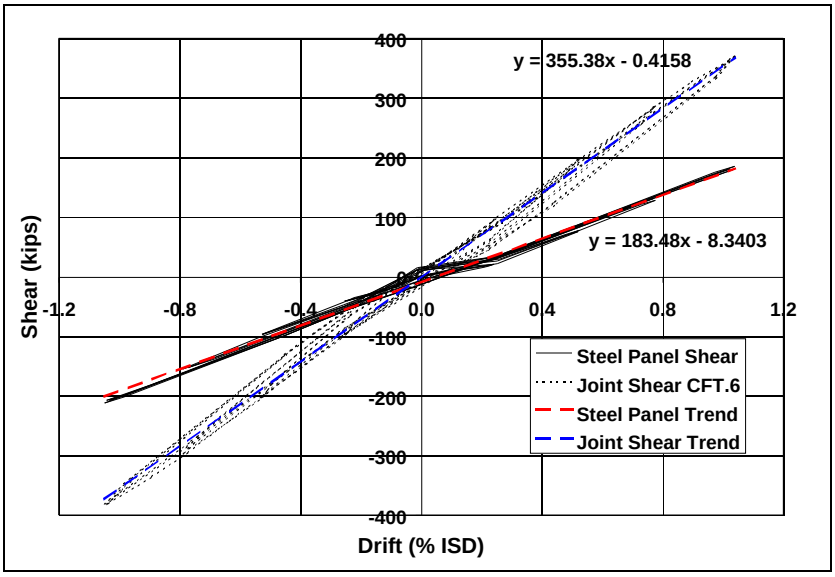

Figure 6.36 - Steel Panel Shear Contribution for CFT.6

6.13 Synopsis

The changing of the width of the tees did not produce significant differences in the overall behavior of comparable CFT system for specimens CFT.1 through CFT.4. The variation between the tee width for CFT.3 and CFT.4 was a small one. The tee of CFT.3 occupied 2/3 of the width of the CFT, while the tee of CFT.4 occupied _ of the CFT width. For those two specimens, it was observed that the larger tee specimen of the two (CFT.4) experienced greater overall panel-zone distortion by the end of the test. The global behaviors of specimens CFT.3 and CFT.4 were not noticeably different.

While the reduction in tee width from 15 inches to 9 inches for specimens CFT.5 and CFT.6 did not affect overall strength or story drift, it did have a

substantial effect on the distribution of panel shear between the steel and the concrete. Although CFT.5 was designed to remain elastic, the presence of the widest tee caused the onset of yield in the steel panel. CFT.6, on the other hand put greater demand on the concrete core within the joint. Whereas CFT.6 had less steel panel distortion than CFT.5, there was a slight increase in overall energy dissipation for CFT.6 when shear vs. story drift is considered. Because concrete was taking a greater percentage of the shear compared to CFT.5, the wider hysteresis loops for CFT.6 can be accountable to minor damage in the concrete core. Upon visual inspection of the exposed concrete core during autopsy, two thin crossing diagonal cracks were observed, but there was no visible extent of damage beyond the existence of the hairline crack.

To produce panel-zone failures in specimens CFT.1 through CFT.4, abnormally large tees had to be fabricated, and larger than reasonable beams had to be used. In practical design, beams or tees will likely fail before the panel zone even has a chance to fail. In the case of panel-zone failure in the specimens tested, ductility allowed specimen distortion up to 5.0% drift, which is an unrealistically high level of drift to be seen in an actual catastrophic event.

7. Summary and Conclusions

7.1 Summary

This research program consisted of: (a) fifteen half-scale panel zone specimens utilizing 8 inch square CFTs, (b) four 12 inch square CFT moment connections, and (c) two 16 inch square CFT moment connections.

A test set-up that simulated tee forces of the split-tee through-bolted moment connection was used to test the half scale 8 inch square CFTs. Specimens were grouped into Series A, B and C. Series A and B specimens were used to compare the effects of changing the tee width on the shear behavior, and were tested cyclically. Series B was used to compare the effects of a thicker tube (lower b/t) against the A series. The tubes of Series C were used to understand the contributions of the concrete and steel to the joint shear strength. Various shapes of steel were removed from the tube panels prior to concrete casting, and were then tested monotonically.

The panel zone tests showed that:

- Changing the width of the tee against the column did not have an effect on the overall strength / displacement characteristics of the specimens.
- Failure was a combination of shear, local bearing and flexure, but strength was not governed by the flexural capacity of the specimen. Specimens remained ductile and robust.

- The concrete term V_c was quantified and verified from tests on the Series C specimens by subtracting the theoretical steel contributions from the cut-out specimens.
- The contribution of the steel panel shear strength is additive in the same way as it was for Deierlein (1988) in his study of composite connections.
- The term V_c (included in Equation 4.4), which is based on the concrete term proposed by the ASCE Task Committee, has been calibrated to test data of specimens with b/t =32. Based on the panel-zone test data, an appropriate coefficient of 28 was chosen for CFTs.

The testing of four 12 inch square CFT moment connections showed that the term V_n on the CFTs in this research program can be predicted with Equation 4.4:

$$V_n = V_s + 28A_c\sqrt{f_c'} \text{ (psi)} \qquad (4.4)$$

$$V_s = 2 \times 0.6 d_{fl} t F_y$$

where d_{fl} is the depth of the flat portion of the steel tube.

V_n is expressed here in pounds.

Four full-scale 12 inch CFT moment connections were designed and tested. Two of the 12 inch tubes were designed for joint failure. Failure consisted of steel panel zone shear failure and internal concrete crushing. Increasing the tee width had a marginal effect on the panel zone distortion when CFT.3 and CFT.4 were compared.

While the low *b/t* ratio of the panel-zone specimens of Series B (*b/t* = 21.3) did not result in permanent out-of-plane deformation of the steel panel as seen in Series A and C (*b/t* = 32), the moment connections CFT.3 and CFT.4 (*b/t* = 24), which also had a lower b/t ratio, did not appear to benefit the concrete in the same sense. Failure of CFT.3 and CFT.4 was marked by inelastic out of plane deformation. Equation 4.4 predicted the capacity of specimens CFT.3 and CFT.4 without an adjustment for *b/t* reasonably well.

Tests on the full-scale connections revealed an interesting phenomenon related to the tee width variable. Of the moment connections tested in this research program, CFT.5 and CFT.6 showed the greatest contrast in the test data for this variable because the change in tee width was significant. The tee width was narrowed for CFT.6 compared to CFT.5, but the tee flange thickness and stem thickness had to be enlarged significantly to handle the same amount of tension with less width.

Data extrapolated from strain rosettes in the elastic range of steel behavior indicated that the tee that occupied the full width of the column face (CFT.5) forced the steel side panels to take 75% of the joint shear. The narrow tee that covered just 56% of the column face (CFT.6) only forced 50% of the joint shear through the steel panel. As a result, hysteresis loops for joint distortion through 3.5% drift showed that CFT.5 had almost twice as much energy dissipation in the steel panels compared to CFT.6. What is interesting is that, regardless of this difference in load path through the joint, both specimens had identical global load-displacement behavior, including overall specimen energy

dissipation. The demand on the concrete core of CFT.6 was greater than that of CFT.5. Narrowing the tee tends to distort the steel panel less, but it puts greater demand on the concrete.

7.2 Recommendation for Shear Calculation

Based on the research, Equation 4.4 should be used for CFT split-tee through-bolted moment connection design. The coefficient of 28 is more appropriate than the coefficient of 20 used in SRC composite connections because 20 is too conservative. In addition, the use of the flat tube width (d_{fl}) is more appropriate than the full depth of the tube for the steel term because of the lack of participation of the rounded corners in shear.

Because the tee width changes the distribution of shear force through the joint in the elastic range, the engineer must decide whether or not early steel yielding is preferred over concrete distress. The tradeoff for less yielding in the steel panel is greater stress on the concrete core. Where material ductility is concerned during reverse cyclic loading, several cycles of steel yielding would be preferred over concrete cracking. In addition, as a strut mechanism develops through the joint, wider tee widths can help reduce compression bearing failures, and will help enlarge the strut in tubes with relatively thin walls (high b/t). One possible advantage of choosing a narrow tee vs. a larger tee is that if construction requirements or congestion of materials warrant the choice, then the smaller tee may be used without compromising overall joint strength. Sound engineering judgment should prevail.

7.3 Limitations

Equation 4.4 was calibrated to test data for specimens with *b/t* ratios near the upper limit of code *b/t* criteria for CFTs. Equation 4.4 has been shown to be conservative for the low *b/t* ratio of specimens, which is consistent with experimental results by Tomii (1988) that showed that lower *b/t* ratios provide conservative results for moment and shear. Specimens CFT.5 and CFT.6 were not significantly more conservative with their *b/t* of 24, so it is possible that other variables not covered in this program warrant investigation. Examples are: amount and degree of holes cut in through the CFT for through bolts, overall tube depth, or tube thickness.

Because the confining effects of concrete in the CFT are assumed to be at least as good or better than reinforced concrete joints, the same limitations on the use of concrete strength in the equation should be adhered to until more data can be collected. The concrete compressive strengths in this testing program ranged from 3.9 to 7.2 ksi.

7.4 Suggestions for Future Research

There is a need to understand the role of *b/t* of the steel tube, and its affects on confinement. Tests should be done to examine the effects of *b/t* within the range of 20 and 40, with an emphasis on low *b/t* ratios, where the effects effects confinement may be more significant. In addition, the tee-width variable should be studied especially for relatively large CFT systems in which the beams and tees are less than 50% of the full width of the column.

Appendix A: Finite Element Analysis

The following joint research report was published in:
The Journal of Fujita Technical Research Institute, No.9, 1998

Panel-Zone Behavior of Moment Connections between Steel Beams and Concrete-filled Steel Tube Columns

Kazuhiro Uchida[1], Hiroshi Noguchi[2], Bradley D. Koester[3]
James O. Jirsa[4], Joseph A. Yura[5]

Abstract

Experimental and analytical studies were carried out to study the behavior of the split-tee through-bolted moment connection between steel beams and rectangular concrete-filled steel tubes. The aim of the study is to determine the role of the concrete core in transferring joint shear forces due to earthquake loads. The test specimens and reaction frame were designed to idealize the connection zone. The main variables of the experimental study were: the area of the contact width of the beam flange forces applied to the side of the steel tube,

[1] Ph.D. Candidate, Chiba University, Japan
[2] Professor, Chiba University, Japan
[3] Ph.D. Candidate, The University of Texas at Austin
[4] Professor, The University of Texas at Austin
[5] Professor, The University of Texas at Austin

tube wall thickness (b/t ratio), and concrete strength. Finite element models of the both the panel-zone tests and of an actual joint detail were developed and analyzed. FEM analysis was used to determine how well the model could correlate with the panel-zone test data, and to determine how well the test set up could accurately model the stress condition of an actual joint. Test results showed that changing the footprint of the simulated beam flange forces had negligible effect on the capacity of the joint. The FEM analysis showed satisfactory comparison between the test data and the analytical model. It was also shown that the stress condition of the panel-zone test specimens is similar to that of a beam-column joint with the split-tee through-bolted connection.

A.1 Introduction

The behavior of steel wide flange beam to rectangular concrete-filled tubular column moment connections utilizing the split-tee through-bolted connection is studied by testing specimens idealizing the connection zone, and by comparing results of the tests with finite element models.

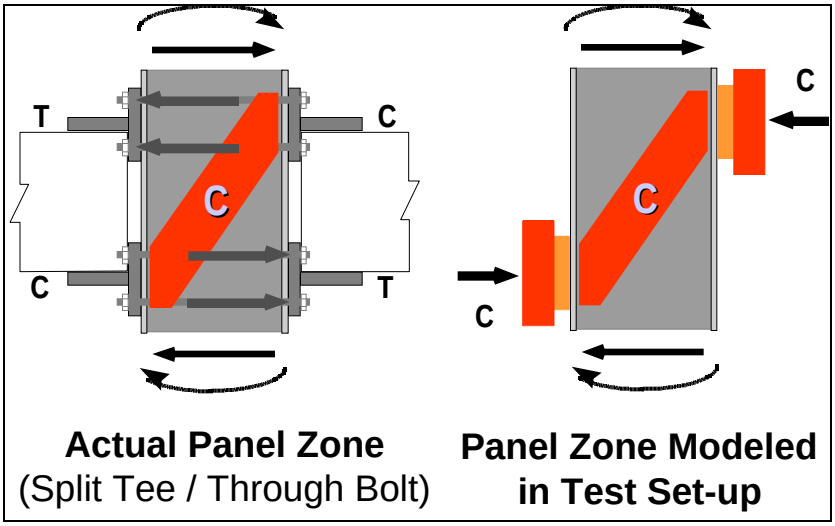

Figure A.1- Modeling of Panel Zone in Experimental Program

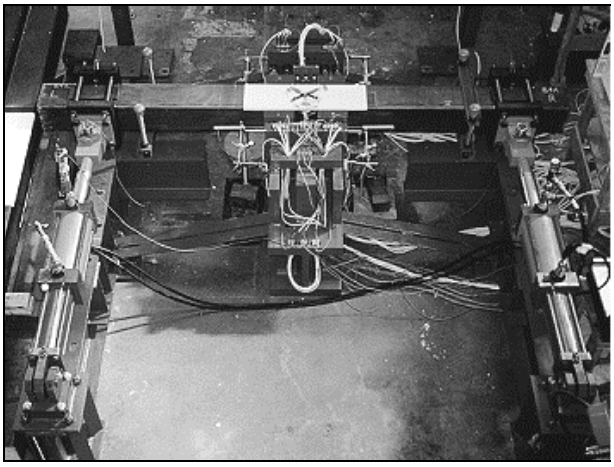

Figure A.2 - Panel-Zone Testing Frame

Figure A.1 shows how this connection zone was idealized. The forces were applied through the use of a stiff reaction frame (Figure A.2) designed to simulate the transmission of beam flange forces into the connection region under severe reverse cyclic (seismic) loads. The schematic of the test is shown in Figure

A.3. Cross section dimensions for the specimens were scaled from earlier Lehigh tests on full-scale connections (Ricles *et al* (1997)).

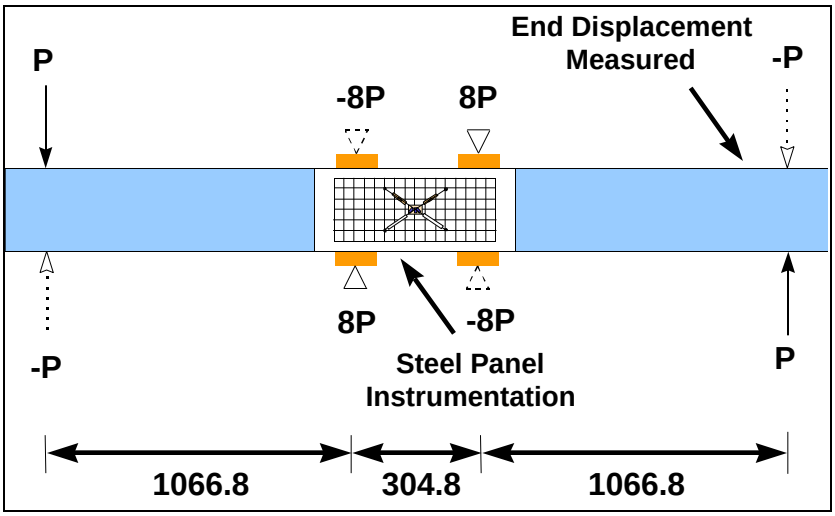

Figure A.3 - Schematic of Test Setup

Because the concrete compression strut within the split-tee through-bolted connection is a significant means of shear force transfer through the joint, and because no internal or external diaphragms are in place to aid in the force transfer, it is important to understand the role of the concrete in transferring large beam flange forces through the joint during significant reverse cyclic loading. Design recommendations for the panel-zone region of such connections will be developed based on: (a) the results of the panel-zone tests, (b) finite element models of the tests, and (c) the results of future tests on actual moment connections.

A.2 Experimental Program

A.2.1 Panel-Zone Test Specimens and Variables

The list of specimens is shown in Table A.1. The steel tube outer dimensions were held constant at 203 mm X 203 mm (8 in. X 8 in.). Two material thicknesses were used in this investigation: 6.4 mm (0.25 in.) and 0.5 mm (0.375 in.). The specimens were grouped into two series (A and B) according to steel batch. Series A utilized 6.4 mm (0.25 in.) thick material, and Series B used 9.5 mm (0.375 in.) material. The nominal concrete strengths, 41 MPa (6 ksi) was used. The experimental program and test set-up were developed and completed at The University of Texas at Austin (Koester *et al* (1997)).

Table A.1 - Panel Zone Specimens

ALL : 203X203 ASTM A-500 Cold Formed Welded HSS					
Series A - tc=6.4mm			**Series B -** tc=9.5mm		
	σ_y=372MPa			σ_y=365MPa	
Specimen	***b(%)***	**fc'(MPa)**	**Specimen**	***b(%)***	**fc'(MPa)**
8.4-A	50	42	8.4-B	50	41
8.6-A	75	42	8.6-B	75	42
8.8-A	100	42	8.8-B	100	41

In both Series A and Series B, the main variable was the width of the bearing block, simulating the width of the split tee, relative to the width of the steel tube. Figure A.4 shows the way in which the test set-up simulates beam-flange force application through the use of variable-width reaction blocks. By varying the width of the contact area from 50% to 100% of the tube wall width

(or tube depth, b), the effect of having a split-tee through-bolted connection that does not fully cover the width of the face of the CFT column could be simulated.

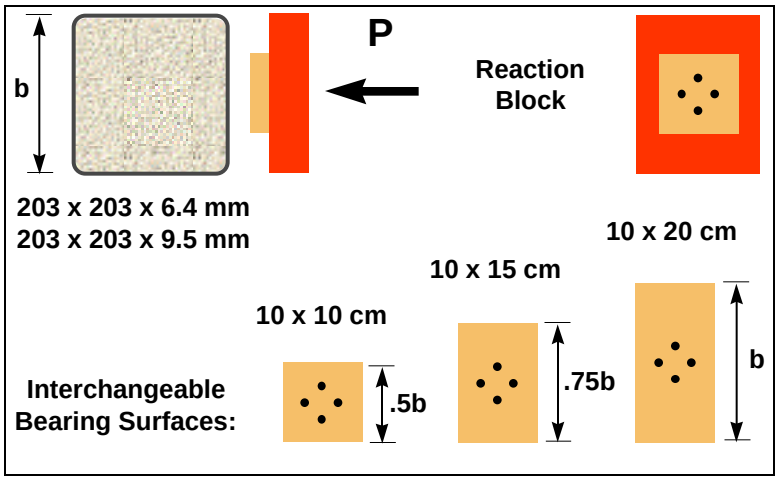

Figure A.4 - Varying the Reaction Area

A.2.2 Testing Procedure

Cyclic loads were applied to all specimens. The test was displacement-controlled in the sense that the displacement at one end of the specimen (including the effects of test set-up flexibility) was monitored and controlled during loading. Hydraulic rams were double-rodded, cross-linked, and used to apply equal and opposite pressures to the two rams. Symmetry in the displacements at both ends of the first pilot specimen was observed. Displacements were not chosen based on "story-drifts" because the introduction of flexibility at and around the reaction blocks created a situation in which story-drifts would be difficult to define. Instead, an arbitrary selection of a displacement history was used based on data from the pilot specimen, and then used in subsequent tests to make comparisons between specimens.

A.2.3 Experimental Results

For specimens in Series A and B, failure was observed to include a combination of significant panel-zone shear distress in both the steel and concrete, and localized bearing failure at the location of the reaction blocks against the steel tube surface. Bearing distress was less severe in the series B specimens, in which the b/t ratio of the tube wall was 21 compared to the series A b/t ratio of 32. Flexural yielding of the tube just outside of the panel zone was observed in all of the above specimens. In addition to visual inspection of the exterior, specimen 8.4-A was carefully examined by removing the steel from around the joint region. No concrete crushing due to flexure was observed. Most of the concrete was left intact, with small diagonal crack patterns, and localized indentations in the concrete due to high bearing stresses from the reaction blocks. The force-displacement relationship for the tip deflection of specimen 8.8-A is shown in Figure A.5.

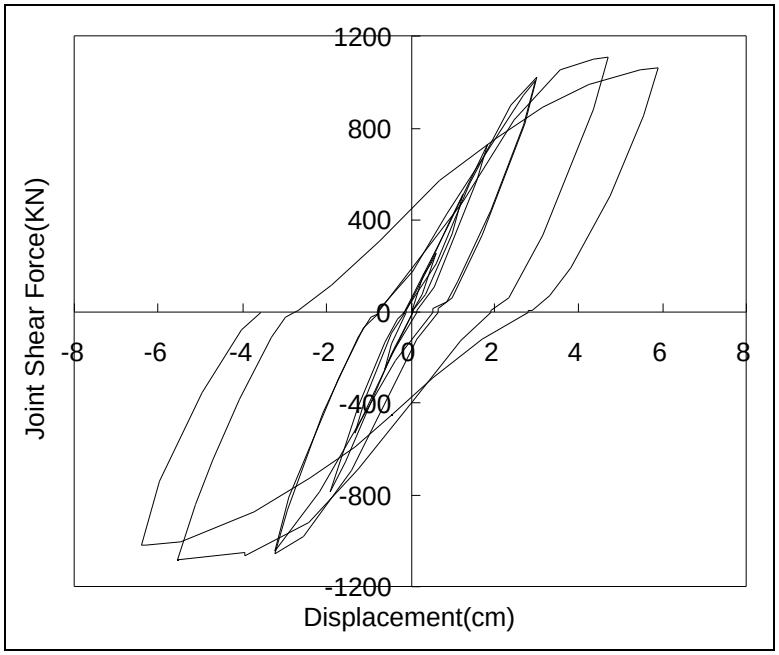

Figure A.5 - Joint Shear Force vs. End Displacement

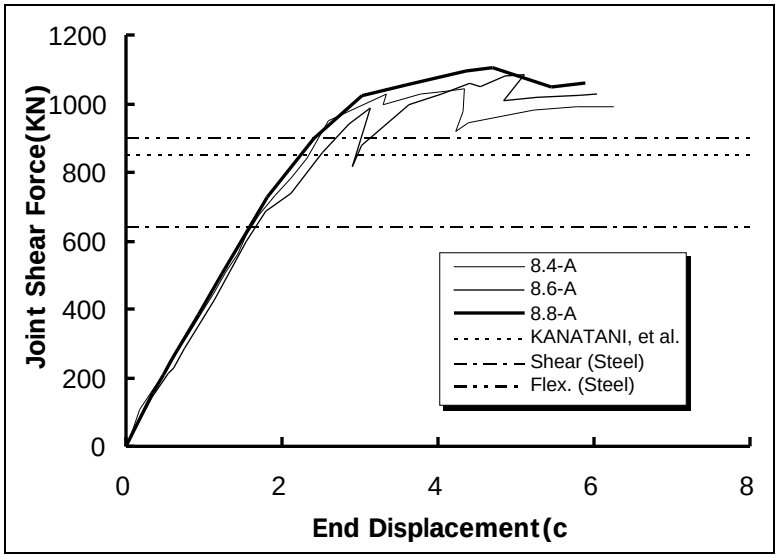

Figure A.6 - Comparisons of Series A Specimens

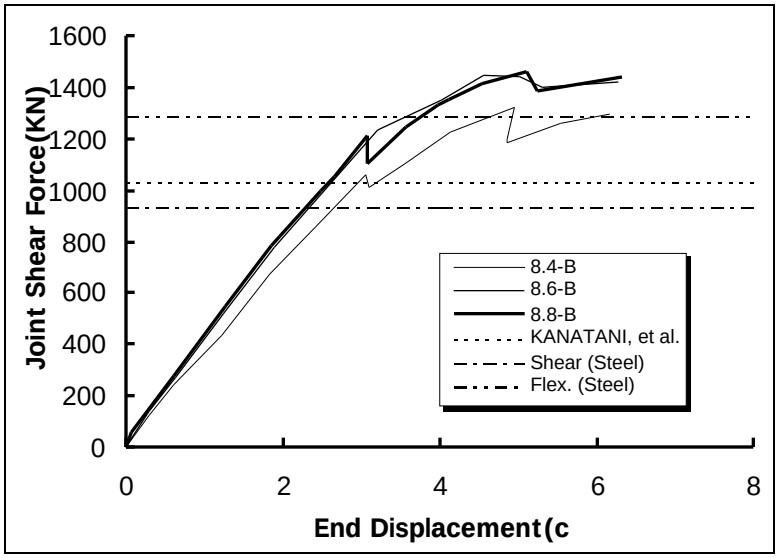

Figure A.7 - Comparisons of Series B Specimens

Within series A and B, changing the area of the reaction blocks did very little to change the ultimate load at failure. Comparisons of series A and B are shown in Figure A.6 and Figure A.7. Although bearing distress was more severe with the smaller area, the load carrying capacity was not significantly changed. Confinement helped to prevent further degradation due to bearing failures. It was determined that the panel zone tests within series A and B did not develop full plastic hinging outside of the panel zone. This supports the observation that the failure of the panel zone specimens was due to the combination of shear and bearing, and not limited by plastic hinging. The influence of the flexural yielding of the steel tube on the shear capacity of the panel zone is discussed analytically in the following section.

Figure A.6 and Figure A.7 show that the panel zone specimens in series A and B were able to achieve values of shear that were 80% and 60% higher than

the shear capacity for the steel section. In addition, the values of shear at ultimate were approximately 30% and 50% higher than the shear capacity of the composite section predicted by the Kanatani, *et al* (1985) method.

A.3 Finite Element Analysis

In this research, nonlinear three-dimensional finite element analyses of a panel zone test specimen and a beam - column joint test specimen with a split-tee, through-bolted connection were conducted. The analyses were shown to be effective for understanding the behavior of CFT. The three-dimensional nonlinear FEM analytical program used was developed by Uchida, Noguchi *et al*. (1994, 1997).

The concrete and the steel tube were modeled by solid elements and shell elements, respectively. The interaction characteristics between the concrete and the steel tube were represented using interface elements. A nonlinear-elastic model based on the equivalent uniaxial strain concept (Darwin and Pecknold (1974)) was used for the concrete. The isotropic hardening model based on Mises yield condition was used for the steel. The modeling of the interface elements under compressive normal stress, which was obtained using the results of bond tests (Kim *et al* (1994)), was shown in Fig.8. The ratio of the bond stress to the compressive normal stress was expressed by an exponential function. The initial bond stiffness was assumed to be 1 $N/mm^2/mm$. After the tensile normal stress exceeded 0.1 MPa, 1/100 of the initial stiffness was used.

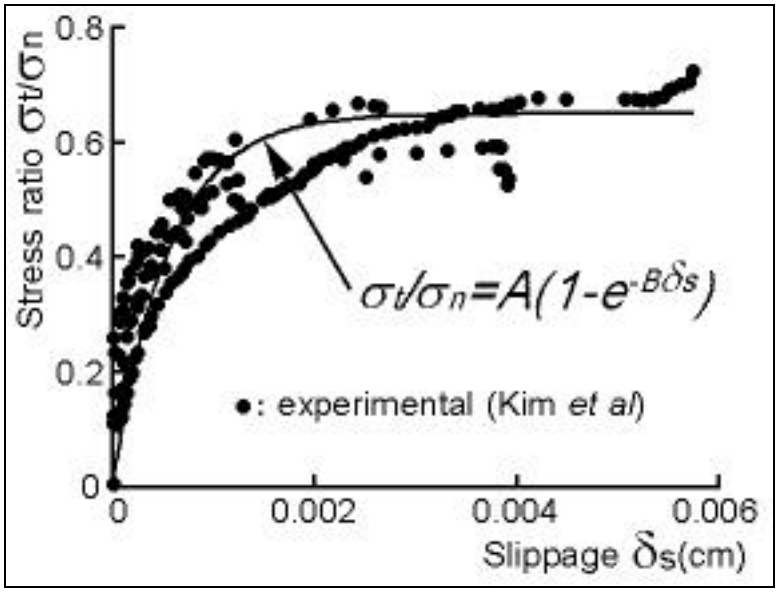

Figure A.8 - Characteristics of Interface Element

A.3.1 Finite Element Analysis of Panel Zone Test

A.3.1.1 Outline of Analysis

Specimens 8.8A and 8.4A were selected for analysis. The tube thickness of both specimens was 6.35mm. The ratio of the reaction plate width to the tube width of specimens 8.8A and 8.4A was 1.0 and 0.5, respectively. The finite element idealization of specimen 8.8A is shown in Figure A.9. Material properties used in the analysis are shown in Table A.2. If the loading condition is modeled ideally as shown in Figure A.3, the boundary condition becomes a pin support. However, the reaction block was supported by four high strength bolts in the test as shown in Figure A.10, and the actual boundary condition in the test was different than a pin support. Therefore spring supports were used in the

analysis as shown in Figure A.10. The stiffness of the spring was calculated from the property of high strength bolts.

Table A.2 - Material Properties for Analysis

Concrete		
Young's Modulus	2.85? 10^4	(MPa)
Compressive Strength	42.4	(MPa)
Strain at the Compressive Strength	2.28? 10^{-3}	
Tensile Strength	3.2	(MPa)
Steel		
Young's Modulus	2.00? 10^5	(MPa)
Yield Point	372.3	(MPa)

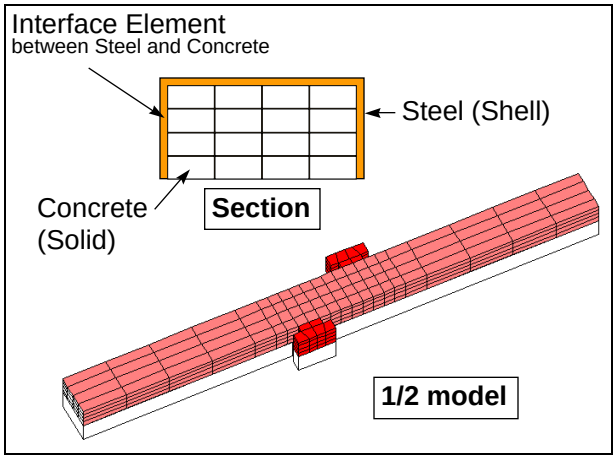

Figure A.9 - Finite Element Idealization

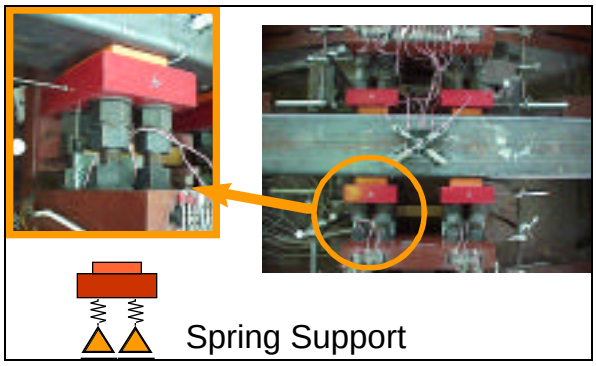

Figure A.10 - Boundary Condition of Reaction Block

In the tests, the flexural yielding of the columns and the shear yielding of the panel-zone were observed. In the analyses, the numerical specimens were planned in order to investigate the effect of the flexural yielding of the column on the shear capacities of the panel zone. Because the numerical steel tube specimens had elastic flanges, the flexural yielding of the column was avoided.

A.3.1.2 Analytical Results

The relationships between joint shear force and deformation are shown in Figure A.11 and Figure A.12. FEM1 is a simulation analysis of the test specimen, FEM2 is an analysis of the numerical specimen with elastic flanges. Elastic theoretical stiffness is indicated in these figures. Modified deformation was obtained by deducting the measured deformation of the reaction block from the original deformation. The initial stiffness in all analytical cases was larger than that in the experiment. The measured initial stiffness was similar to the elastic theoretical stiffness of the steel tube. It is considered that the concrete didn't contribute to the stiffness. For the maximum load of both specimens, the analytical results (FEM1) agree with the experimental results.

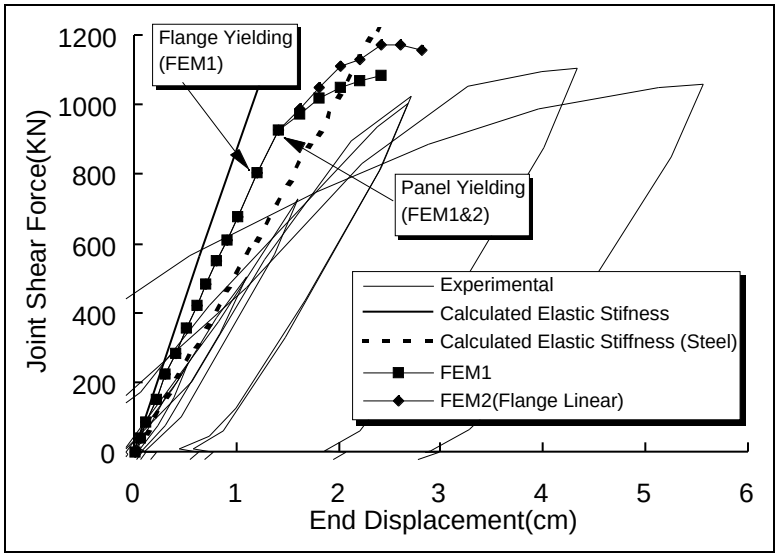

Figure A.11 - Joint Shear Force vs. End Displacement (8.8-A)

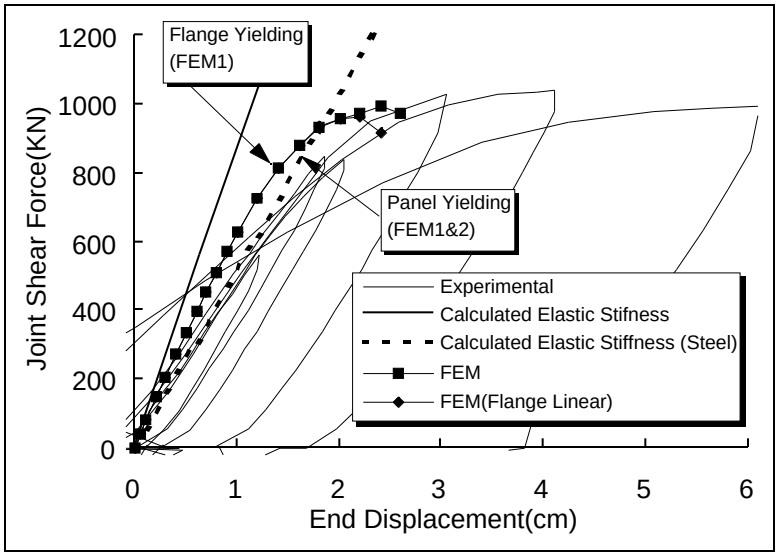

Figure A.12 - Joint Shear Force vs. End Displacement (8.4-A)

The analytical results (FEM1 : Simulation, FEM2 : Elastic flange) are compared in Figure A.11 and Figure A.12. For 8.8-A, the capacity of FEM2 was 8% higher than FEM1. For 8.4-A, the capacities of both cases are similar.

Therefore the measured capacity of 8.4-A was considered to be the shear capacity of the panel zone. However the measured capacity of 8.8-A depended on flexural yielding of the flange.

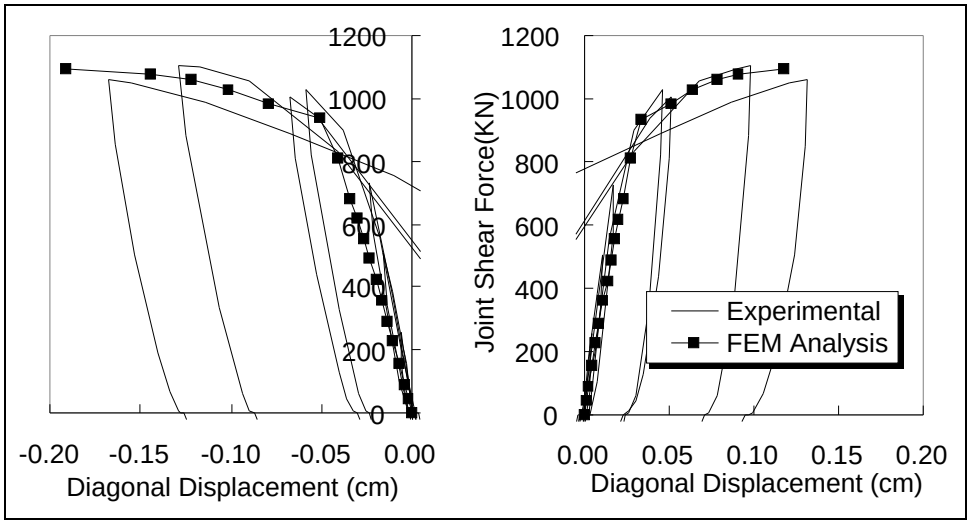

Figure A.13 - Diagonal Displacement of Panel Zone (8.8-A)

In Figure A.13, diagonal deformation measured in the panel zone and the corresponding deformation calculated in FEM1 (8.8-A) are compared. In compression and tension, the computed stiffness showed good agreement with measured. Therefore in the panel zone the analytical model simulated experimental results well. Comparing to analytical and experimental results, total deformation was different, but panel zone deformation was similar.

A.3.2 Finite Element Analyses of Beam - Column Joint Test

A.3.2.1 Outline of Analysis

Specimen C6 was a cross shaped beam - column joint specimen with a CFT column and steel beams using split-tee, through bolted connections (Ricles

et al (1997)) in Figure A.14. C6 was selected in order to compare with the results of the panel zone test specimen analysis. Using prestressing for the bolts, a pretension force of 356 KN was applied to each bolt. An axial load of 2000 KN was applied to the top of the column. Cyclic lateral loads were applied to the top of the column. The failure mode was beam yielding.

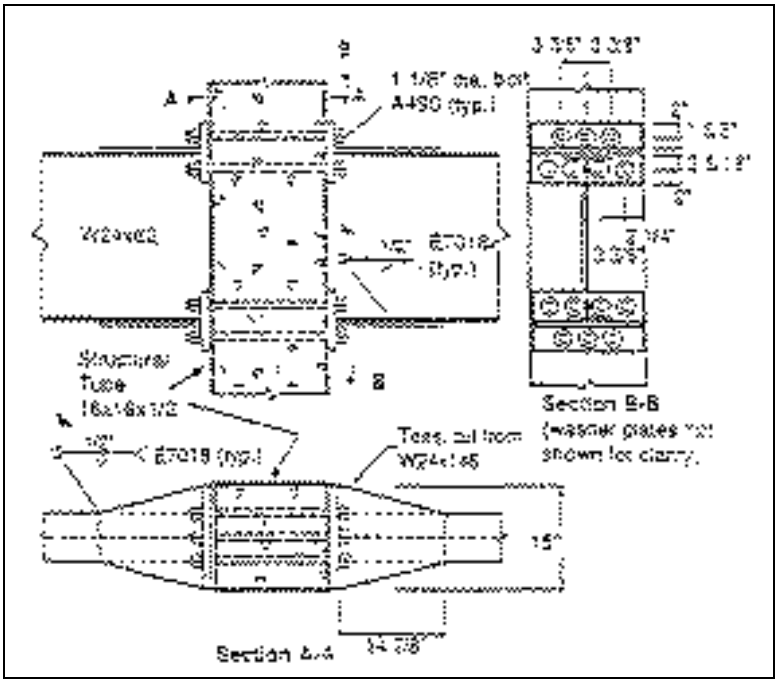

Figure A.14 - Connection Details, Specimen C6

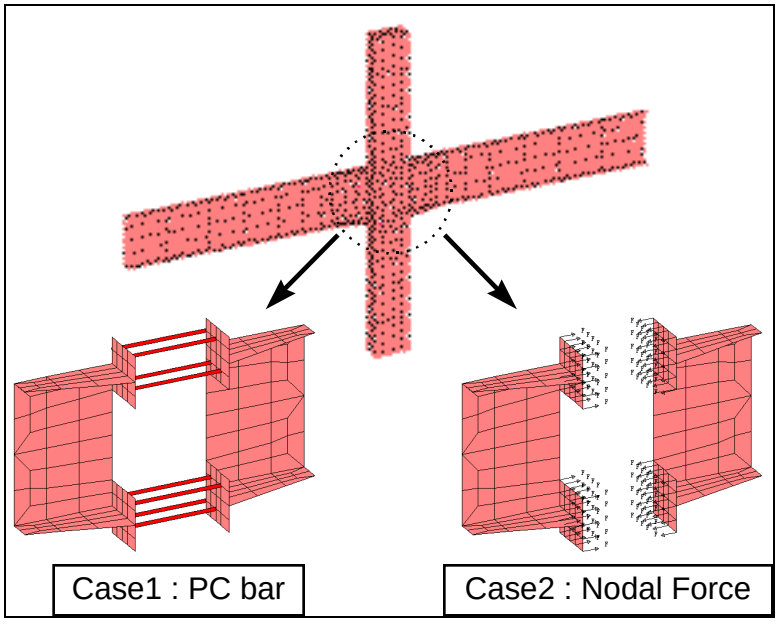

Figure A.15 - Modeling of Prestress

Finite element idealization of specimen C6 is shown in Figure A.15. For the application of the pretension force on the bolts, two cases were considered for modeling of prestressing. In Case 1, unbond bolts only were modeled without prestressing. In this case, tensile forces from the steel beam were assumed to be transferred by bolts to the opposite face split-tee. It is considered that the stress condition of the panel zone test is similar to this case. In Case 2, average normal stresses at the split-tee surface produced by prestressing were modeled as equivalent nodal forces. In this case, the stiffness of the bolts was assumed to be the same as the compressive stiffness of the concrete. An axial load was applied to the top of the column and monotonic load was applied to the end of each steel beam. In Case 2, nodal forces were applied to split-tees before axial loading was applied.

Table A3 - Material Properties for Analysis

Concrete		
Young's Modulus	3.06×10^4	MPa
Compressive Strength	50.9	MPa
Strain at Compr. Strength	2.40×10^{-3}	
Tensile Strength	3.6	MPa
Steel		
Young's Modulus	2.00×10^5	MPa
Yeild Point (CFT)	379	MPa
Yeild Point (Beam Flange)	298	MPa
Yeild Point (Beam Web)	342	MPa
Yeild Point (Split-tee)	428	MPa
PC Bar		
Young's Modulus	2.00×10^5	MPa
Yeild Point	896	MPa

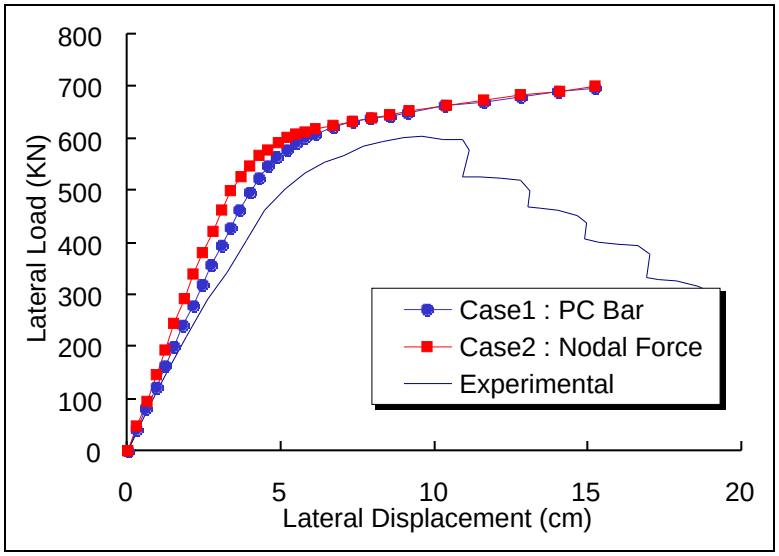

Figure A.16 - Lateral Load vs. Displacement

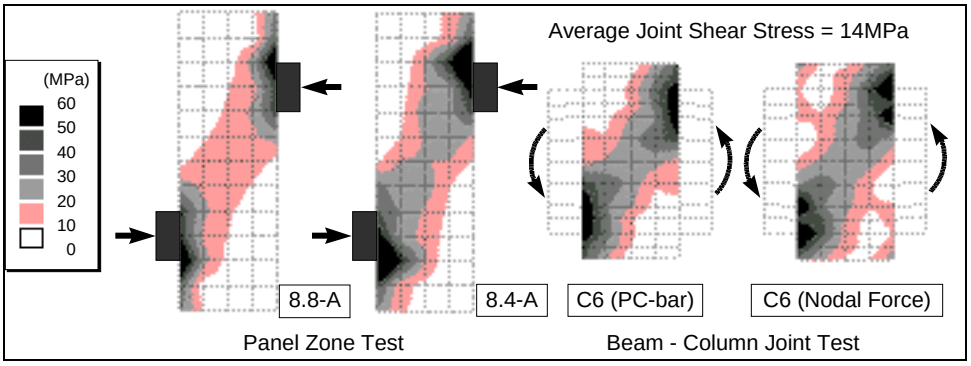

Figure A.17 - Minimum Principal Stress Distribution

A.3.2.2 Analytical Results

The relationship between the lateral load and deformation is shown in Figure A.16. The stiffness and the capacity from both analyses were larger than measured. Comparing Case 1 (bolts without prestressing) and Case 2 (nodal forces prestressing), the stiffness of Case 2 is larger than that of Case 1. The capacities of Cases 1 & 2 are similar, because the capacity depended on yielding of the steel beam. Minimum principal stress distributions of Case 1, Case 2, and the panel zone test (8.8-A and 8.4-A) at the average shear stress of 14 MPa are shown in Figure A.17. Shown are the stress distributions at the plane including the second node from mid-plane of column. Average shear stress was calculated from the analytical results by considering the steel web section area as an equivalent cross-section area. Because the reaction plate width of 8.8-A is wider than that of 8.4-A, the principal stresses of 8.8-A are distributed on the average compared with 8.4-A. In Case 2, compressive stress is observed in the tension area due to nodal force prestressing. The distribution of C6 (Case 1 & 2) and that of the panel zone tests (8.8-A and 8.4-A) are compared. For C6, the stresses tend

to concentrate to the mid-plane of the beam-column joint due to the existence of the web. Therefore it is considered that the stress condition of beam-column joint tests is simulated well by the panel zone test of 8.4-A with narrow reaction plate.

A.4 Conclusions

An experimental testing method and a finite element analysis for simulating the stress condition within the panel-zone region of the split-tee through-bolted moment connection were developed and executed. The experimental tests were conducted to examine the effects of varying: the contact width of the reaction plate, the tube wall thickness (b/t ratio), and concrete strength. A finite element method model was developed to compare the stress condition from this testing method against the stress condition that exists in the FEM model of an actual moment connection detail. A case that compared the stress condition of a panel-zone specimen to that of an actual connection detail was also analyzed. The following conclusions were made:

Varying the contact width of the reacting blocks against the CFT from 50% to 100% of the tube depth had negligible effect on the capacity of the panel-zone.

Varying the b/t ratio of the steel tubes did not appreciably change the failure mode except in the sense that localized bearing distress was less severe.

The failure of the panel-zone was the result of a combination of shear yielding in the steel, bearing failure at the location of the reacting blocks, and some cracking within the concrete core.

The finite element analysis satisfactorily simulated the behavior of the panel-zone test. The shear capacity of the panel zone tests was influenced by the flexural yielding of the steel tube according to the analytical results.

From the comparison of analytical results, the stress condition of the panel zone test is similar to that of a beam - column joint with the split-tee, through bolted connection.

Acknowledgements

This research was carried out as the cooperative study of Fujita Cooperation, Chiba University and University of Texas at Austin under the U.S.-Japan cooperative structural research project on composite and hybrid structures.

References

1) Darwin, D., and Pecknold, D., A., W. (1974), Inelastic Model for Cyclic Biaxial Loading of Reinforced Concrete, University of Illinois, July
2) Kanatani, H., Tabuchi, M., and Kamba, T. (1985), A Study on Concrete Filled RHS Column to H-Beam Connections Fabricated with HT Bolts in Rigid Frames. Proc. Of the 1st Composite and Construction in Steel and Concrete Conference, Henniker, NH., 614-635
3) Kim, K. and Noguchi, H.(1994), Experimental Study on Bond Characteristics of Concrete and Steel Plates, Summaries of Technical Papers of Annual Meeting of Architectural Institute of Japan, pp1631-1632, September (in Japanese)

4) Ricles, J.M., Lu, L.W., Peng, S.W., Split-Tee Seismic Connections for CFT Column-WF Beam MRFs. Proceedings of Structures Congress XV, 2, ASCE, 1997, 959-963

5) Uchida, K., Mikame, A., Noguchi, H., Three-Dimensional Nonlinear Finite Element Analysis of Connections between Steel Beams and Reinforced Concrete Columns in Hybrid Structures. Computational Structural Engineering for Practice, Civil-Comp Press, 1994, 143-150

6) Uchida, K., Mikame, A., Satoh, T., Noguchi, H., Three-Dimensional Nonlinear Finite Element Analysis of Frames Consisting of RC Columns and Steel Beams. Transactions of JCI, 18, 1997, 243-250

7) Koester, B.D., Uchida, K., Noguchi, H., Yura, J.A., Jirsa, J.O., Panel-Zone Behavior of Moment Connections between Steel Beams and Concrete-Filled Steel Tube Columns, Strctural Engineering World Congress, 1997

Short Comment: The finite element analyses are effective for understanding the behaviors of hybrid and composite structures. Modeling of the interaction between Concrete and Steel is very important to simulate the behaviors of these structures.

Kazuhiro Uchida

8. Appendix B: Design Shear Check

The following example illustrates a check of the joint shear in a moment connection utilizing a concrete-filled square tube column and steel wide-flange beams. Through analysis, the designer has decided that a 16 inch square tube with a 5/8 inch wall thickness is sufficient for use as a column in a high-rise building. W24 x 68 beams are chosen to frame into the moment connection in order to satisfy strength requirements and to ensure strong-column/weak-beam design. Split-tee through-bolted connections are specified and properly designed to carry flange forces through the joint. Design calculations are complete except for the joint shear check:

Material properties:

Beams: W24 x 68, Grade 50

Z = 177 in^3

Columns: 16 x 16 x 5/8 in., Grade 50

Wall thickness = 0.625 in.

Concrete specified f'_c = 6000 psi

Story Height = h = 12 ft. = 144 in.

Calculate Joint Shear:

Assume that inflection points for the column are at mid-height, so the following simplified analysis can be made (refer to Figure B1):

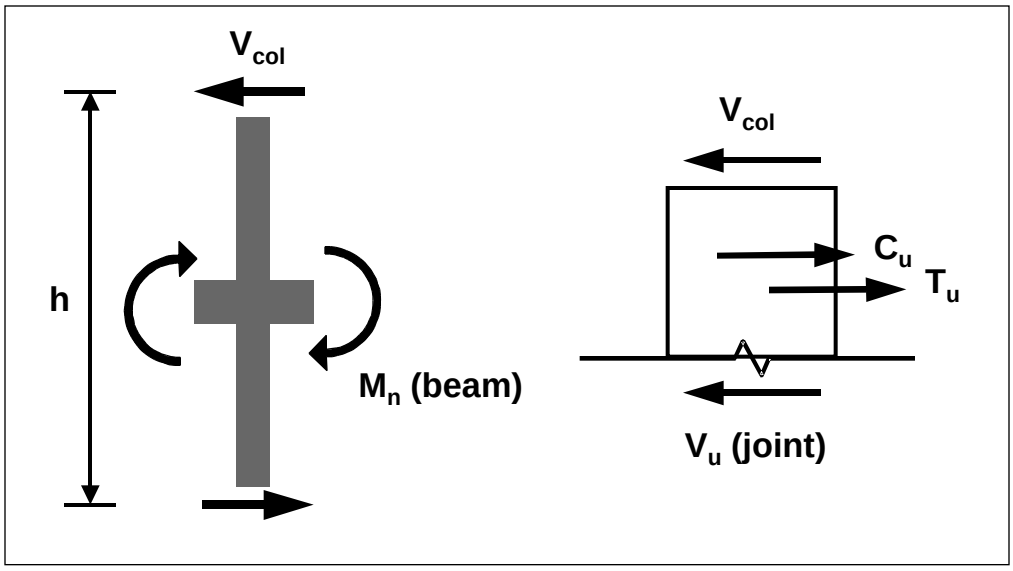

Figure B1 - Joint Shear Design Assumptions

$M_n = ZF_y$ = 177(50) = 8850 k-in.

V_{col} =2 M_n(beam) / h = 2(8850) / 144 = 123 kips

T_u = M_n(right beam) / 24 in. = 369 kips

C_u = M_n(left beam) / 24 in. = 369 kips

V_u(joint) = T_u + C_u - V_{col} = 369 + 369 – 123 = **615 kips**

Check joint shear capacity:

$$V_n = V_s + 28A_c\sqrt{f_c'} \text{ (psi)} \qquad (4.4)$$

$$V_s = 2 \times 0.6 d_{fl} t F_y$$

where d_{fl} is the depth of the flat portion of the steel tube.

d_{fl} = 13.5 inches (measured flat steel shear panel)

A_c = [16 - 2(.625)]^2 = 218 in^2 (shear area of concrete)

V_s = 2(0.6)(13.5)(0.625)(50) = 506 kips

V_c = 28(218)(6000)$^{1/2}$ = 473 kips

Using a φ factor of 0.85 for shear,

φV_n = 0.85(506 + 473) = **832 kips > 615 kips** (joint is okay for shear)

Appendix C: As-Built Connection Dimensions

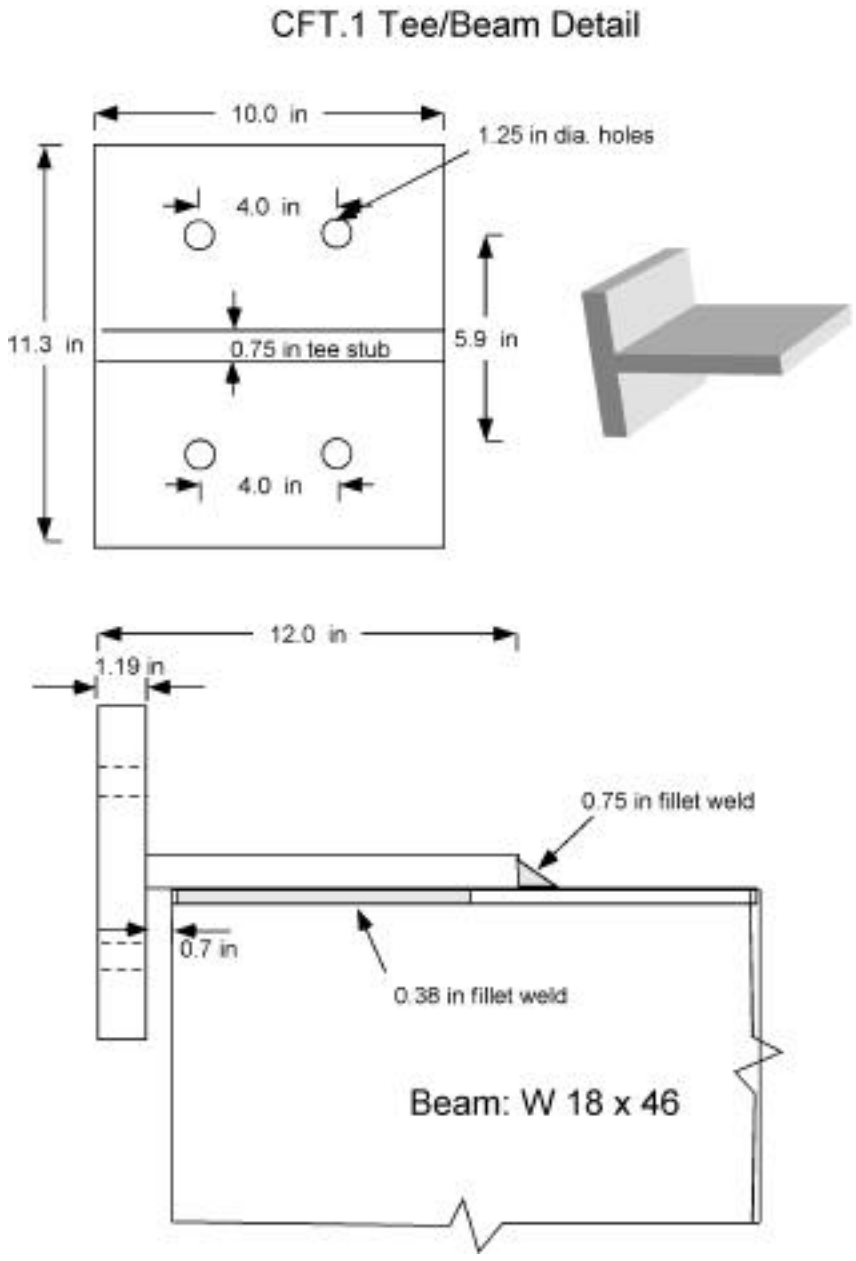

Figure C.1 – Connection CFT.1

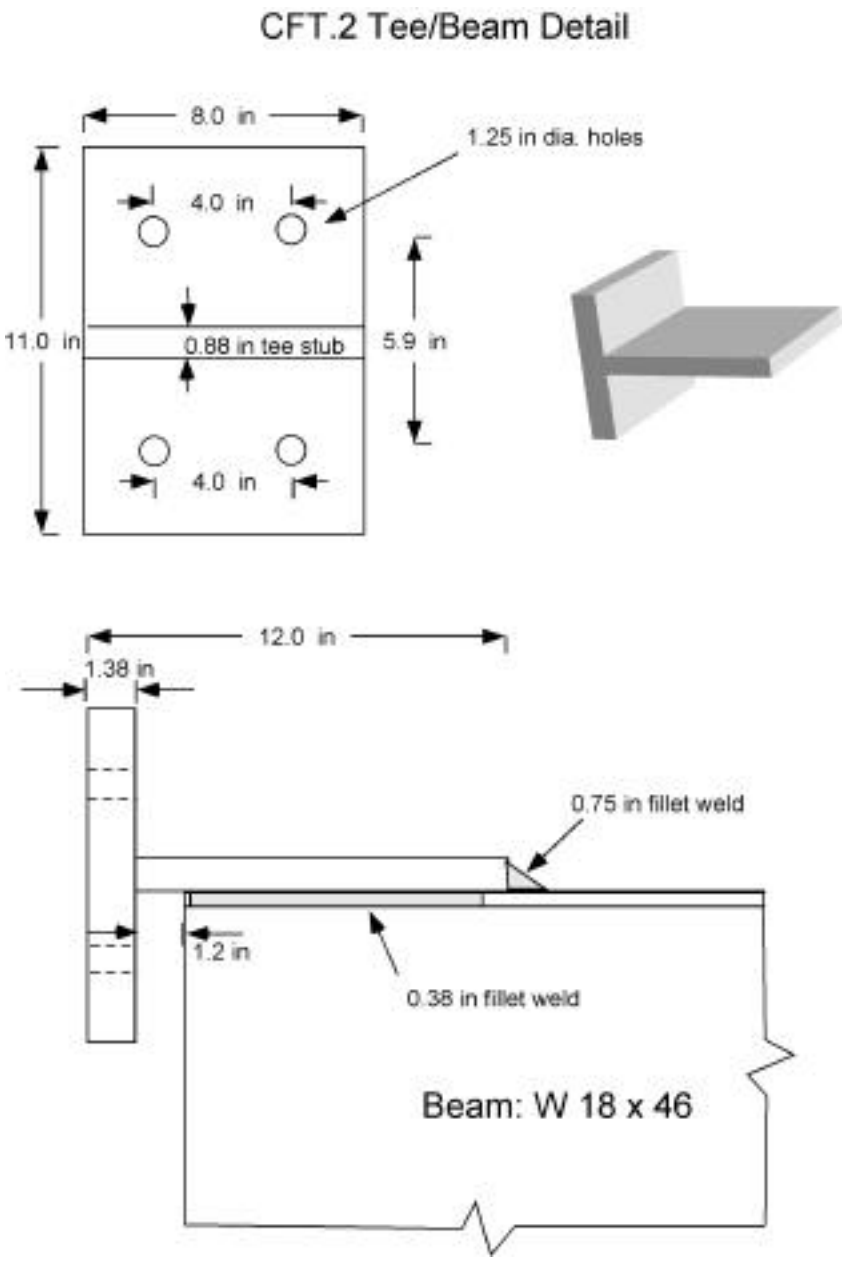

Figure C.2 – Connection CFT.2

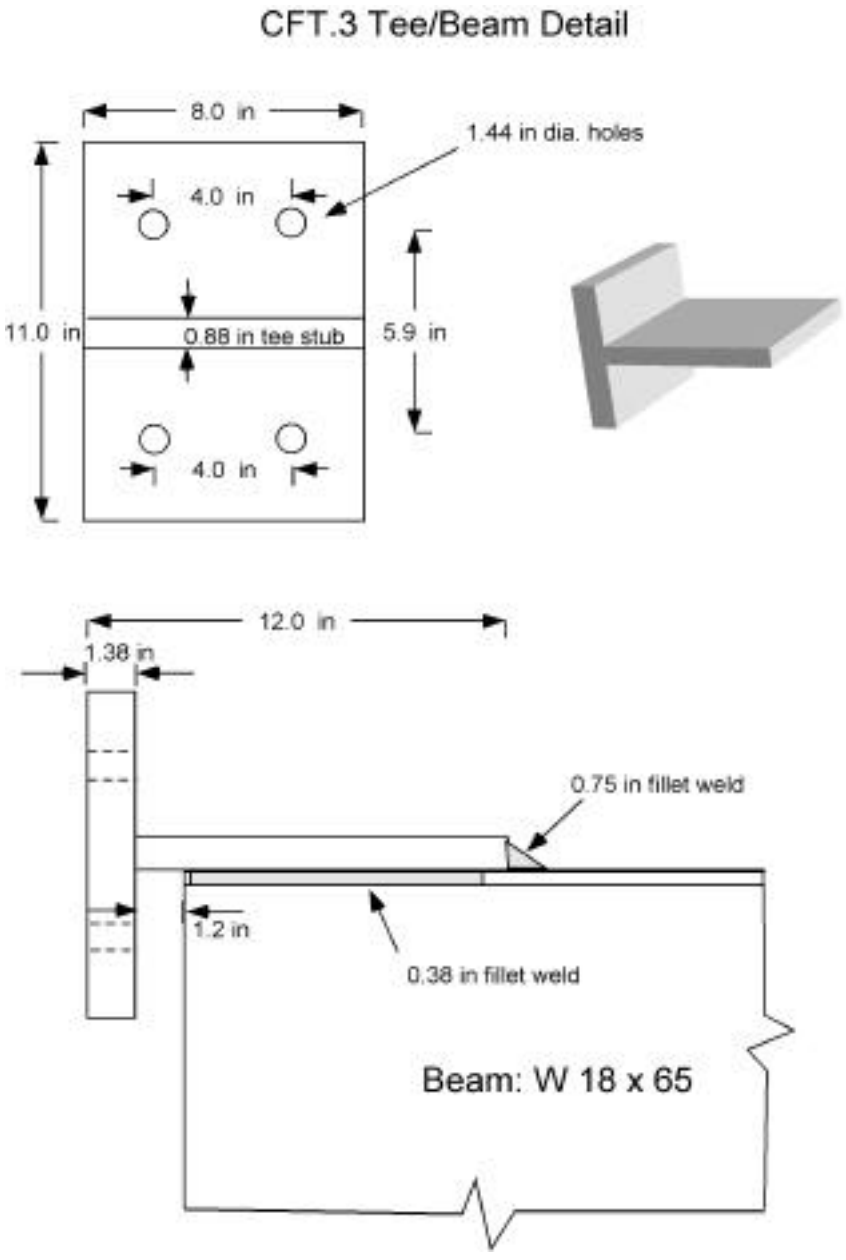

Figure C.3 – Connection CFT.3

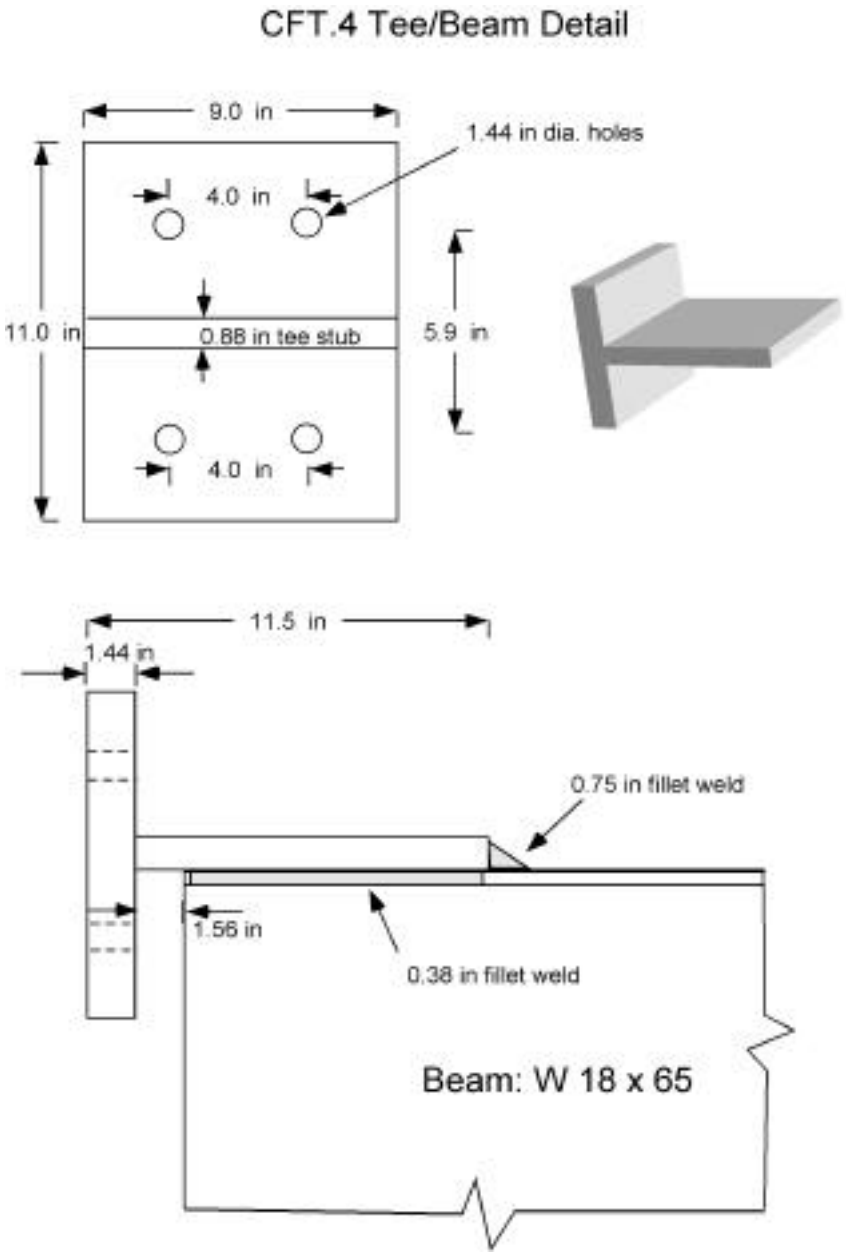

Figure C.4 – Connection CFT.4

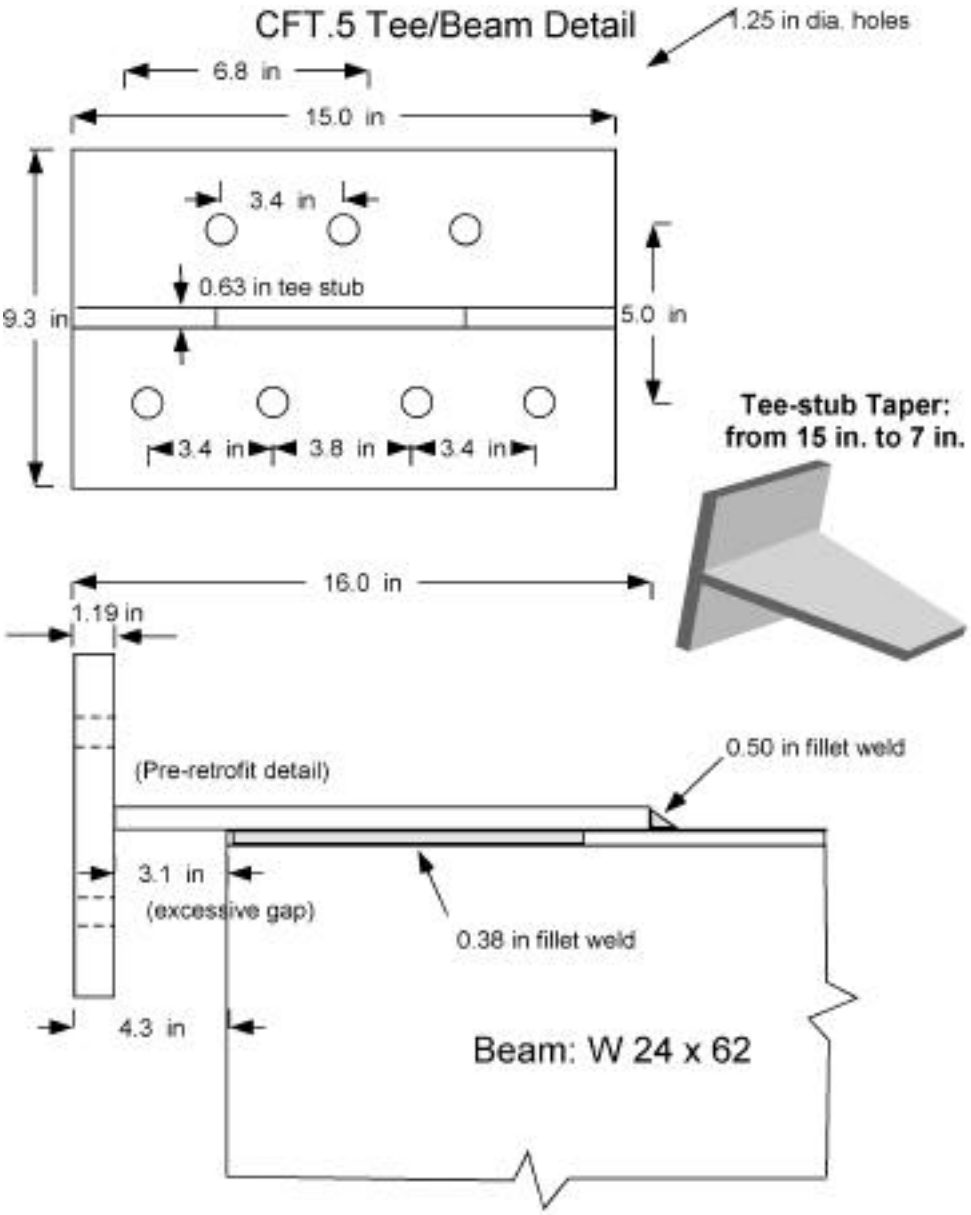

Figure C.5 – Connection CFT.5 (pre-modification)

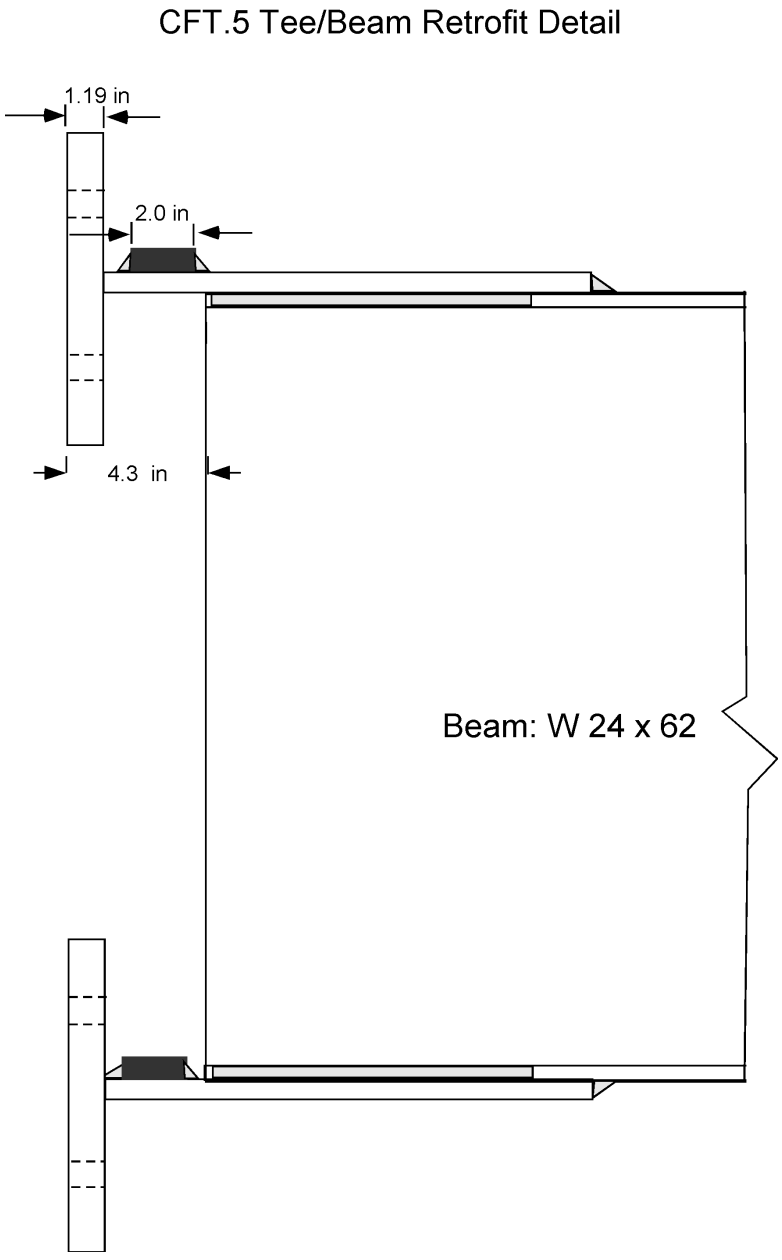

Figure C.6 – Modification to Connection CFT.5

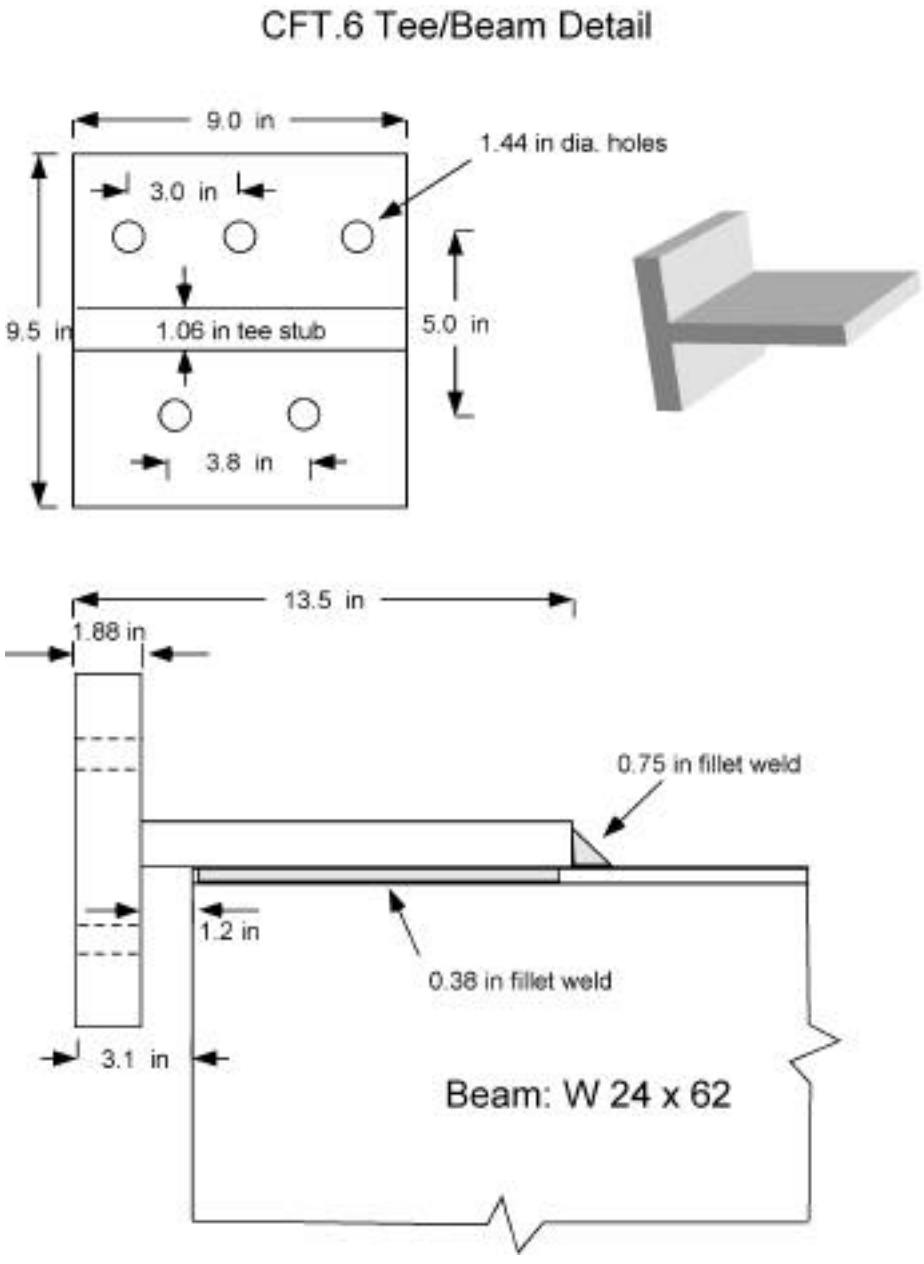

Figure C.7 – Connection CFT.6

Bibliography

Aboutaha, R. S., and Machado, R. I. (1999). "Seismic Resistance of Steel-Tubed High-Strength Reinforced-Concrete Columns" Journal of Structural Engineering, ASCE, 125(5), 485-494.

ACI (1995). "Building Code Requirements for Structural Concrete (ACI 318-95) and Commentary (ACI 318R-95)" American Concrete Institute, 1995.

ACI-ASCE Committee 352 (1998). "Recommendations for Design of Beam-Column Joints in Monolithic Reinforced Concrete Structures" ACI Manual of Concrete Practice, Part 3, American Concrete Institute, 1998, 352R-1 to 352R-21.

Advisory Group on the Specification for the Design of Cold-Formed Steel Structural Members (1990). "Load and Resistance Factor Design Specification for Cold-Formed Steel Structural Members", Report CF 90-1, American Iron and Steel Institute, 1990.

AISC (1994). "Manual of Steel Construction, Load and Resistance Factor Design, Structural Members, Specifications & Codes", Vol. I & II, American Institute of Steel Construction, 1994.

Architectural Institute of Japan (1988). "Standard for Structural Calculation of Steel Reinforced Concrete Structures & Composite Steel Tube and Concrete Structures (Draft Translation)" AIJ, 1998.

ASCE Task Committee on Design Criteria for Composite Structures in Steel and Concrete (1994). "Guidelines for Design of Joints between Steel Beams

and Reinforced Concrete Columns" Journal of Structural Engineering, ASCE 120(8), 2330-2357.

Ballio, G., Plumier, A., and Thunus, B. (1990). "Influence of Concrete on the Cyclic Behavior of Composite Connections" IABSE Symposium Brussels 1990, Mixed Structures including New Materials, 203-208.

Deierlein, G. G. (1988). "Design of Moment Connections for Composite Framed Structures" Ph.D. Dissertation, The University of Texas at Austin, 1998.

El-Tawil, S., Vidarsson, E., Mikesell, T., and Kunnath, S. K. (1999). "Inelastic Behavior and Design of Steel Panels" Journal of Structural Engineering, ASCE, 125(2), 183-193.

Fielding, D. J. (1994). "Frame Response Considering Plastic Panel Hinges" Engineering Journal, AISC, 1st Quarter 1994, 31-37.

Kanatani, H., Tabuchi, M., Kamba, T., Hsiaolien, J., and Ishikawa, M. (1987). "A Study on Concrete Filled RHS Column to H-Beam Connections Fabricated with HT Bolts in Rigid Frames" Composite Construction in Steel and Concrete, Proceedings of an Engineering Foundation Conference, ASCE, Henniker, NH, 1987, 614-635.

Knowles, R. B., and Park, R. (1969). “Strength of Concrete Filled Steel Tubular Columns” Journal of the Structural Division, ASCE, 95(12), 2565-2587.

Krawinkler, H. (1978). "Shear in Beam-Column Joints in Seismic Design of Steel Frames" Engineering Journal, AISC, 3rd Quarter 1878, 82-91.

Krawinkler, H., Bertero, V. V., and Popov, E. P. (1975). "Shear Behavior of Steel Frame Joints" Journal of the Structural Division, ASCE, 101(11), 2317-2336.

Krawinkler, H., and Popov, E. P. (1982). "Seismic Behavior of Moment Connections and Joints" Journal of the Structural Division, ASCE, 108(2), 373-391.

Meinheit, D. F., and Jirsa, J. O. (1981). "Shear Strength of R/C Beam-Column Connections" Journal of the Structural Division, ASCE, 107(11), 2227-2244.

Mirza, S. A. (1989). "Parametric Study of Composite Column Strength Variability" Journal of Construction Steel Research, Elsevier Science Publishers Ltd., 14(1989), 121-137.

Ogura, K., Tanaka, R., and Noguchi, H. (1990). "Development of Mixed Structures in Japan" IABSE Symposium Brussels 1990, Mixed Structures including New Materials, 437-442.

Park, R., Priestley, M. J. N., and Gill, W. D. (1982). "Ductility of Square Confined Concrete Columns" Journal of the Structural Division, ASCE, 108(4), 929-951.

Parsley, M. A. (1998). "Push-Out Behavior of Concrete-Filled Steel Tubes" Masters Thesis, The University of Texas at Austin, 1998.

Ricles, J. M., Lu, L. W., and Peng, S. W. (1997). "Split-Tee Seismic Connections for CFT Column-WF Beam MRFs", ASCE Structures Congress, Portland, 1997.

Saatcioglu, M., and Razvi, S. R. (1990). "Strength and Ductility of Confined Concrete", Journal of Structural Engineering, ASCE, 118(6), 1590-1607.

Schneider, S. P. (1998). "Seismic Behavior of Steel Frames with Deformable Panel Zones" Journal of Structural Engineering, ASCE, 124(1), 35-42.

Sheikh, T. M. (1987). "Moment Connections Between Steel Beams and Concrete Columns" Ph.D. Dissertation, The University of Texas at Austin, 1987.

Tomii, M. (1988). “Investigations on Transversely Super Reinforced Concrete Structures and Concrete Filled Steel Tube Structures” Report to the Ministry of Education, Science and Culture, Department of Architecture, Faculty of Engineering, Kyushu University, Japan, 1988.

Uchida, K., Noguchi, H., Koester, B. D., Jirsa, J. O., and Yura, J. A. (1998). "Panel-Zone Behavior of Moment Connections between Steel Beams and Concrete-filled Steel Tube Columns" Journal of Fujita Technical Research Institute, No. 9, 1998

Viest, I. M., Colaco, J. P., Furlong, R. W., Griffis, L. G., Leon, R. T., Wyllie, L. A. (1997). “Composite Construction Design for Buildings”, ASCE, McGraw Hill Publishing

Vita

Bradley Donald Koester was born in Minneapolis, Minnesota on June 4, 1965 to parents Donald and Carol Koester. Following graduation from Alexander Ramsey Senior High School in Roseville, Minnesota, Brad entered the Institute of Technology at the University of Minnesota. After obtaining his Bachelor of Science degree in Civil Engineering, he entered the Graduate School of The University of Texas at Austin where he pursued his Masters degree in the Department of Civil Engineering. He earned his Masters in the fall of 1995, and continued toward a Ph.D. of the same. In addition to his interests in the many fields of engineering, Brad is also a part-time film actor and voice-over talent, having taken on starring and supporting roles in independent and short films. Brad is Executive Vice President of CDstreet.com of Dallas, Founder and Executive Producer of AustinActors.net, and President of Koester Media, a multi-media and web development firm in Austin, TX that has been in business since 1996.

Permanent Address: 3605 Steck Avenue, #2103
Austin, TX 78759-8834

This dissertation was typed by the author.